DESIGN AND TESTING OF A PHASELOCK RECEIVER FOR A V.H.F.-F.M. IONOSPHERIC FORWARD SCATTER COMMUNICATION SYSTEM

A Thesis

Submitted to the Faculty of Graduate studies

in Partial Fulfillment of the Requirements

for the Degree of

Master of Science

in the Department of Electrical Engineering

University of Saskatchewan

by

Gary H. Beuker

Saskatoon, Saskatchewan

March, 1965

ACKNOWLEDGMENTS

This work was carried out under the direction of Professor A. G. Wacker, whose encouragement and assistance are gratefully acknowledged. I am also indebted to Professor A. Michalenko and Mr. A. Krause for criticisms and assistance in the preparation of this thesis.

I wish to acknowledge the Department of Natural Resources for its financial assistance and the department radio operator at Uranium City for his aid in operating the transmitter.

ABSTRACT

In this thesis, a start has been made on the design of a low power frequency modulated VHF ionospheric forward scatter communication system, to provide reliable radio transmission between points located in the auroral zone.

Previous work suggested the feasibility of a system using a 50 watt transmitter and a phaselock receiver with a lock range of 300 cps and signal bandwidths between 5 and 100 cps.

To substantiate former work in which recommendations were based on test results using an unmodulated carrier, a similar system was designed with provisions for frequency modulation. Dictated by the frequency stability of the entire system, the lock range was increased to 775 cps.

Much of this thesis is devoted to the design and analysis of the phaselock detector and to the testing of the receiving system. Some pertinent properties of the receiver have been theoretically predicted and tested under simulated field operating conditions.

In order to test the system under actual field conditions the 50 watt transmitter and the phaselock receiver were placed at Uranium City and Saskatoon, Saskatchewan, respectively. It was observed that sufficient signal to lock the system could be received for only a small portion of the total propagation time. This fact tentatively has been attributed to the effect which Doppler frequency shifts may have on a phaselock system with a relatively large lock range. The geometry of propagation and atmospheric conditions were not as favourable as during previous experiments.

Recommendations have been made regarding improvements of the present receiver design and regarding the analysis of other, possibly superior, receiving systems.

GENERAL INDEX

Title			Page
I.	INTRODUCTION		
	1.0	The Problem Defined........................	1
	1.1	Previous Work on VHF Ionsopheric Forward Scatter...........................	3
	1.2	General Discussion of the Scope of this Thesis...............................	7
II.	TRANSMITTING EQUIPMENT DESIGN AND ITS OPERATION		
	2.0	Transmitter................................	14
	2.1	Transmitter Modulator......................	15
		2.1.1 Modulation Method Number 1..........	15
		2.1.2 Modulation Method Number 2..........	15
		2.1.3 Modulation Method Number 3..........	15
	2.2	Transmitter Identification.................	19
III.	ANTENNAS AND ASSOCIATED EQUIPMENT		
	3.0	Physical Dimensions........................	21
	3.1	Antennas-Radiated Power....................	22
IV.	RECEIVING EQUIPMENT		
	4.0	Commercial VHF and IF Receivers............	26
	4.1	Phaselock Detector.........................	28
		4.1.0 Basic Description of the Phaselock Detector..................	28
		4.1.1 The Low Pass Signal Filter..........	31
		4.1.2 Total System Transfer Function......	33
		4.1.3 Lock Range..........................	33
		4.1.4 Capture Range.......................	36
		4.1.5 Signal Bandwidth....................	37
		4.1.6 Noise Bandwidth.....................	39
		4.1.7 Other Phaselock Detector Properties.	39

...2

V. PHASELOCK DETECTOR COMPONENTS AND ASSOCIATED CIRCUITS
5.0 Block Diagram of the Entire Detector System.......................... 40
5.1 The Local Oscillator (VCO)................ 43
5.2 Phase Comparison Circuit.................. 47
5.3 Miscellaneous Circuits
5.3.1 Non-Linear Circuit to Correct VCO Gain Irregularities............. 49
5.3.2 Twin T Output Filters............... 49
5.3.3 Schmitt-Trigger..................... 49
5.4 System Circuit Diagram.................... 54

VI. PHASELOCK DETECTOR TESTS
6.0 General Discussion........................ 58
6.1 Phase Response Test....................... 59
6.2 Output Voltage-Frequency Response Test..... 63

VII. SYSTEM OPERATION TESTS
7.0 General Discussion........................ 68
7.1 Threshold Considerations
7.1.1 Theoretical Predictions............ 72
7.1.2 Experimental Threshold Observations
7.1.2.1 Measurements........... 77
7.1.2.2 Discussion of the Experimental Curves..... 86
7.2 Field Test Discussion
7.2.1 Field Test Preparation............. 91
7.2.2 Field Test Observations............ 92

VIII. CONCLUSIONS AND RECOMMENDATIONS
8.0 Conclusions............................... 98
8.1 Recommendations........................... 102

...3

LIST OF REFERENCES.. 104

APPENDIX A - ANTENNA CALCULATIONS.................................. 107

APPENDIX B - SIGNAL BANDWIDTH...................................... 109

APPENDIX C - NOISE BANDWIDTH....................................... 111

APPENDIX D - PHASE RESPONSE EQUATIONS.............................. 112

APPENDIX E - PHASE RESPONSE EQUATIONS (20 cps).................... 115

APPENDIX F - PHASE PEAKING RATIO................................... 116

APPENDIX G - OUTPUT VOLTAGE RESPONSE EQUATIONS..................... 117

APPENDIX H - THEORETICAL THRESHOLD PREDICTIONS..................... 121

APPENDIX I - GALACTIC NOISE TEMPERATURE AND NOISE FIGURE........... 123

APPENDIX J - NOISE VOLTAGE USED IN CALCULATIONS OF S/N............. 124

APPENDIX K - S/N RATIO BANDWIDTH CONVERSION........................ 125

LIST OF FIGURES

Title	Figure No.	Page
Actual Forward Scatter IF Recording	1.1	5
IF Recording Antenna Directions	1.2	9
Transmitter Frequency Stability Test	1.3	10
System Frequency Stability Test	1.4	11
Local Oscillator Frequency Stability Test	1.5	12
Block Diagram of the System Showing the Parts Which Affect the Frequency Stability	1.6	13
Modulator Varicap Response	2.1	16
Modulator Circuit	2.2	18
Transmission System Block Diagram	2.3	20
Yagi Antenna	3.1	23
Antenna Pattern	3.2	24
Locations of Sites on the Great Circle	3.3	25
Receiving System IF Frequency Response	4.1	27
Servo Diagram	4.2	29
Servo Diagram	4.3	29
Servo Diagram	4.4	30
Lead-Lag Network	4.5	32
Open Loop Gain Curves	4.6	35
Relation Between Lock and Capture Range; and Noise and Signal Bandwidth	4.7	38
System Block Diagram	5.1	41
V.C.O. Circuit	5.2	45
V.C.O. Voltage - Frequency Response	5.3	46
Phase Comparison Circuit	5.4	48
Non-Linear Circuit	5.5	50
Active Twin T Filter Frequency Response	5.6	51

...2

FM Caused by AM	5.7	53
System Circuit Diagram -- Input	5.8.1	55
System Circuit Diagram -- Filter	5.8.2	56
System Circuit Diagram -- Output	5.8.3	57
Phase Response Curve	6.1	60
Curve Showing Relationship Between Filter and Output Response	6.2	64
System Output Response	6.3	66
FM/AM Curves	7.1	70
Typical FM Threshold Curve	7.2	71
Predicted Threshold Curves	7.3	74
Equipment Used in Determining FM Thresholds	7.4	78
Threshold Region -- 5 cps Bandwidth --	7.5	80
Threshold Curve -- 10 cps Bandwidth --	7.6	81
Threshold Curve -- 20 cps Bandwidth --	7.7	82
Threshold Curve -- 40 cps Bandwidth --	7.8	83
Threshold Curve -- 100 cps Bandwidth --	7.9	84
Comparison of Experimental Thresholds	7.10	87
Possible Noise Spectrum	7.11	88
Calibration of IF Recording	7.12	93
Galactic and Receiver Noise	7.13	94
Modulation (.5 cps) Recording	7.14	95
Recording Showing Modulation Over Period of Time	7.15	96

...3

LIST OF TABLES

Title	Figure No.	Page
Phaselock Detector System Data	6.I	67
Experimental Threshold Data	7.II	97

I. INTRODUCTION

1.0 The Problem Defined

In the far northern scarcely populated areas of Canada, radio communication is commonly carried on by ionospheric propagation. Because of the great distances involved, this type of communication is often the only practicable system. However, signal propagation at high frequencies (below 30 Mc) is at times completely unreliable in the areas located in the auroral zone. [1] [2] [24] . Disturbances in the ionosphere, especially when associated with auroral storms, cause the radiated signal to be absorbed. [1]

There are ways in which this difficulty can be partially overcome. For example, the following systems can be used:

(1) -- A groundwave radio system using low frequencies, large antennas, high power transmitters, and occasional repeater stations when the large distances necessitate them.

(2) -- Tropospheric forward scatter at ultrahigh frequencies ranging from 300 Mc to 3,000 Mc and up. Scattering will take place at heights near 10 Km, below the ionosphere. [16] [17] . One such a system is presently in use between Fort Smith, North West Territories, and Uranium City, Saskatchewan.

(3) -- Normal point-to-point microwave communication.

(4) -- Ionospheric scattering at VHF.

The use of any one of the first three systems might be costly, especially when remotely controlled repeater stations have to be located at nearly inaccessible locations. The financial restrictions for much of the private as well as commercial communication are such as to prevent the use of the more expensive, reliable systems.

Some existing communication systems employ radio-teletype high power ionospheric forward scattering at VHF. The use of VHF frequencies (30 - 300 Mc) has proved to be more reliable than normal HF and more economical than tropospheric scattering or microwave. [1] [2]. However, the cost of high power VHF propagation systems is a limiting factor.

Therefore, it was decided to examine the feasibility of a low power, low cost VHF ionospheric forward scatter communication system, to complement existing systems.

The purpose of the research, described in this thesis, is to design and test such a system and to make recommendations regarding its feasibility.

1.1 Previous Work on VHF Ionospheric Forward Scatter

During the past decade, much research has been conducted in the field of VHF ionospheric propagation. Previously, amateur radio operators had noticed that during periods of ionospheric disturbances, and consequently absorption of normal HF energy, VHF communication was still possible.

Morgan [24] , explains how ionospheric propagation can take place between 30 and 300 Mc by means of at least five distinct methods. These are:

Regular F_2 layer ionization.

Sporadic E layer ionization.

Scattering from regular ionization.

Auroral ionization.

Meteoric ionization.

It is the third method, that of scattering from regular ionization, which is of interest at the moment. This mechanism of propagation has been investigated by Bailey [1] , Booker [25] [30] , and Forsyth [26] . Some of their more meaningful observations and conclusions are listed below:

(1) VHF forward scattering takes place from the bottom of the "E" layer and possibly the "D" layer, and is not affected by sudden ionospheric disturbances known as SID's.

(2) Some VHF scattered signal can be detected all the time, provided sufficient transmitter power is used.

(3) Periods of signal absorption in the HF range are often characterized by periods of signal enhancement in the VHF range.

(4) Some of the irregularities in propagation are caused by meteor trail ionization and by turbulent mixing of inhomogeneities in the "E" layer. (See the spikes in Figure 1.1.)

(5) Scattering takes place in a relatively small volume, explaining, therefore, the preference for directional antennas.

(6) The background noise level often decreases during periods of absorption, but otherwise remains constant except for diurnal variations. (See Figure 1.1. (5 pm))

(7) There is a relationship between ionospheric absorption, distance of communication and frequency. The intensity of the ionospheric forward scattered signal is found to depend on both distance and frequency. [1][17] .

Figure 1.1 shows that during a period of absorption the meteor spikes disappear and that the background noise level drops. Two conclusions can be drawn from this observation.

(1) -- Energy reaching the absorption layer from both the inside and the outside of the ionosphere is absorbed.

(2) -- The absorption layer must lie below the location of the ionized meteor trails.

It has been suggested that some form of communication by VHF forward scatter is possible using a low power transmitter. In order to attain signal to noise ratios which compare favourably with those from high power transmitters, certain sacrifices have to be made. Unless the gain of the antennas can be increased, the signal bandwidth will have to be made narrower. This will result in a reduction of the rate at which communication can take place.

If the received signal is discrete in frequency, then the signal bandwidth can be reduced to the extent that only the signal frequency and noise at that frequency are present. However, the signal is not discrete in frequency if modulation and Doppler frequency shifts exist.

Fig. 1.1 Actual Forward Scatter I.F. Signal Recording

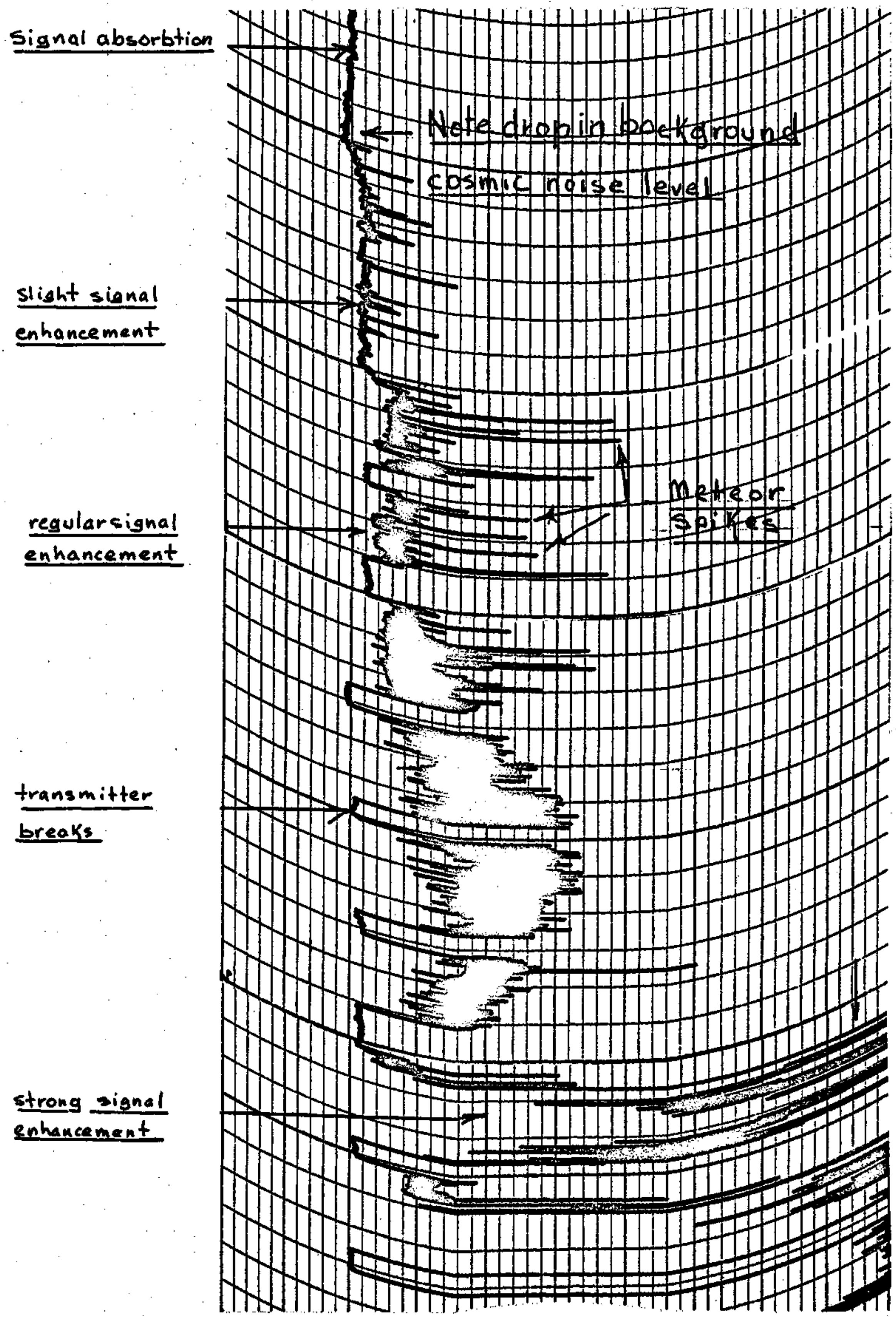

In 1961, Koehler [2] studied the signal spectral bandwidth caused by Doppler shifts. He concluded that this bandwidth was about 10 cps. This meant that narrowing the receiver bandwidth beyond 10 cps no longer increased the received signal to noise ratio.

Koehler used a transmission system similar to that shown in Figure 1.2, except that his 50 watt, 40 Mc transmitter was located at Fort Smith, North West Territories, instead of at Uranium City, Saskatchewan.

To achieve narrow bandwidth operation, Koehler used the phase-lock detector. This detector, to which a large portion of this thesis is devoted, allowed him to utilize transmitter frequency deviations up to 300 cps, while using signal bandwidths as low as 5 cps.

Koehler observed that his system operated during periods of signal absorption and concluded that communication would be possible, most of the time, in signal bandwidths near 10 cps. This communication would have to be at a rate determined by Shannon as:

$$C = B \log_2 (1 + S/N)$$

where C is the number of binary digits which can be transmitted with arbitrarily small frequency of error, B is the system signal bandwidth, and S/N is the received signal to noise ratio.

1.2 General Discussion of the Scope of This Thesis

Upon examination of Koehler's results, it was decided to test the existing receiver with a frequency modulated carrier. To carry out this task by modifying Koehler's circuit, proved to be nearly impossible. To explain some of the problems involved, a short discussion of the phase-lock detector is presented.

Basically the phaselock receiver system detects a difference in the phases of two signals. This phase difference is used to equalize the frequencies of the two signals, by correcting the frequency of one. The corrected frequency is usually associated with the signal from a voltage controlled oscillator and is said to track the frequency of a reference source. The system is referred to as being "locked" when the two signal frequencies have been equalized by the tracking method. The "lock range" is the maximum frequency range over which tracking can take place. Automatic locking results if the unlocked frequencies are close enough to be in the "capture range," which is either equal to or smaller than the lock range. The system includes a filter, which determines the receiver signal bandwidth and controls the difference between the lock and capture range.

The lock range used by Koehler was 300 cps. However, he stated that the system would not remain locked for any significant length of time, due mainly to frequency instability of both the transmitter and receiver components. Some of these instabilities are indicated in Figures 1.3 to 1.6, inclusive.

Subsequently, the local oscillator was placed in an oven, which substantially improved the frequency stability. However, there remained some drift at very small rates of change. (See Figure 1.5.)

Several parts of Koehler's receiver circuit could, by his own admission, be removed. Therefore, it was decided to rebuild the entire detector part of the receiving system. At the same time, the lock range was increased to 775 cps. Two reasons for increasing the lock range are:

(1) The total frequency drift of the system, even with all the pertinent oscillators placed in ovens, was almost 90 cps. This did not leave any frequency spectrum allocation for modulation frequency deviation and other incidental frequency shifts, unless the capture range was exceeded in certain bandwidths. Since automatic relocking was desirable, the choice of a fairly large lock range was necessary.

(2) With a wider lock range, the modulation index could be increased. It was assumed that in such a case, Doppler shifts would have less effect on the received signal to noise ratio. This made the choice of a larger lock range desirable.

Much of this thesis is devoted to the design of the system and to the testing of the receiver. Information on modulation frequency response, phase response, and threshold criteria has been obtained. The system was also field tested using a sinusoidally modulated transmitter at Uranium City, Saskatchewan, and receiver and output circuits located at Saskatoon, Saskatchewan. (See Figure 1.2.)

Numerous problems were encountered which limited the time during which the system could be operated and tested. For example; no radio frequency shielded room was available for threshold determination. Also, occasionally the transmitter would break down and since no experienced technical aid was available at the transmitter site, the transmitter would have to be packaged and sent air express to Saskatoon.

The field tests indicated that the communication system could be locked only occasionally. The results of the tests are fully analyzed in this thesis, and recommendations are made regarding improvements in this system, and regarding the use of other communication systems.

Fig. 1.2

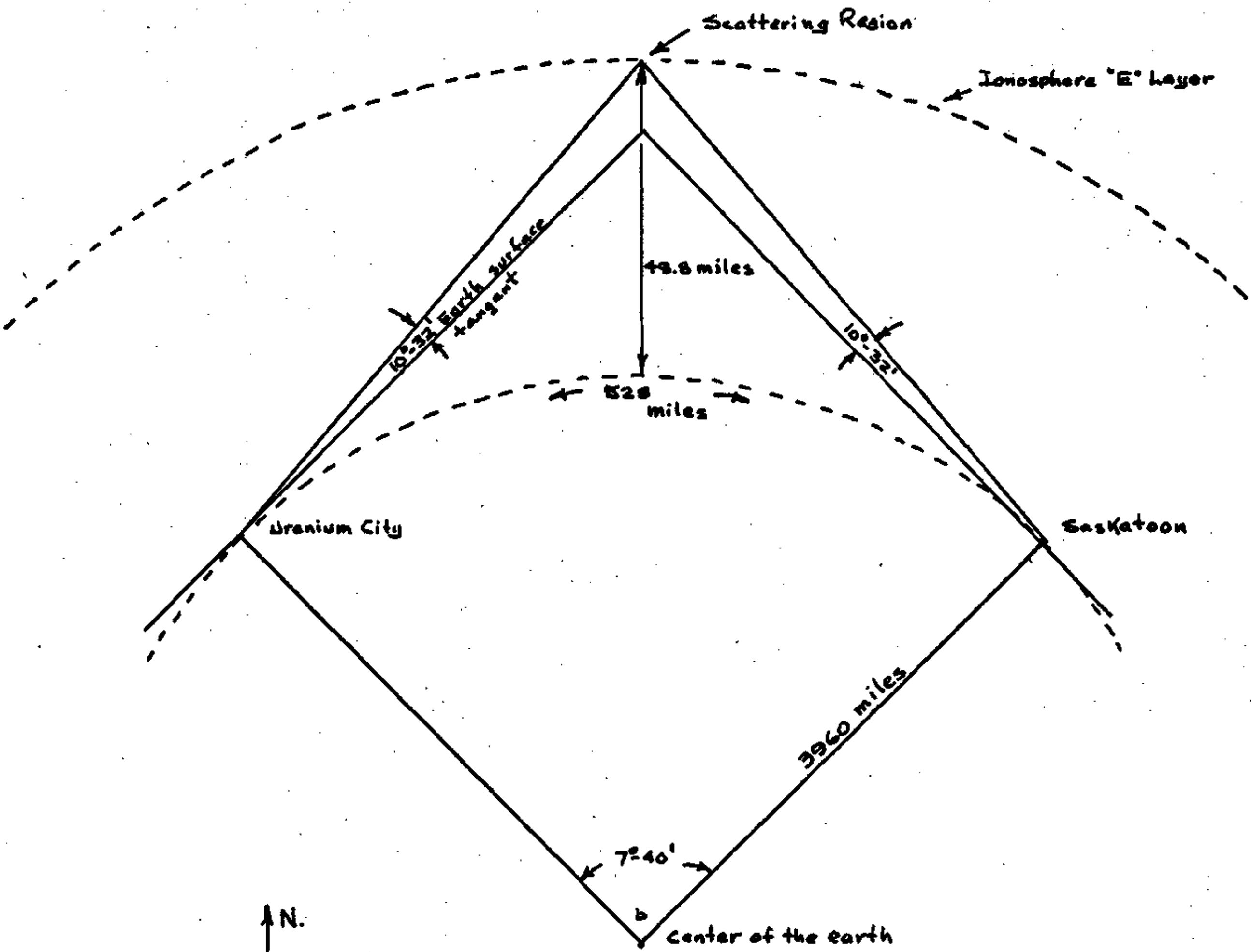

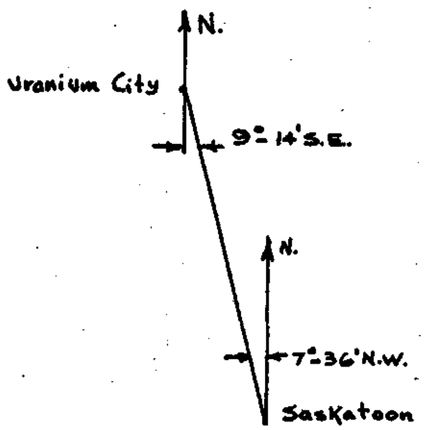

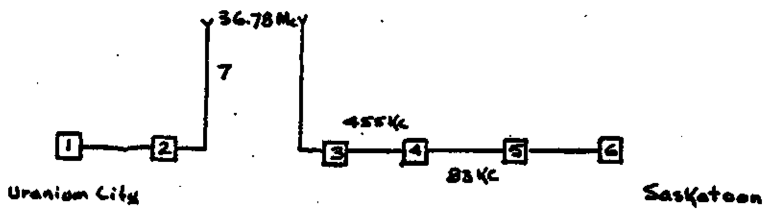

1 - Modulator
2 - Transmitter (50W.)
3 - Receiver
4 - I.F. Receiver
5 - Phase detector
6 - Output stage
7 - Antennae (Yagi)

ANTENNA DIRECTIONS

Fig. 1.3

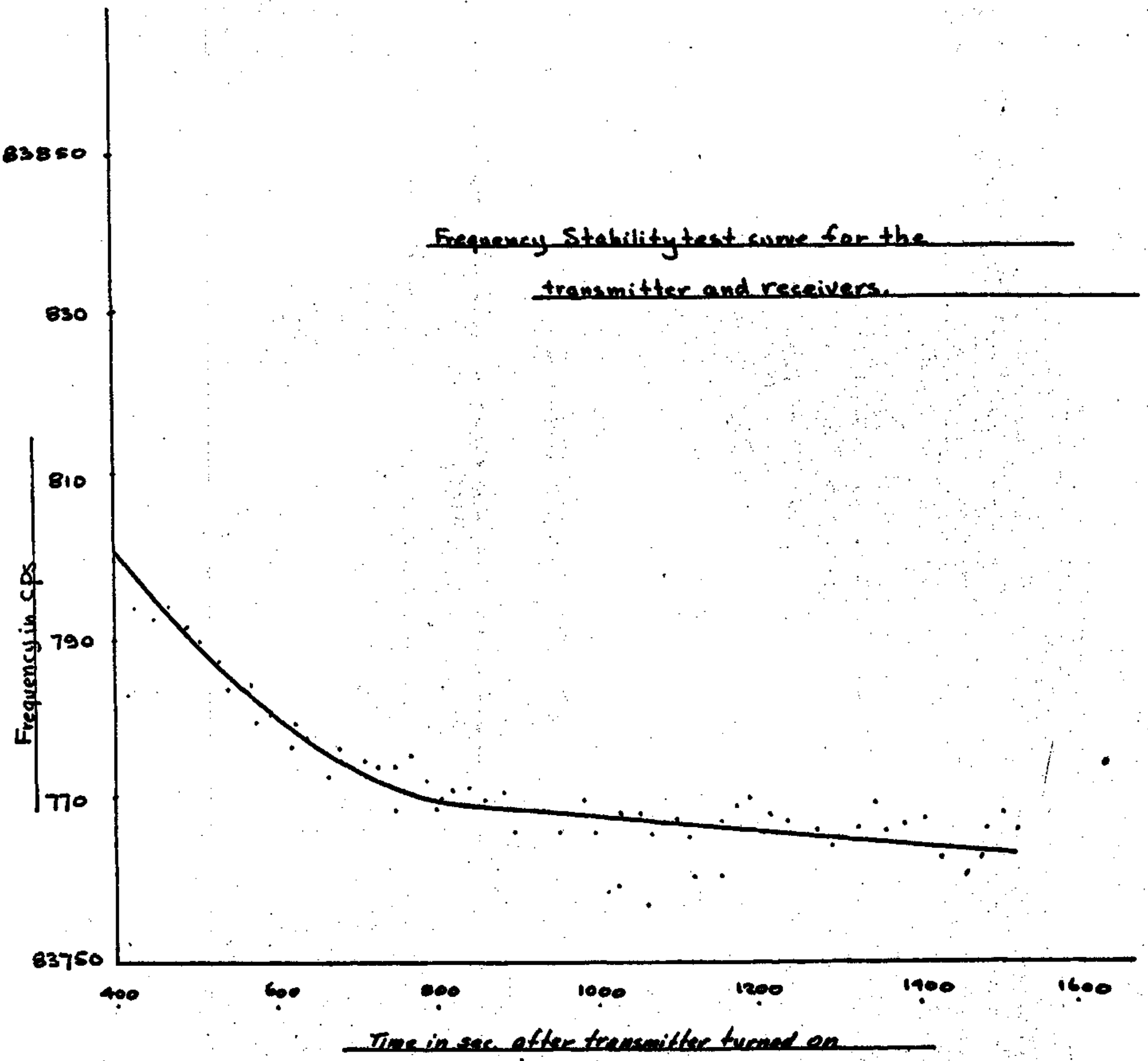
Frequency Stability test curve for the
transmitter and receivers.
83850
830
810
790
770
83750
Frequency in CPS
400
600
800
1000
1200
1400
1600
Time in sec. after transmitter turned on

Fig. 1.4 Chart showing the Frequency Stability of the Transmitter, receivers and voltage controlled oscillator. (Please refer to fig. 1.6)

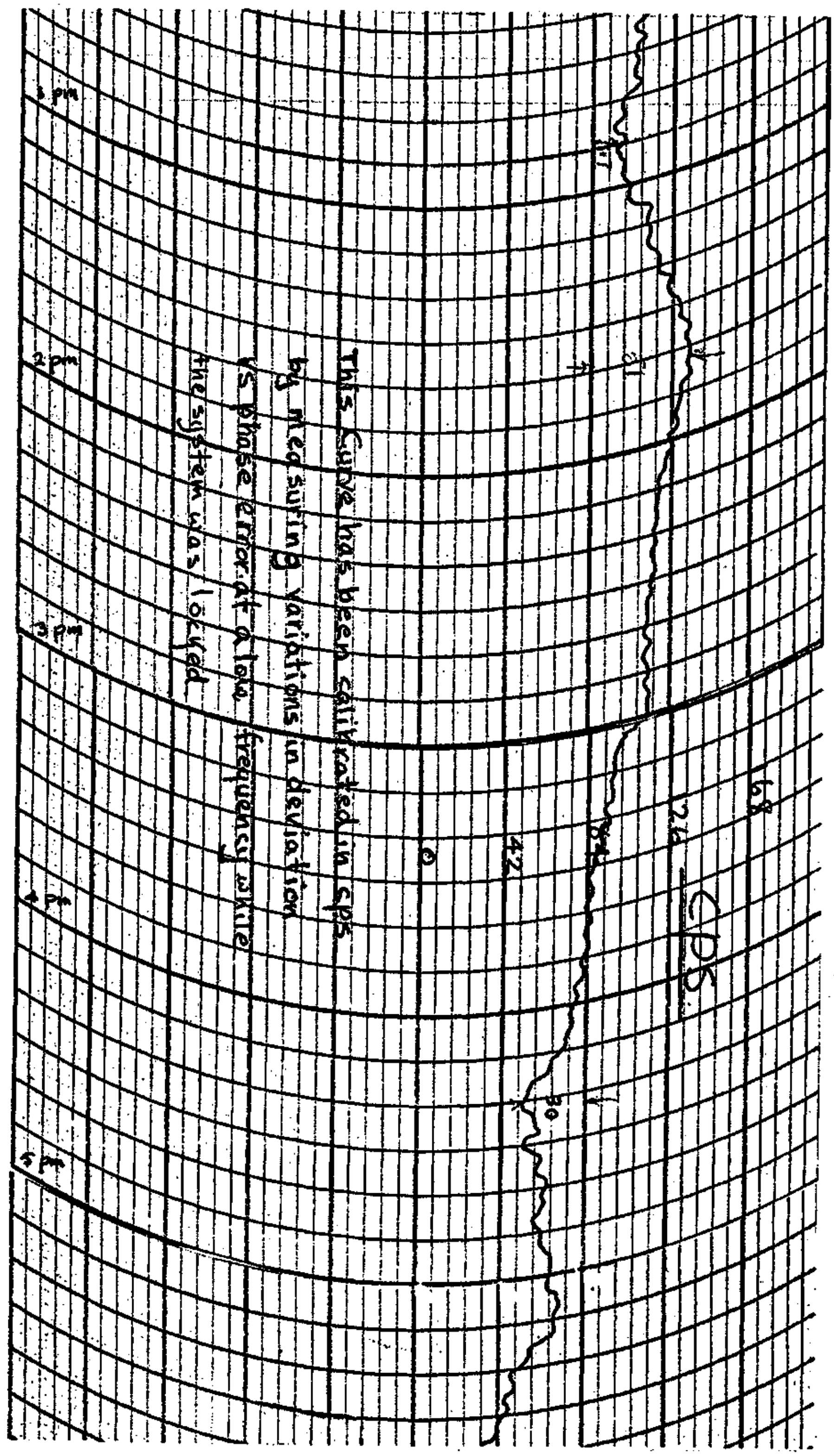

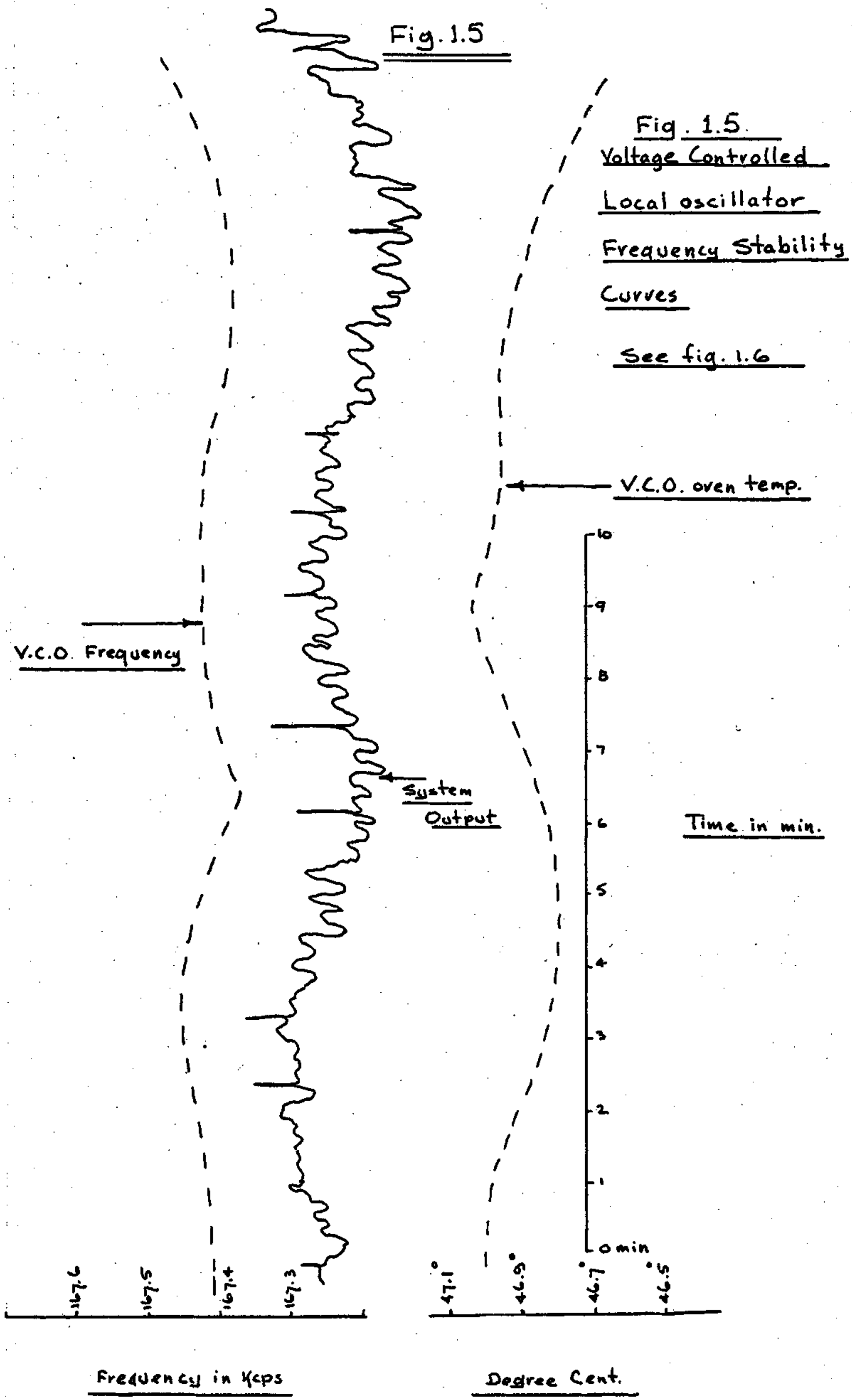
Fig. 1.5
Fig. 1.5.
Voltage Controlled
Local oscillator
Frequency Stability
Curves
See fig. 1.6
V.C.O. oven temp.
V.C.O. Frequency
System
Output
Time in min.
10
9
8
7
6
5
4
3
2
1
0 min
167.6
167.5
167.4
167.3
47.1°
46.9°
46.7°
46.5°
Frequency in Kcps
Degree Cent.

Fig. 1.6

Block Diagram Showing System components which affect Frequency Stability.

See fig. 1.3 for frequency stability.

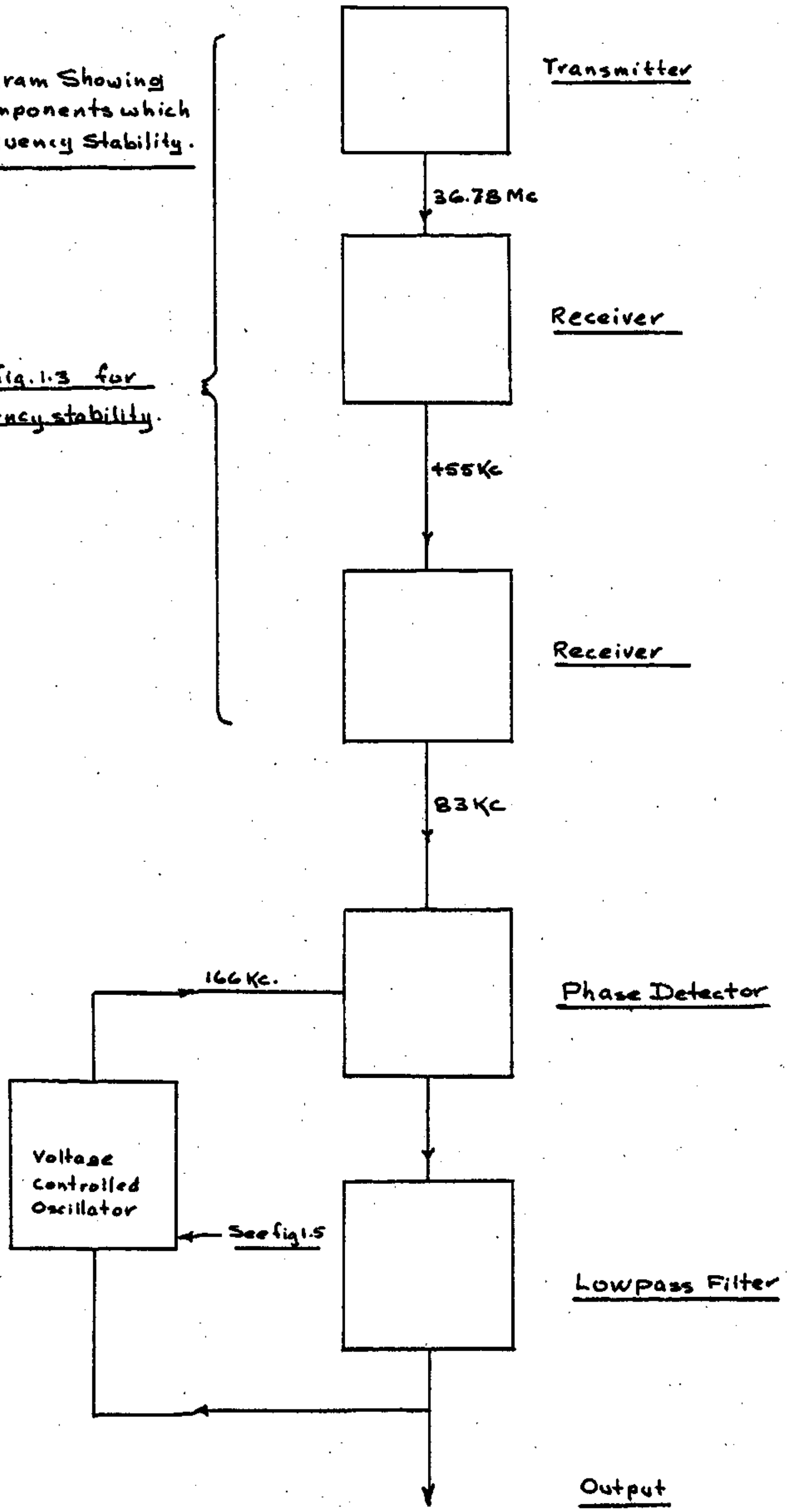

II. TRANSMITTING EQUIPMENT DESIGN AND ITS OPERATION

2.0 Transmitter

The transmitter, located at Uranium City, was a unit made by General Electric, 60 watt model 4ET23A1, 25-54 Mc, 50 ohms output impedance. The transmitter oscillator operated at a frequency of about 3 Mc, and three stages of frequency multiplication produced the final output frequency of 36.776 Mc. This frequency could be deviated approximately 2,500 cps manually by means of a variable capacitor located on the transmitter chassis.

The transmitter came equipped with a standard FM modulator, which proved to be unsuitable for use at low modulation frequencies and small frequency deviations. Since low modulation frequencies were desired, it was necessary to design an external modulator.

As shown in Figure 1.3, considerable incidental frequency drift occurred, caused by the transmitter or the receiver. After an initial warm-up period of 15 minutes, drifts of 20 to 30 cps were frequently present. Subsequently, the transmitter oscillator was placed in an oven capable of regulating the temperature within .5 degrees centigrade. This did not reduce the total drift significantly, although the frequency of the drifts was reduced to coincide with the on-off cycle of the oven.

2.1 Transmitter Modulator

To simplify the analysis of test results, sinusoidal modulation was preferred. However, square wave modulation could be used and its possibilities were examined as well. Several factors were considered in the design of the modulator; such as: size, weight, cost and ease of operation. The following paragraphs describe a few of the methods tested:

2.1.1 Modulation Method Number 1: Two capacitors, ranging in size between 3 and 10 pfs, were connected in parallel with the transmitter oscillator crystal. These capacitors were switched in and out, alternatively, by means of a variable speed relay. This method resulted in square wave modulation. However, many transients were present and only one frequency deviation could be obtained for each combination of two capacitors.

2.1.2 Modulation Method Number 2: A reactance tube modulator was used. Not only were the circuits associated with this modulator quite bulky, but the response indicated that the frequency range of this modulator did not extend to D.C. For these reasons, this modulator was discarded.

2.1.3 Modulation Method Number 3: This particular method was used in the final experiment. Its operation is based on the fact that a variable voltage applied across a variable capacity diode can be used to vary the frequency of the transmitter oscillator. The particular diode used was a Hughes 7001, silicon type, inserted in parallel with the transmitter oscillator crystal, to produce the voltage-frequency curve shown in Figure 2.1.

Fig. 2.1

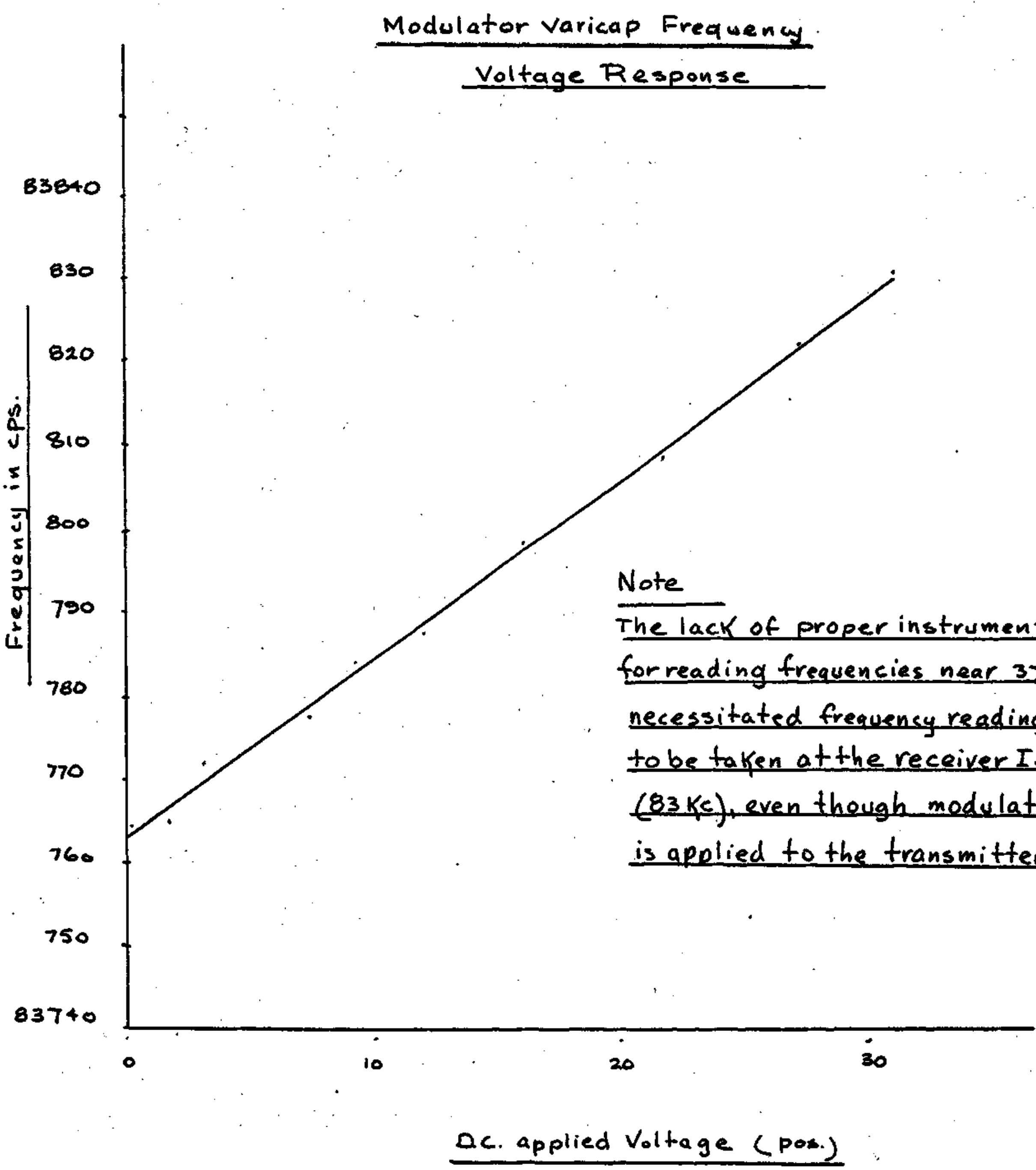
Modulator Varicap Frequency Voltage Response
Frequency in cps.
83840
830
820
810
800
790
780
770
760
750
83740
0
10
20
30
D.C. applied Voltage (pos.)
Note
The lack of proper instruments for reading frequencies near 37 Mc necessitated frequency readings to be taken at the receiver I.F. (83 Kc), even though modulation is applied to the transmitter.

The circuit used to produce the desired frequency variation is shown in Figure 2.2, within the circle labeled, "modulator." A sinusoidal voltage, superimposed on a 12 V dc supply, was applied across a 8.2 K ohm resistor. The 470 pf. capacitor served to eliminate any 3 Mc frequency feedback to the ac voltage generator. A 16 pf. capacitor was connected to couple the modulator to the transmitter oscillator circuit.

A variable frequency generator (.01 cps to 15 kc), with a variable sinusoidal voltage output, was used to drive the modulator. The transmitter modulation frequency and frequency deviation were controlled by the function generator frequency and output, respectively.

In order to simplify the operating procedure for the personnel in Uranium City, the function generator voltage output was set at maximum. A step attenuator was installed between the function generator and the modulator. (See Figure 2.2, "frequency deviation selector.") Thus, five discrete deviations could be obtained, merely by operating this switch.

A schedule, left with the D.N.R. radio operator at Uranium City, indicated the times at which a particular switch position and modulation frequency was to be used.

Fig. 2.2.

Modulation Circuit.

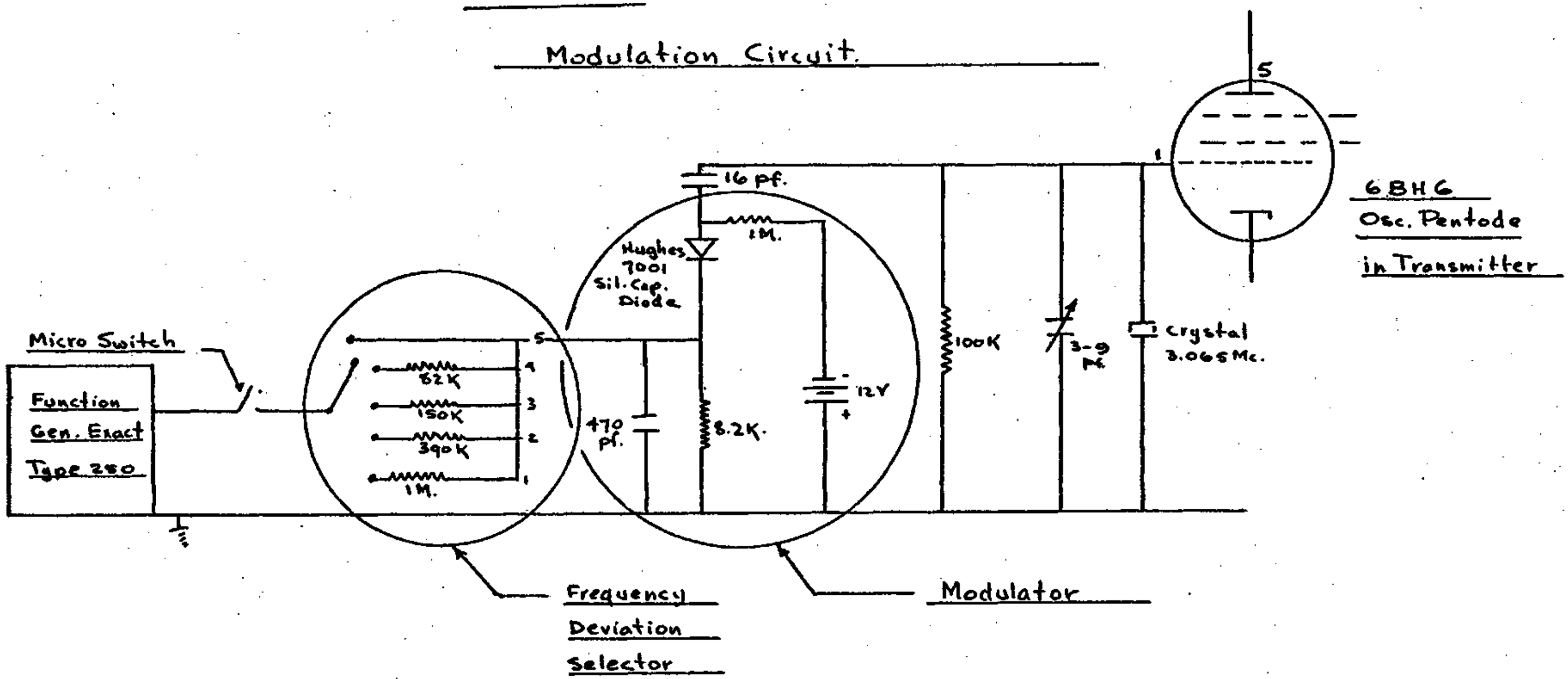

Dev. Selector Position	36.78 Mc. Carrier freq. Deviation
#1 pos.	3 cps
2	8
3	15
4	22
5	49

2.2 Transmitter Identification

In order to observe at the receiving end if the transmitter was operating, transmitter breaks were inserted. This was accomplished by means of a clock keying unit, consisting of a rotating disc (1 rph) and a micro switch which switched the transmitter to "stand-by" every 15 minutes. (Figure 2.2) The transmitter was switched on and off automatically during one of the "stand-by" periods, which positively identified the transmitter. During periods of signal enhancement, the transmitter breaks were clearly observed. (Figure 1.1)

To obtain a modulation break, a second micro switch was installed on the same clock keying unit. This made it possible to observe incidental frequency modulation noise and Doppler frequency shifts.

Fig. 2.3

Transmission System Block Diagram

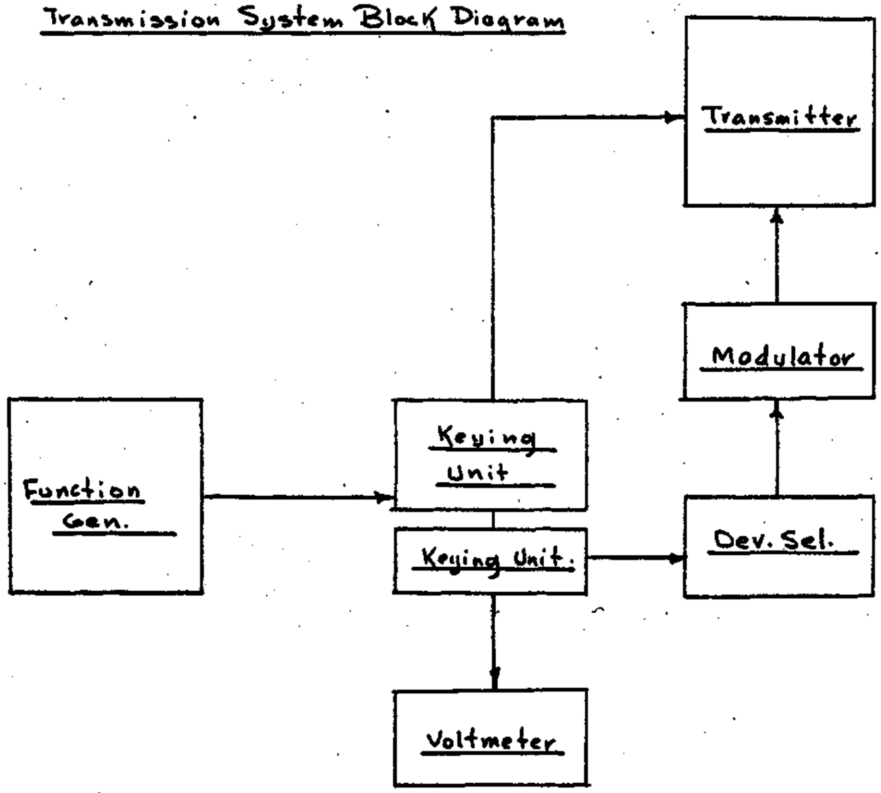

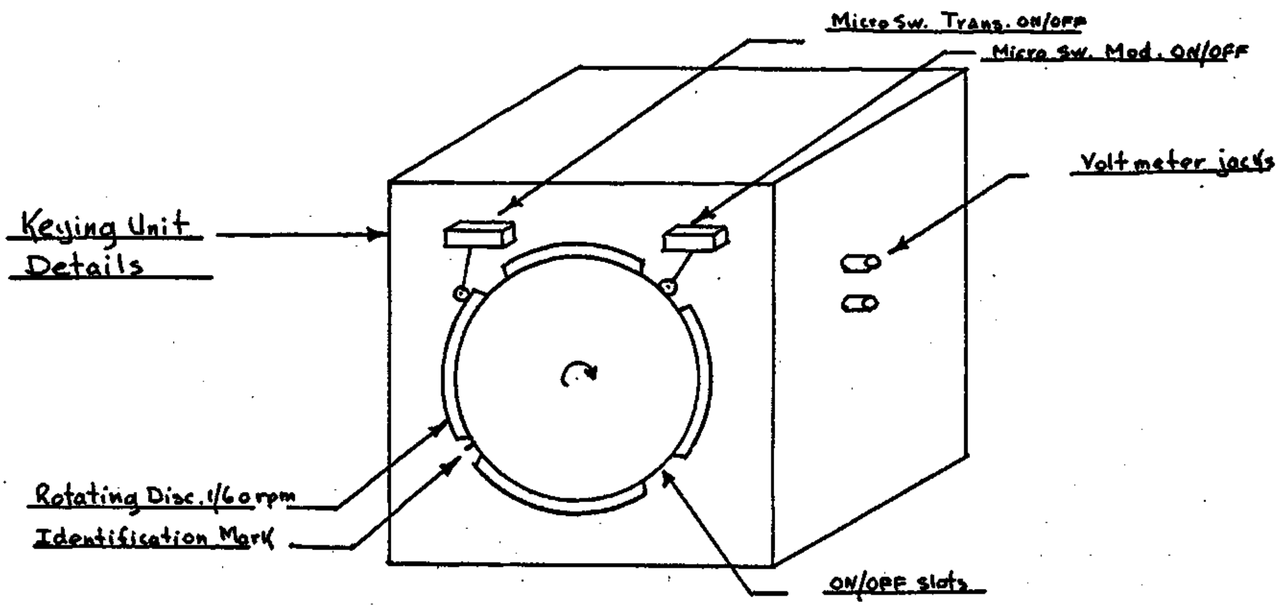

III. ANTENNAS AND ASSOCIATED EQUIPMENT

3.0 Physical Dimensions

Since relatively little carrier power was supplied by the transmitter, antennas with a reasonable gain (approximately 12 db) were used in this experiment. Gain, of course, is dependent on the price that one is prepared to pay; and since this design called for a low-power, low-cost system, elaborate equipment was not used.

Two Yagi type antennas were assembled. The structure and radiation pattern of these antennas are shown in Figures 3.1 and 3.2, respectively. It should be pointed out that Figure 3.2 shows the vertical radiation pattern of an isotropic source, 36.5 feet above ground, at a frequency of 36.78 Mc. It only approximates the vertical radiation pattern of the Yagi as the Yagi's pattern is quite broad in the vertical direction. Approximately 200 feet of coaxial 50 ohm cable was used at each end of the system. A balun impedance matching transformer, 17.91 feet in length, was installed to couple the coax. cable to the actual metal structure.

The antennas were mounted on aluminum columns at a height of 36.5 feet. This height was chosen so that the first maximum of the vertical radiation pattern illuminated the region of the ionosphere responsible for forward scatter propagation. (See Figures 3.2 and 1.2.) Since ionospheric scattering takes place at a height of 80 km (49.8 miles), [2] , the angle of elevation for the antennas was found to be $10^{\circ}\ 32'$. The antennas were subsequently mounted and properly directed at Uranium City and Saskatoon, respectively. (See Figures 1.2 and 3.3.) Calculations regarding antenna mounting are shown in Appendix A.

3.1 Antennas-Radiated Power

After one of the antennas was erected, a signal at 36.78 Mc was applied to it, in order to establish the radiated power level and to calculate the V.S.W. ratio on the coaxial cables. This level was recorded daily at the transmitter end, by the operator at Uranium City.

On the average, 50 watts of power was supplied to the system by the transmitter, and approximately 1.3 watts was returned, as measured by an M. C. Jones Micromatch power meter. Taking into account the 2.5 db loss in the coax. feeder cable, the power radiated into space was approximately 26.2 watts.

Fig. 3.1

Typical Yagi Antenna

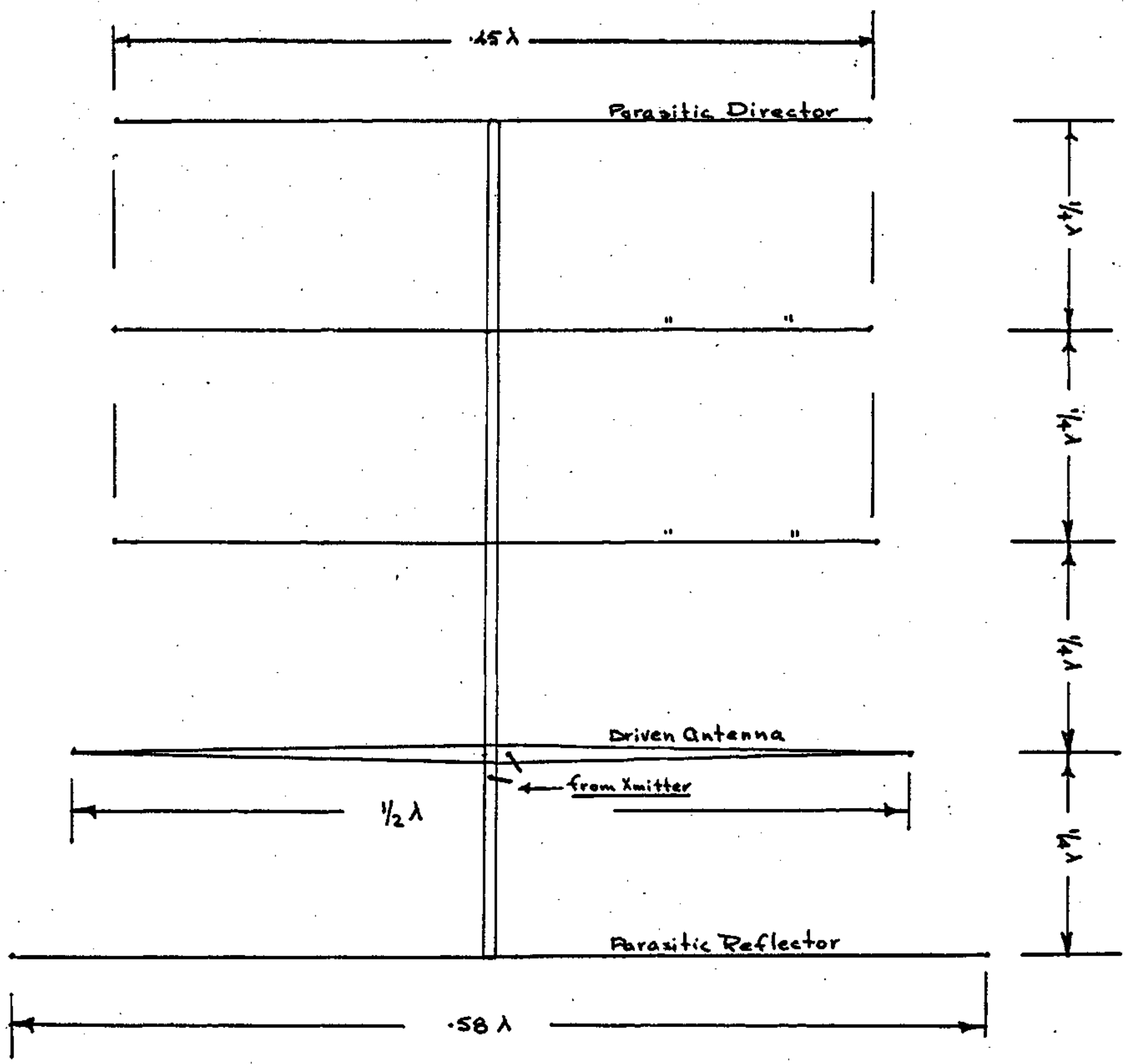

Fig. 3.2

Approximate Vertical Radiation Pattern of the Yagi antenna at 36.78 Mc. when h = 36.5 feet.

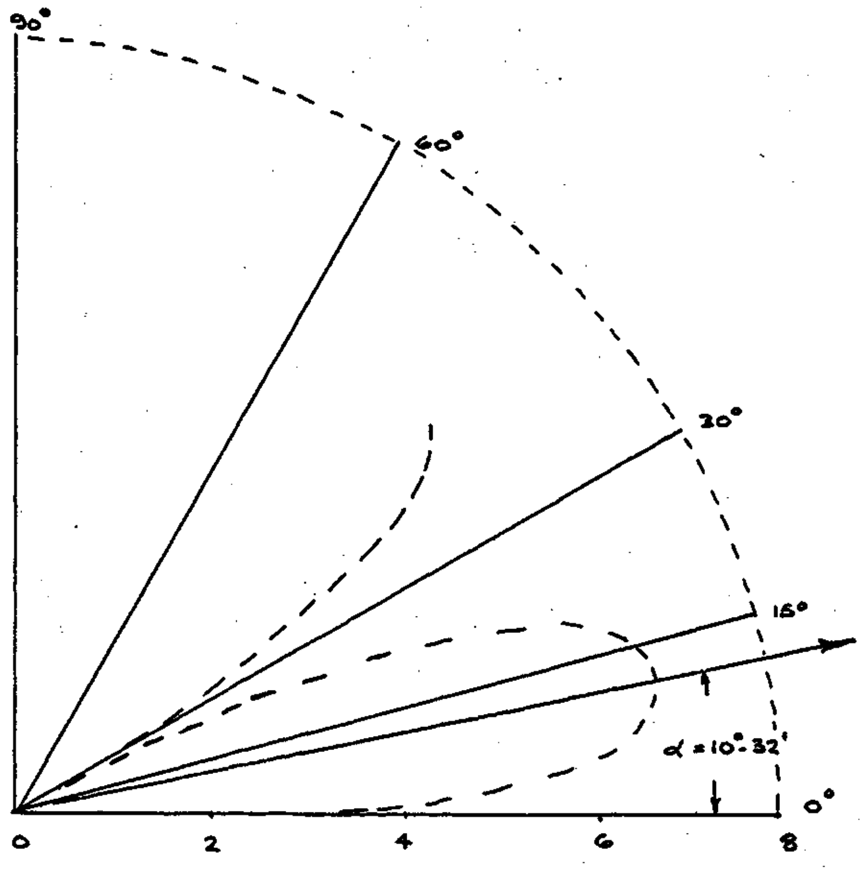

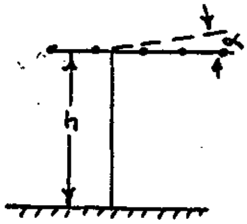

Fig. 3.3

Location of sites on the great circle

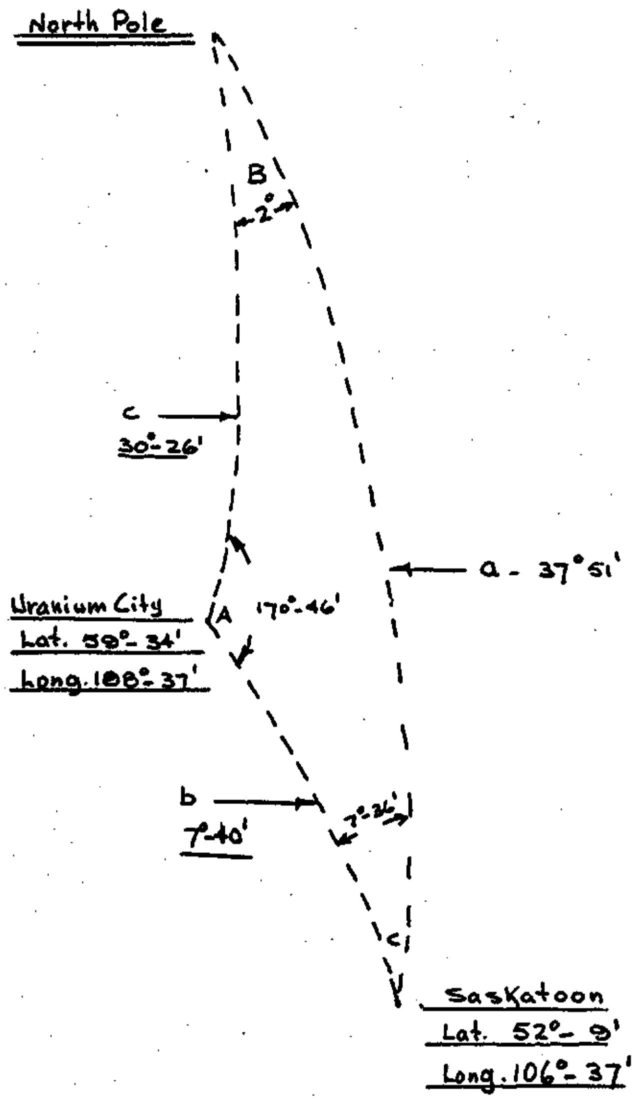

4. RECEIVING EQUIPMENT

4.3 Commercial VHF and IF Receivers

Two commercial receivers were used in the system, one of them being a Ferranti Packard Model No. 155 FM receiver tuned to a frequency of 36.77[illegible] Mc. This receiver had a signal bandwidth of 2.3 kc and its IF frequency was 455 kc. (See Figure 1.6.)

The best possible noise figure of the receiver that could be obtained was 7 db. Since the receiver had a recorder output stage, the IF signal and noise amplitudes were recorded, as shown in Figure 1.1.

The IF signal from the Ferranti Packard receiver was fed into a BC 453 receiver, which was modified to produce an output at 83.[illegible] kc.

The frequency response curve for this section of the receiving system is shown in Figure 4.1.

The Ferranti receiver was modified slightly by inserting one of the oscillator crystals in a constant temperature oven.

Fig. 4.1

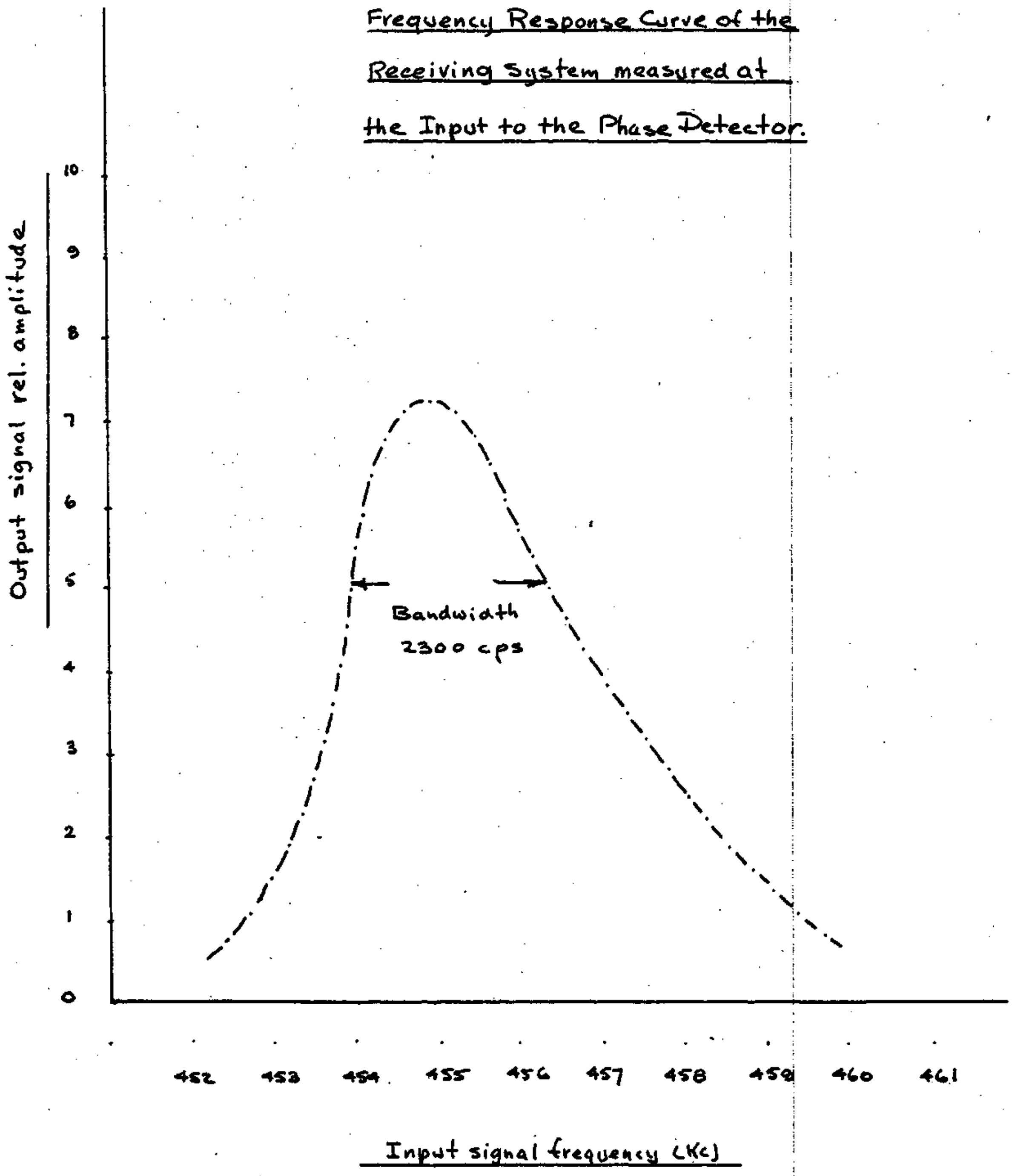
Frequency Response Curve of the
Receiving System measured at
the Input to the Phase Detector.
Output signal rel. amplitude
0
1
2
3
4
5
6
7
8
9
10
Bandwidth
2300 cps
452
453
454
455
456
457
458
459
460
461
Input signal frequency (Kc)

4.1 Phaselock Detector

4.1.0 Basic Description of the Phaselock Detector: The phase-lock detector provides a communication system with two advantages:

(1) The carrier frequency drift is allowed to be larger than the signal bandwidth. [2], [4].

(2) The threshold can be improved several db over "conventional" FM systems. [5] [15] [18].

As stated previously, a phaselock detector is a device detecting the difference in the phases of two discrete signal frequencies. Usually the two frequencies are associated with a voltage controlled local oscillator and a reference carrier, respectively.

If a difference in the two frequencies exists, this difference is integrated. The result of the integration is used to regulate the dc bias of the voltage controlled oscillator, so that the VCO frequency will "track" the frequency of the reference carrier.

Some common methods of representing the phaselock detector used in this experiment are shown in Figures 4.2, 4.3, and 4.4. Referring to Figure 4.2, let ω_{m1} represent the change in the carrier frequency from the IF stage of the conventional receivers, and let ω_{m2} represent the (resulting) change in the frequency of the VCO. Consequently, $\Delta\omega_m$ represents the difference between ω_{m1} and ω_{m2}. This difference, when integrated, produces $\Delta\phi_m$, a difference in the phases of ω_{m1} and ω_{m2}.

The gain of the phase detector in volts/radian, and the gain of the VCO (or local oscillator) in rad./sec./volt are represented by K_1 and K_2, respectively. $F(s)$ represents the low pass filter transfer function.

It should be noted that when the VCO is tracking the carrier frequency from the IF receivers (referred to henceforth as the IF frequency), the

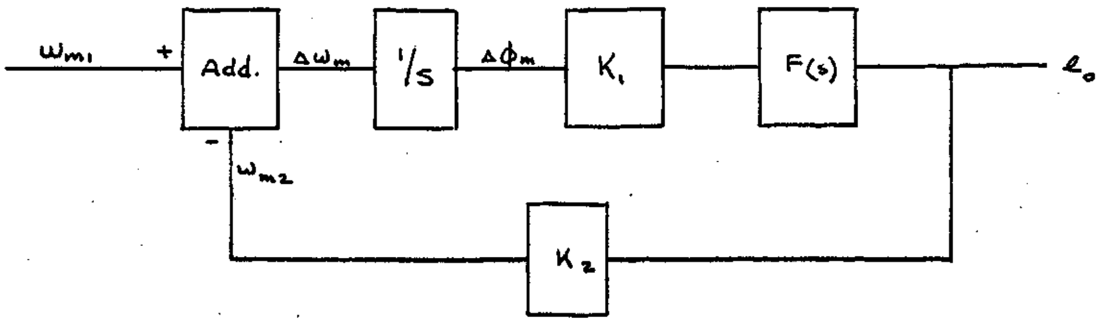

Fig. 4.2

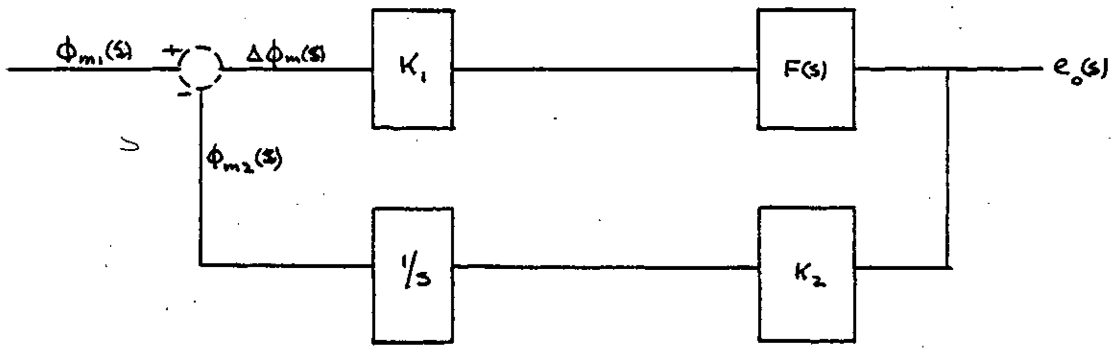

Fig. 4.3

SERVO DIAGRAMS

ω_m - Modulation Frequency

ϕ_m - Modulation Phase

K_1 - Gain of the Phase Detector in Volts/Radian

K_2 - Gain of the Local Oscillator (V.C.O.) in rad./sec./volt

1/S - Integrator

F(s) - Transfer Function of the Narrowband Filter

Fig. 4.4

Alternate Servo Diagram

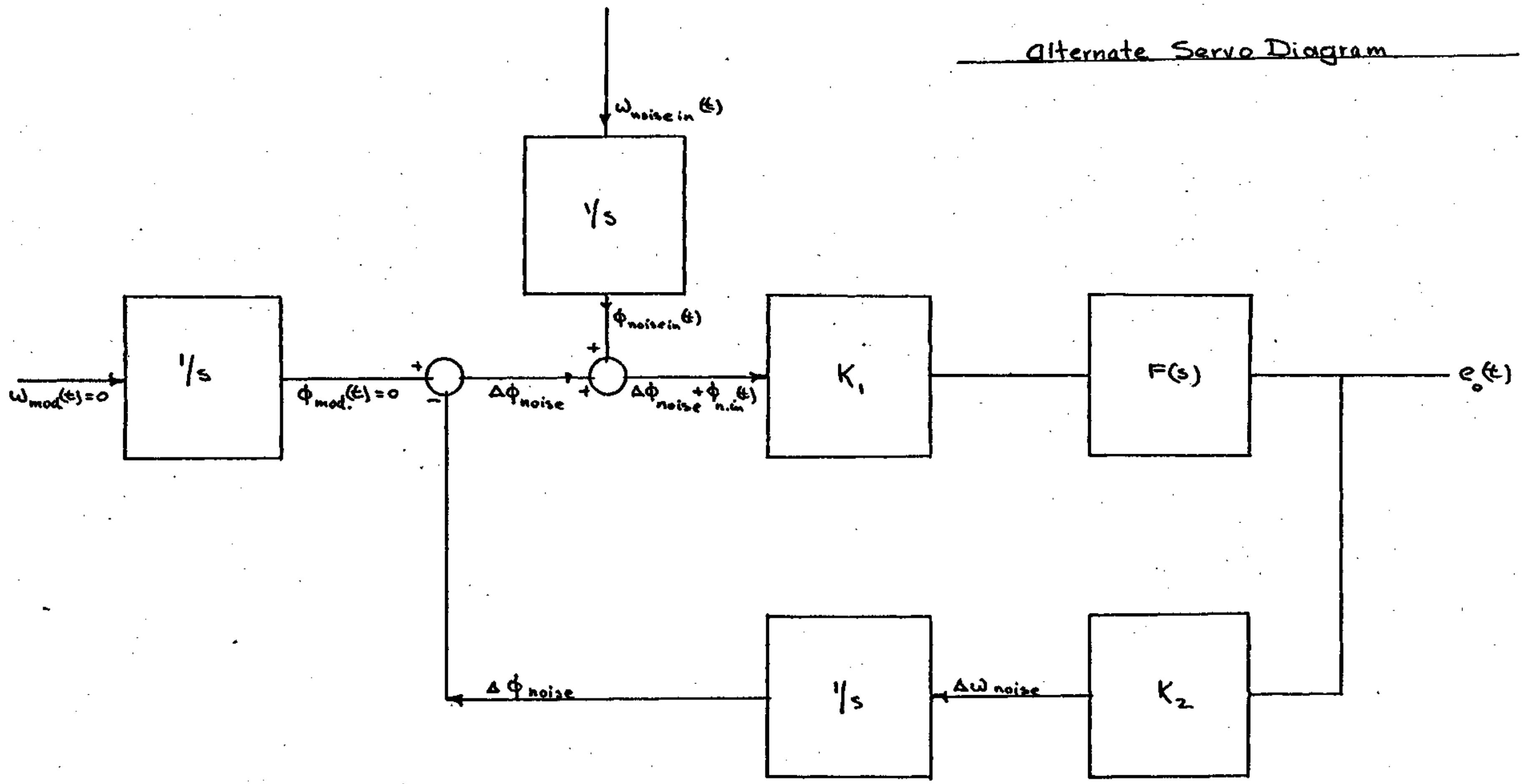

system is said to be "locked," and ω_{m1} and ω_{m2} are equal except for their instantaneous phases.

The adder and integrator units can be shown as separate identities in the servo model. However, they cannot be separated in the actual circuit, since one gating circuit functions as both an adder and integrator.

Several functions and properties of the phaselock detector are discussed next.

4.1.1 The Low Pass Signal Filter: A lead-lag network, as shown in Figure 4.5, was used to provide the phaselock detector with the proper signal bandwidth. McAleer [4] and Gruen [32] have reported this type of filter to be optimum with respect to noise bandwidth and capture range.

The following terms are associated with this type of lead-lag filter:

(1) lag break time constant - $t_1 = (R_1 + R_2)C$

(2) lead break time constant - $t_2 = R_2C$

(3) transfer function $F(s) = \dfrac{1 + t_2s}{1 + t_1s}$

The cut-off frequency for this filter was adjustable to 5 cps, 10 cps, 20 cps, 40 cps, and 100 cps. The filter could be bypassed entirely.

Calculations for R_1, R_2, and C to provide the proper signal bandwidths are shown in Appendix B.

There are disadvantages associated with the lead-lag filter. For example the phase change $\Delta \phi_m$ does not vary linearly with changes in the modulation frequency ω_m. Also at high frequencies the attenuation of this filter approaches R_1/R_2, as compared with a 6 db octave attenuation for a simple RC filter.

Fig. 4.5

A lead-lag network

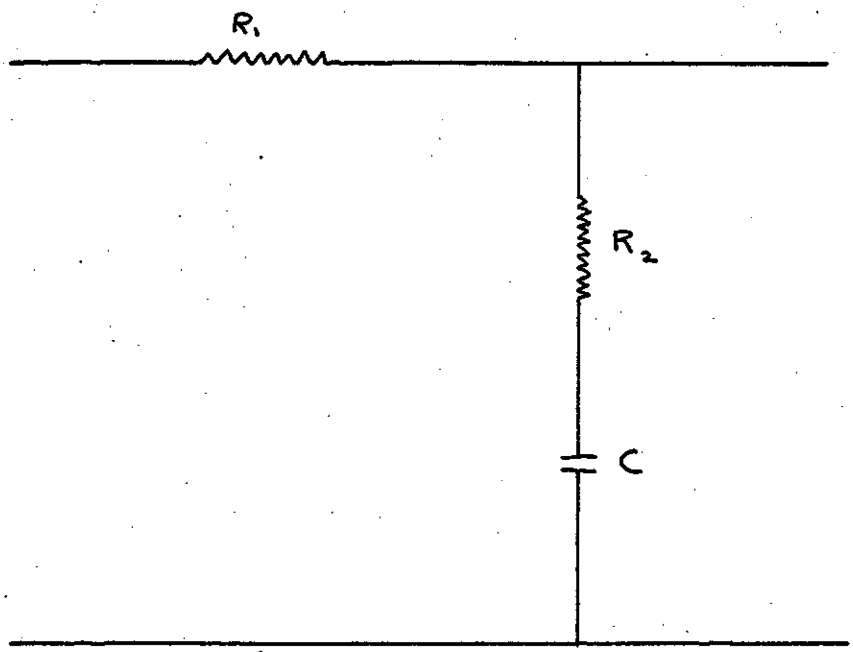

4.1.2 Total System Transfer Function: The system transfer function is defined as the output over the input. With reference to Figure 4.2, the servo input is ω_{m1} (or $\omega_{m1}(s)$) and the servo output is ω_{m2} (or $\omega_{m2}(s)$). Since

(1) $\omega_{m2}(s) = \Delta\omega_m(1/s)(K_1)(K_2)\left(\frac{1 + t_2 s}{1 + t_1 s}\right)$

(2) $\Delta\omega_m(s) = \omega_{m1}(s) - \omega_{m2}(s)$

the system transfer function becomes; [4]

$$\omega_{m2}(s)/\omega_{m1}(s) = K(1 + t_2 s)\Big/t_1\left\{ s^2 + s\left(\frac{1}{t_1} + \frac{Kt_2}{t_1}\right) + \frac{K}{t_1} \right\} \qquad 4.3$$

where $K = (K_1)(K_2)$

If the natural resonant frequency is represented by $\omega_n = (K/t_1)^{\frac{1}{2}}$ and the damping ratio by γ, where $\gamma = (1 + Kt_2)/2\omega_n t_1$, see [4], then equation 4.3 can be rewritten as:

system transfer function $= H(s) = \omega_{m2}(s)/\omega_{m1}(s)$

$$= \omega_n^2(1 + t_2 s)/(s^2 + 2\gamma\omega_n s + \omega_n^2)$$

As pointed out by McAleer in [4], the value of the damping factor γ ranges from a value of 0.7 at $\omega_c = K$ to 0.5 for $\omega_c \lll K$ where ω_c represents the signal bandwidth cut-off frequency.

4.1.3 The Lock Range: The lock range of the APC (automatic phase control) system can be defined as the maximum range over which the VCO frequency will "track" the output reference (or IF) frequency from the conventional receivers. In other words, it can be defined as the total drift in unlocked output frequency which can be compensated by the system. [4] In this particular experiment, once the system was locked ($\omega_{m1} = \omega_{m2}$) it would remain locked until the unlocked frequency difference between the two inputs produced a phase difference, $\Delta\Phi_m$, which exceeded π radians or was less than 0 radians. If the two input unlocked frequencies were exactly the same and the servo loop was then closed, the phase difference $\Delta \phi_m$ was equal to $\pi/2$ radians.

In reference to Figure 4.2, K_1 is the gain of the phase detector in volts/radian. K_2 is the gain of the reactance modulator-oscillator combination in radians/second/volt. In this experiment, the phase changed linearly with frequency deviation over the entire (phase) lock range of π radians, when observed at a constant modulation frequency. A maximum change in the IF frequency produced π radians change in phase, which resulted in πK_1 volts change in the output of the phase detector. Consequently, the frequency of the VCO was changed by $\pi K_1 K_2$ radians/second.

Therefore, the (frequency) lock range was equal to $\pi K_1 K_2 = \pi K$ radians/second (or K/2 cps).

After examining the total incidental drifts of the IF and VCO frequencies and with some knowledge of Doppler frequency shifts, the following values of K_1 and K_2 were chosen.

$K_1 = 2.65 \text{ volts} / \pi \text{ radians} = .84 \text{ volts/rad.}$

$K_2 = 1{,}840 \text{ rad./sec./volt}$

$K = .84 \times 1{,}840 = 1{,}550 \text{ rad./sec.}$

This produced a lock range (πK rad/sec.) of $1{,}550\,\pi$ rad./sec. which is equivalent to 775 cps.

The open loop gain response for the system phase detector loop curve is plotted in Figure 4.6. With the system filter bypassed, the curve crosses the zero axis at K, at a slope of 6 db/octave. Due to the insertion of an additional RC filter, the slope changes to 12 db/octave near 3 kc. The crossover frequency is referred to as ω_n, the natural resonant frequency.

Fig. 4.6

Open loop gain response curve

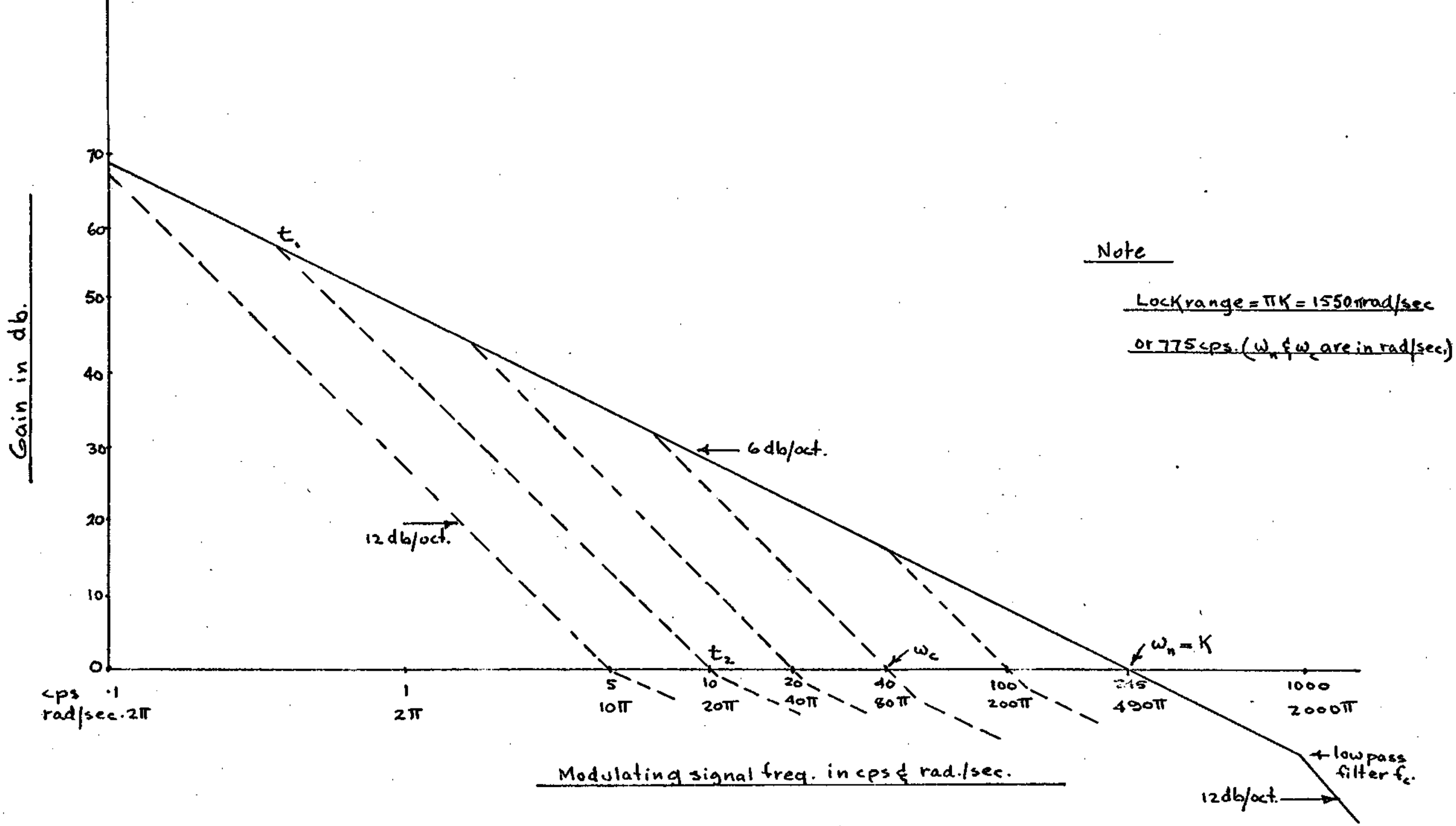

Had no system filter been used, then a reduction in signal bandwidth would have necessitated a reduction in the system gain (K). The solid curve in Figure 4.6 would have been shifted to the left, and the lock range would have been reduced.

By using the lead-lag filter, the slope of the curve could be changed to 12 db/octave, with a new crossover frequency of ω_c, without necessitating a reduction in the lock range. Values for ω_c corresponded to signal bandwidths of 5, 10, 20, 40, and 100 cps, respectively, while the lock range remained at π K radians/second. (775 cps.)

Many phaselock detectors have been designed in which the phase does not change linearly with frequency deviations [6], [7], [8], [9], [10], [11]. Most of the work on non-linear phase detectors has been reported in the last two years.

4.1.4 Capture Range: The capture range of the phaselock detector is defined as the largest unlocked frequency difference, between the local oscillator and the transmitter, at which the system will lock in.

If the unlocked frequency of either the local oscillator or the transmitter drifts to the extent that the difference in unlocked frequencies is larger than the capture range, then if the system was originally locked, it will not necessarily unlock. However, if it does unlock for one reason or another, the system will not lock again automatically until either one of the frequencies is adjusted to where the difference is again within the capture range. This means that the total frequency deviation, including allowances for incidental drifts, can be made equal to the lock range. However, it is better to keep this deviation smaller than the capture range, so that if unlocking occurs, automatic relocking will take place. In this experiment the deviation was at all times smaller than the capture range.

The capture range, unlike the lock range, varies with the signal bandwidth in the following manner, [4] :

$$\text{Capture range} \approx \text{Lock range} \times (\omega_c/K)^{\frac{1}{2}} \tag{4.5}$$

where; (1) lock range = π K rad./sec.

(2) ω_c = signal bandwidth in rad./sec.

(3) K = system gain = K_1K_2

Note: For a simple RC filter, [4] :

$$\text{Capture range} \approx \text{Lock range} \times \omega_c/K \tag{4.6}$$

Comparison of equations (4.5) and (4.6) indicates that the capture range for the lead-lag filter changes less rapidly with signal bandwidth than is the case for the simple RC filter. This definitely is an advantage.

The calculated values of lock range and capture range are shown in Figure 4.7. Both the lock and capture ranges were determined experimentally, and very close correlation was observed between theoretical and experimental values.

<u>4.1.5 Signal Bandwidth:</u> Since Koehler [2] stated that the carrier frequency spectral spread was approximately 10 cps, the signal bandwidth values were chosen to be in that vicinity. To verify Koehler's results, a 5 cps bandwidth was also used. Other bandwidths were 10 cps, 20 cps, 40 cps, and 100 cps.

The calculations regarding bandwidth and their dependence on R_1, R_2, and C (See Figure 4.5) are shown in Appendix B.

The value for R_1 was calculated to be 43 K ohms and was held constant for all signal bandwidths. The magnitudes of C and R_2 were changed to produce the required bandwidths.

Fig. 4.7

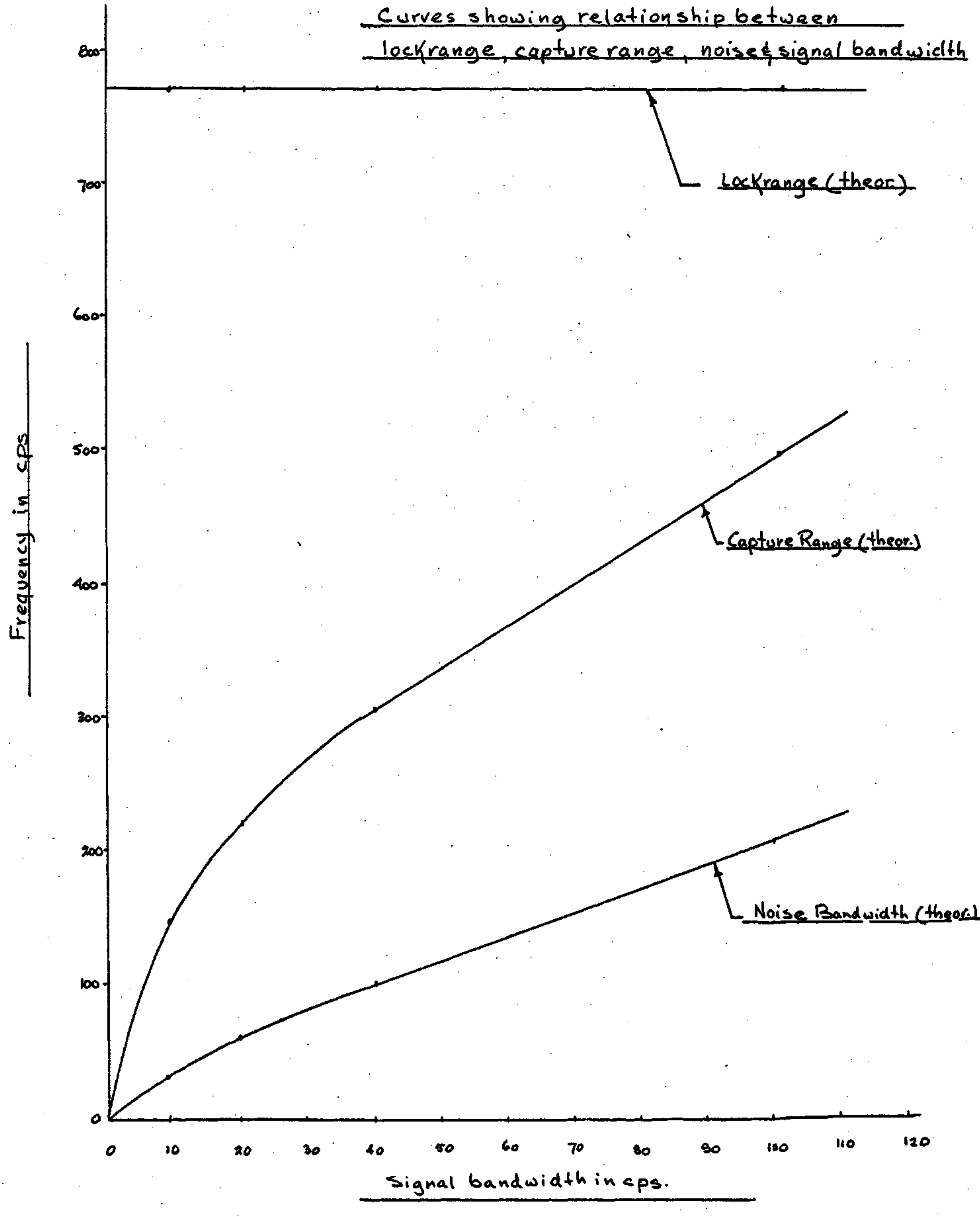
Curves showing relationship between lockrange, capture range, noise & signal bandwidth
800
700
600
500
400
300
200
100
0
Frequency in cps
Lockrange (theor.)
Capture Range (theor.)
Noise Bandwidth (theor.)
0 10 20 30 40 50 60 70 80 90 100 110 120
Signal bandwidth in cps.

4.1.6 Noise Bandwidth: The phaselock system reacts differently to random noise than it does to a discrete modulation frequency. In general, the system is often considered to be an open loop as far as the noise is concerned, and the phase perturbation of the output frequency from the local oscillator is considered to be the important factor, [11] . (See Figure 4.4.) The noise bandwidth can be expressed to be [4] , (see Appendix C):

$$B_n = \int_0^{\infty} \left| H(j\omega) \right|^2 d\omega \tag{4.7}$$

$H(j\omega)$ is the system transfer function as defined in equation (4.5). Consequently, substitution of equation (4.5) in (4.7) yields:

$$B_n = \pi\omega_n/4\zeta \left\{ 1 + (2\zeta - \omega_n/K)^2 \right\} \text{ rad./sec.} \tag{4.8}$$

Equation (4.8) can be calculated in terms of α , the network ratio, to give: (See Appendix B).

$$B_n = \frac{\pi K}{2}(\alpha^2 + Kt_1)/(\alpha^2 + \alpha K t_1) \text{ rad./sec.} \tag{4.9}$$

The noise bandwidth as expressed in equation (4.9) was plotted in Figure 4.7, converted to cps. Note, that when $Kt_1 \rightarrow 0$ then $B_n \rightarrow \frac{\pi K}{2}$, which represents half the lock range. On the other hand, for very small signal bandwidths, $B_n \rightarrow \omega_c$ or π x signal bandwidth.

4.1.7 Other Phaselock Detector Properties: In order to provide a continuity of description in this thesis, two other properties of the phaselock detector are described in Chapter VI. They are the phase-frequency response, and the output voltage frequency response. Both these properties necessitated extensive theoretical and experimental work. Consequently, an entire chapter has been devoted to them.

V. PHASELOCK DETECTOR COMPONENTS AND ASSOCIATED CIRCUITS

5.0 Block Diagram of the Entire Detector System

Since the entire detector system consisted of many components, it was considered advantageous to show the relationship between the various sections and to indicate their various functions. Therefore, a block diagram is shown in Figure 5.1.

Following through on the signal from the receiver, it should be noted that a clipping circuit was used. The function of the clipping was to remove almost all the amplitude modulation from the frequency modulated signal. Since clipping reduced the carrier voltage to a maximum of .6 volts peak to peak, amplification was necessary. After amplification the signal was not suitable to properly trigger a multivibrator circuit, as explained in section (5.3.3) and a Schmitt triggering circuit was used to correct this. Its output triggered a monostable multivibrator which produced a rectangular pulse of approximately 6 usec. duration.

The output from the local oscillator was not clipped, since no amplitude variations were present. Its sinusoidal output was converted to a rectangular output by means of a Schmitt triggering circuit and a bistable multivibrator. This multivibrator reduced the oscillator frequency from approximately 166 kc to 83 kc while its output was a rectangular wave of again approximately 6 usec. length.

The two rectangular waves were next guided through a gating circuit which passed one of the waves, depending on the presence or absence of the other. Next in line was a 3 kc low pass filter. It was found that instability occurred if this filter was eliminated or even if the cut-off frequency of this filter was made too high. By making the cut-off frequency 3 kc, the operation of the lead-lag network was not seriously affected.

Fig. 5.1

System Block Diagram

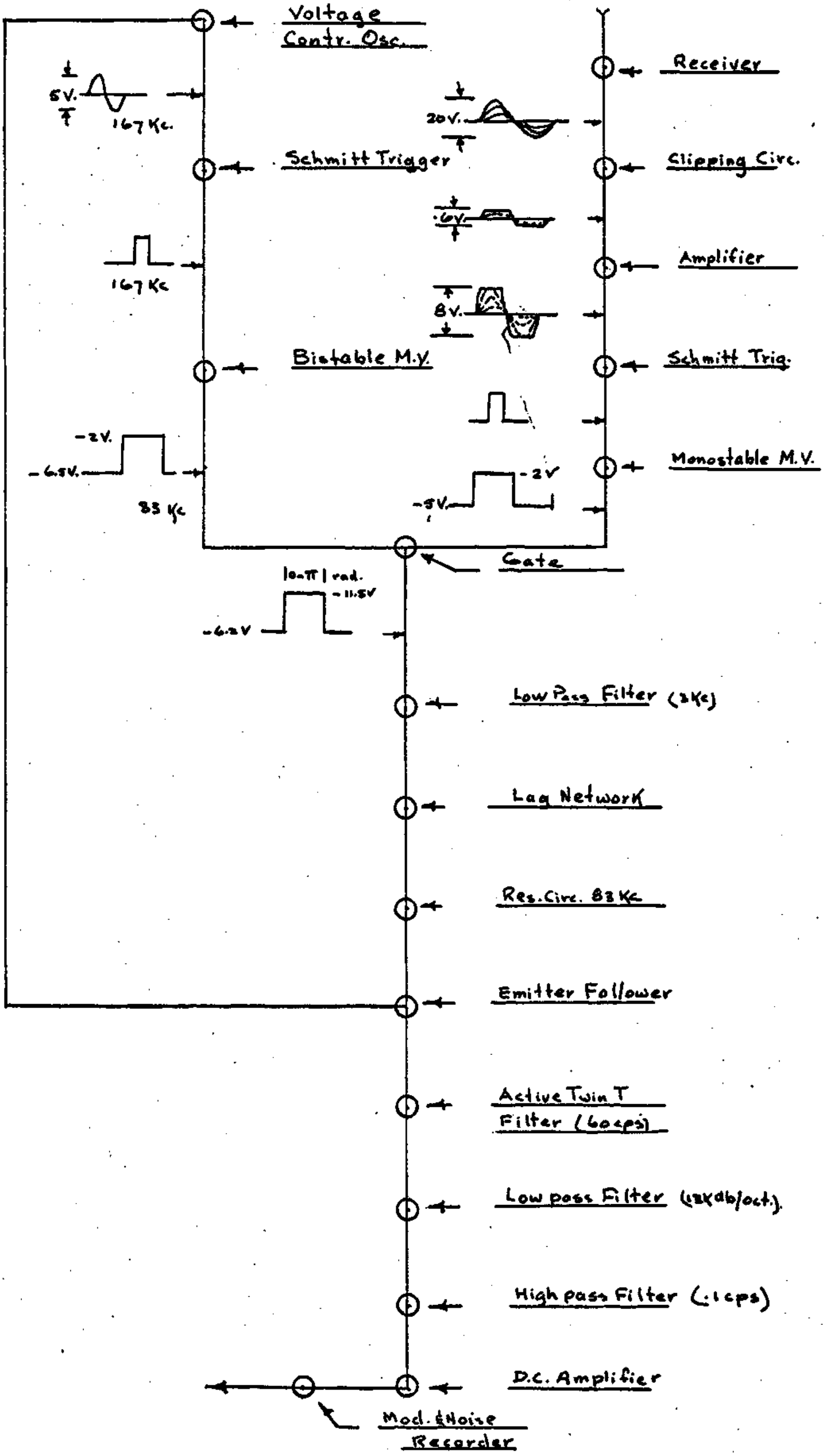

The signal bandwidth dictated the structure of the lag network. Since the cut-off of these filters was not very sharp, a considerable portion of 83 kc and its harmonics remained. In order to obtain a high signal to noise output, most of the 83 kc energy was filtered out by a shunt resonant circuit.

The output from the lag network was fed back to the voltage controlled local oscillator and also to an output stage, through a twin T filter and another low pass filter.

Since frequency drifts still occurred at less than .1 cps, the dc amplifier, used to provide power to drive the signal and noise recorder, was connected to the system through a high pass filter.

5.1 The Voltage Controlled Oscillator (VCO)

One of the pertinent components of the phase detector system is the voltage controlled local oscillator.

The circuit diagram (Figure 5.2) was taken from an electronics handbook, "Handbook of Selected Semi-Conductor Circuits," published by the United States Navy, Navyships Number 93484. It was modified slightly to suit conditions for this experiment, to operate at a frequency near 166 kc. It should be pointed out that the sensitivity of the local oscillator (VCO) depended on the value of the coupling capacitor (300 pf) as well as the characteristics of the variable capacity diode (V_{10}).

Note that the input stage to the VCO was also a low pass filter, made up of the 100 K ohm resistor, and the capacitor combinations. Its cut-off frequency was found to be near 10 kc.

The input - output response curve for the VCO is shown in Figure 5.3. None of the curves shown in this diagram were linear. Since the gain of the local oscillator (K_2) in cps/volt was represented by the slope of the curves, K_2 could not be expected to remain constant. When the system was modulated the input voltage to the VCO was modulated correspondingly. Consequently, the gain changed periodically. The gain at OV.dc was approximately 600 cps/volt while at - 12V.dc it was 300 cps/volt. A non-linear circuit was designed to correct this condition (Section 5.3.1). However, since the lock range was finally established over a range of 2.65 volts, the gain change became less significant. In addition to this, the frequency deviation used in field tests produced a dc bias change in the order of 0.5 V or less, which diminished the effect of the gain variation even more.

The average gain for the VCO (or local oscillator) during the experiment was set at 293 cps/volt or 1840 rad./sec./volt, with the applied input voltage centered at -9.8 volts dc. These values depended on the setting of the variable capacitor $C_{var.}$ (Figure 5.2), and on the selection of the transmitter (or IF) frequency which was tuneable over 2300 cps.

Fig. 5.2

V.C.O. Circuit Diagram (Local Osc.)

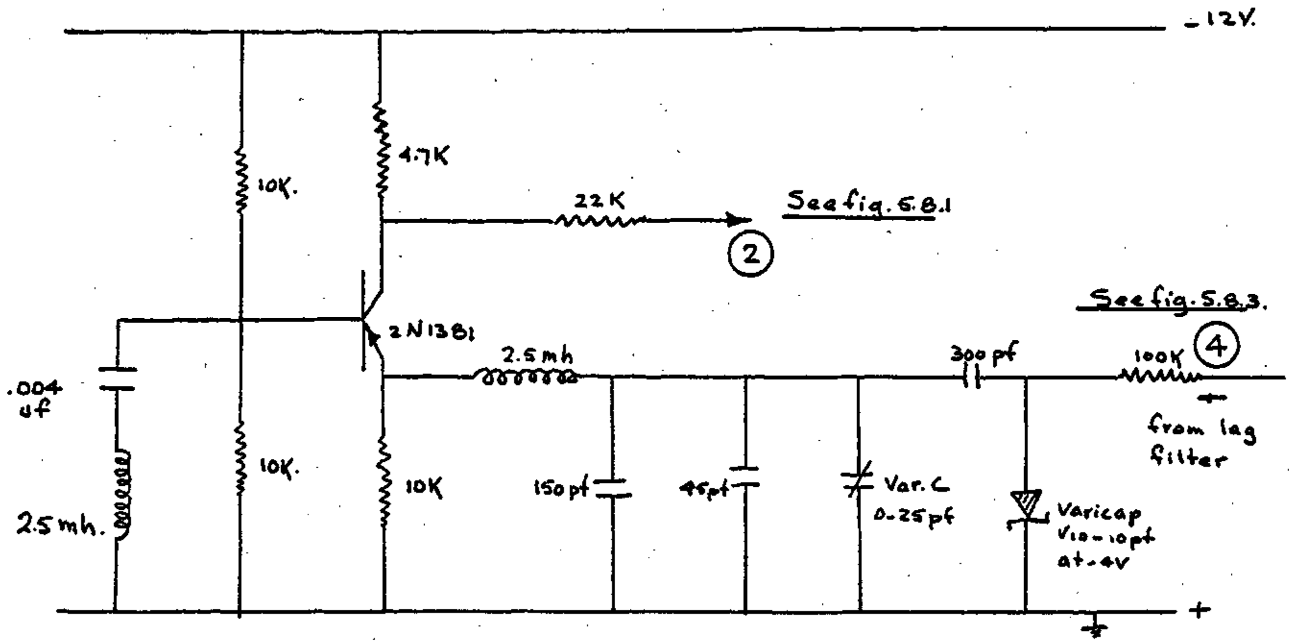

Fig. 5.3

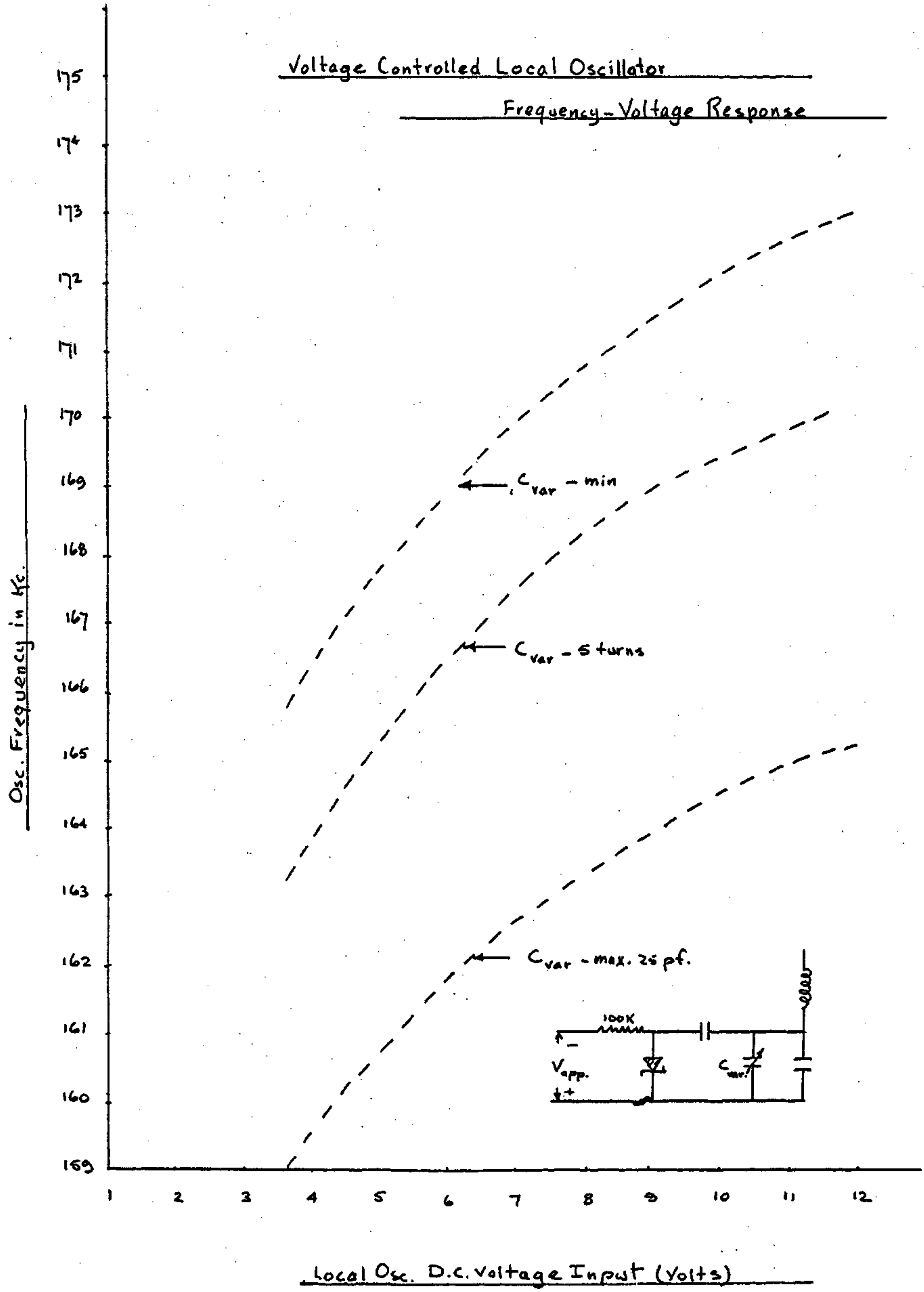
Voltage Controlled Local Oscillator
Frequency-Voltage Response
Osc. Frequency in Kc.
175
174
173
172
171
170
169
168
167
166
165
164
163
162
161
160
159
1
2
3
4
5
6
7
8
9
10
11
12
C_{var} - min
C_{var} - 5 turns
C_{var} - max. 25 pf.
100K
$V_{app.}$
$C_{var.}$
Local Osc. D.C. Voltage Input (Volts)

5.2 Phase Comparison Circuit

A detailed diagram of the phase comparison circuitry is shown in Figure 5.4. When the base of the 2N769 transistor was at -5 V, and the emitter at -2 V, then the transistor would conduct. However, no conduction took place when the base was at -2 V, nor when the emitter was at -6.5 volt. The wave form voltage levels were arranged in the manner shown by the wave form A from the local oscillator (VCO) and the wave form B from the 36.78 Mc receiver. The resulting output wave form is also depicted.

To prevent conduction when both the base and the emitter were at -2 V, a zener diode was inserted to insure that the emitter voltage would never be more positive than -2.5 volts dc.

To prevent loading of the gating circuit and to prevent distortion of the output wave C, an emitter-follower was used as well.

Fig. 5.4

Phase - Comparison Circuit

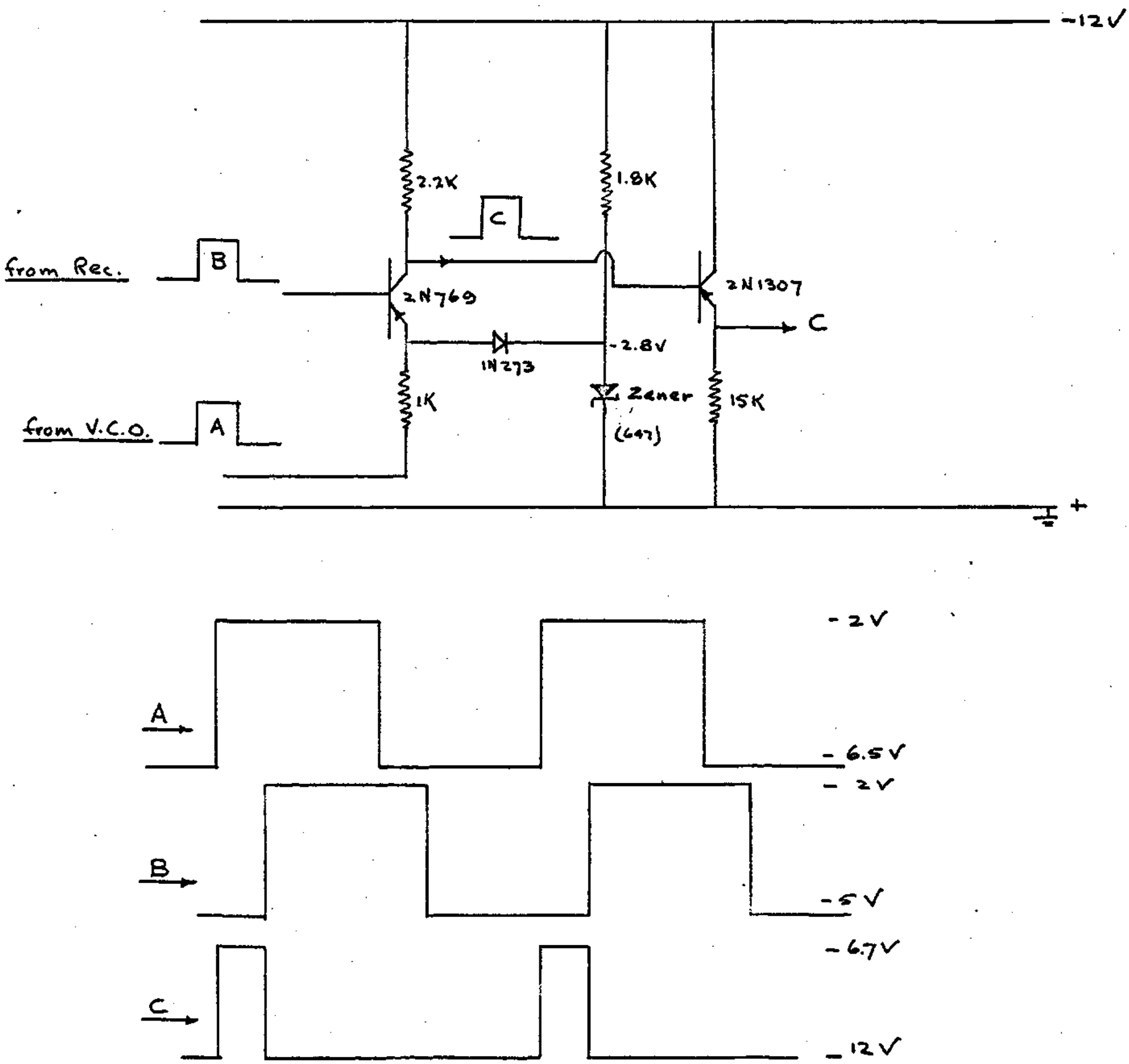

5.3 Miscellaneous Circuits

5.3.1 Non-Linear Circuit to Correct VCO Gain Irregularities: As mentioned previously in section 5.1, the gain of the local oscillator changed with the level of the dc voltage input. The circuit shown in Figure 5.5 corrected the curves shown in Figure 5.3 so that they were linear and the gain of VCO remained constant. Since it was decided to operate over a small fraction of the VCO gain response curve, the non-linear circuit was discarded. For those interested in working with larger lock ranges, this circuit is recorded.

5.3.2 Twin T Output Filters: In order to test the system completely, high signal to noise ratios were required at the system output. However, incidental noise, consisting of 60 cps power frequency and frequencies above 83 kc, was quite significant, its magnitude being in the order of 10 mv (rms). Since the signal output due to modulation could also be of this amplitude, little choice was left but to remove this noise.

To accomplish this, an active filter was inserted using twin T filters to eliminate the 60 cps component and RC filters to eliminate most of the high-frequency remains. The approximate response curve is shown in Figure 5.6. The active RC filter is discussed by Chong and Cobbold. [12]

5.3.3 Schmitt - Trigger: In reference to a previous diagram, Figure 5.1, the output from the conventional receivers passed through a clipping circuit, an amplifier, a Schmitt-trigger, and then a multivibrator.

Although the incoming signal amplitude was clipped, nevertheless, some amplitude fluctuations remained as shown in Figure 5.7, even with the amplifier saturated. If this signal, after amplification, was used to trigger the multivibrator directly and if triggering took place at a voltage other than the zero crossing voltage there would be a corresponding change

Fig. 5.5

Nonlinear Circuit to maintain linear Gain of the Local Osc.

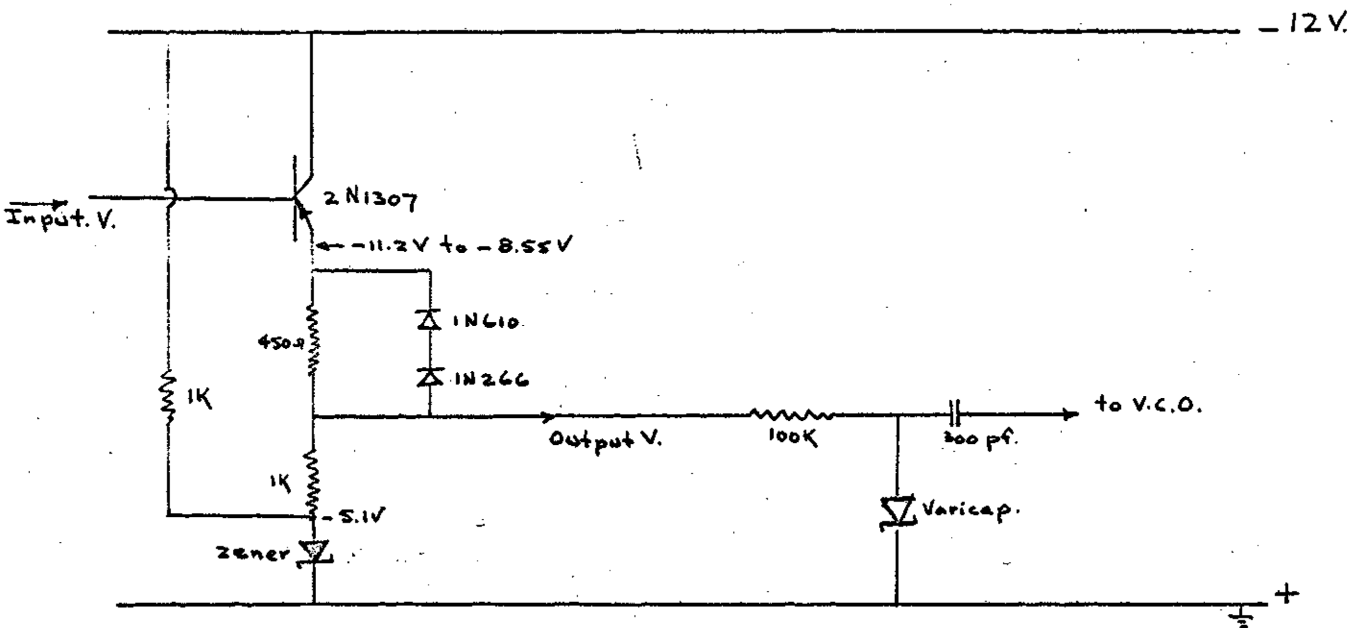

Fig. 5.6

Approx. Freq. Response of the active R.C. filter

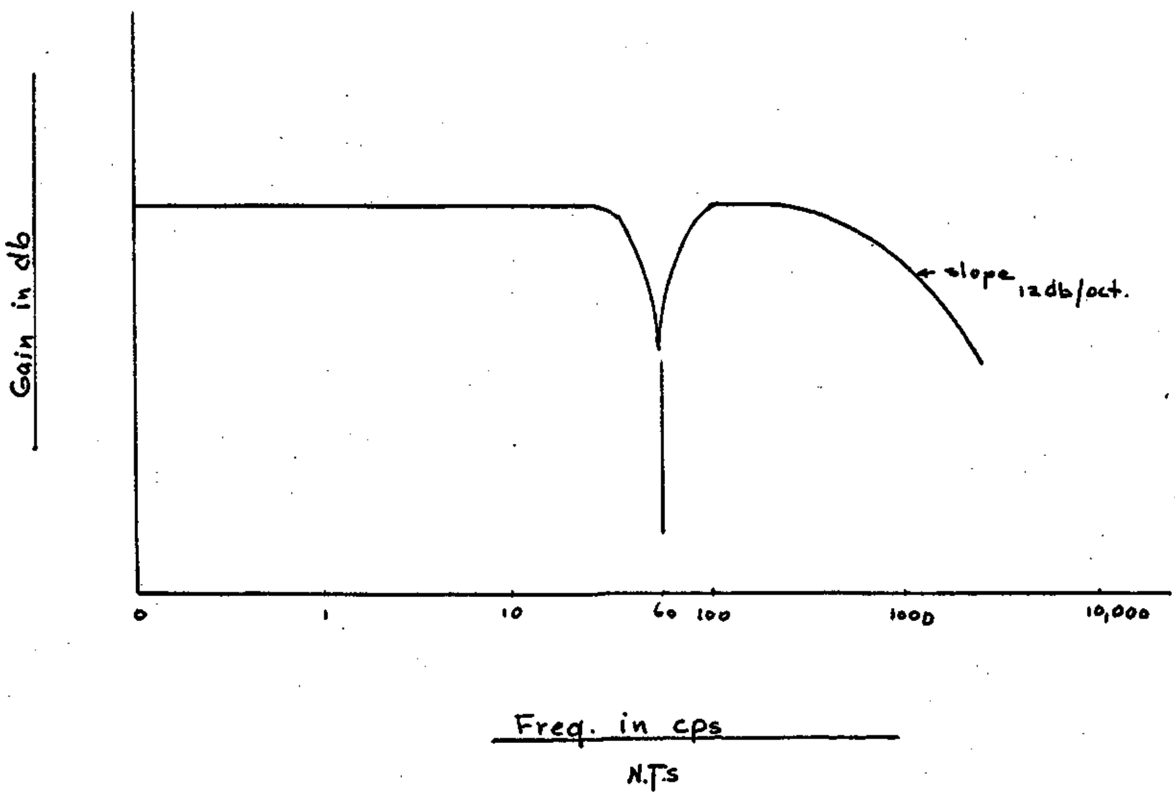

in time Δt at which the multivibrator triggered. In other words, one would obtain incidental frequency modulation due to incidental amplitude modulation of the incoming signal. One could have amplified the signal before triggering, and then clipped it again. However, since a Schmitt-trigger can be made to fire at the zero crossing voltage, this circuit was used to trigger the multivibrator.

The above explanation is not valid for the signal coming from the VCO, since no amplitude fluctuations were present.

Fig. 5.7

Frequency Mod. caused by amplitude modulation

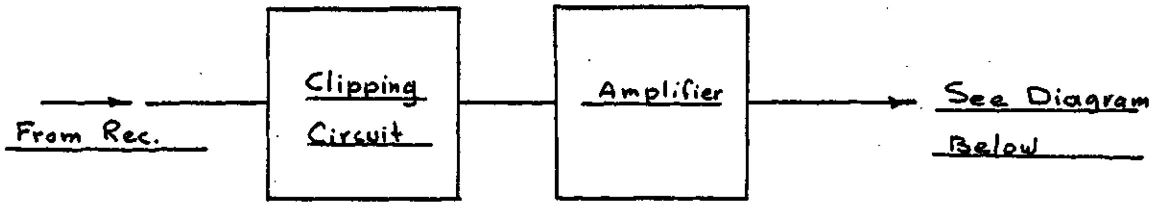

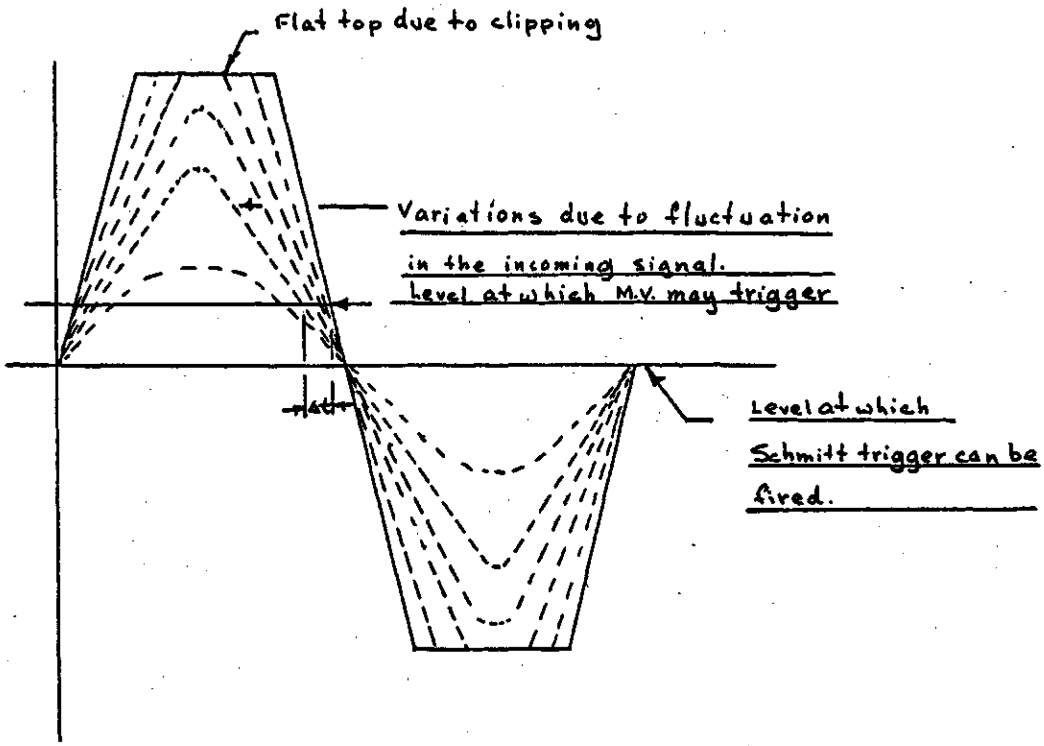

5.4 System Circuit Diagram

The system circuit diagram is shown in three stages: input, phase detector/filter, and output. These are shown in Figures (5.8.1), (5.8.2), and (5.8.3), respectively.

These circuit diagrams do not show any of the commercial equipment circuits.

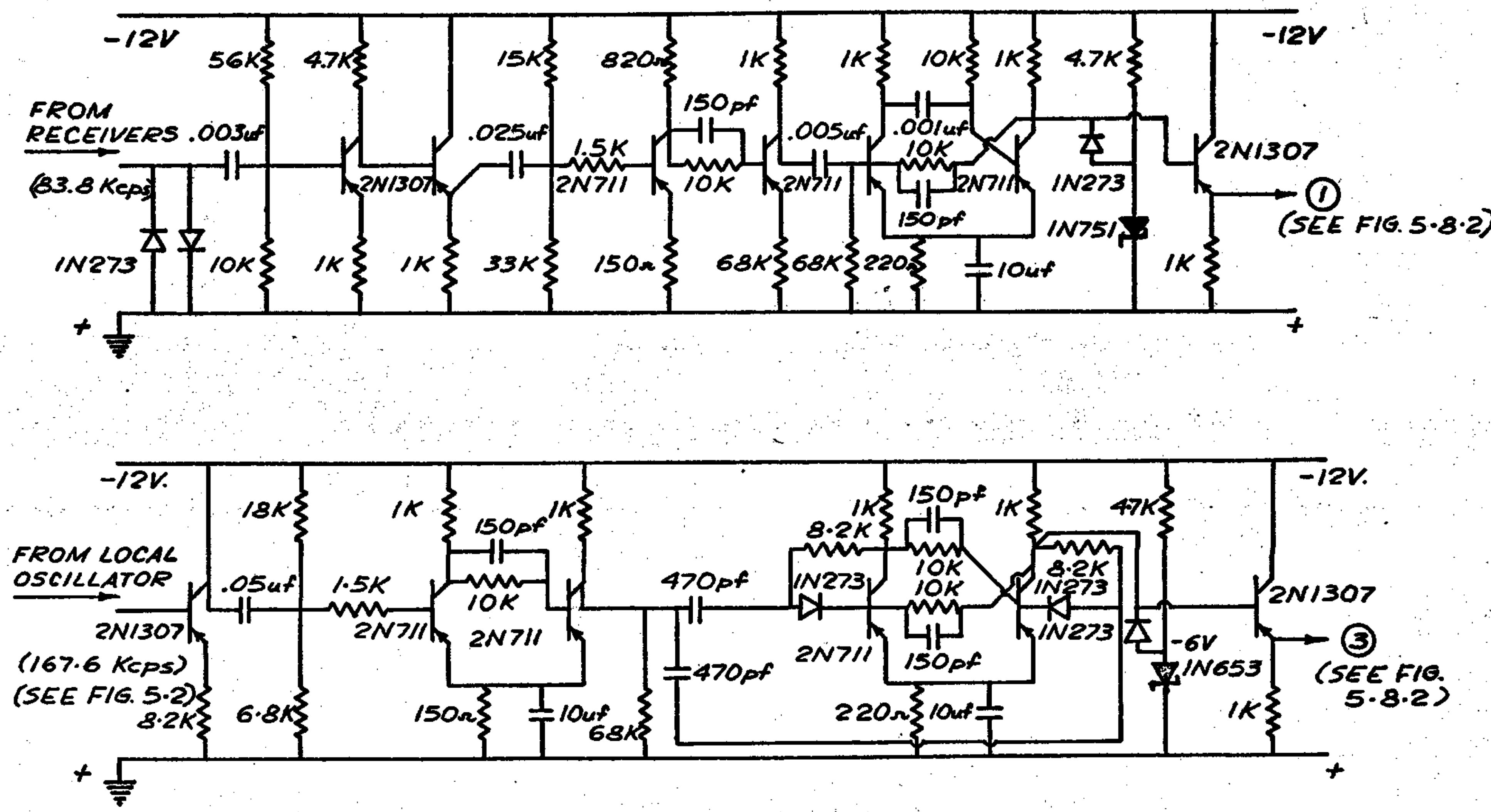
-12V
FROM RECEIVERS
(83.8 Kcps)
.003uf
IN273
56K
4.7K
10K
1K
2N1307
.025uf
15K
1.5K
2N711
33K
820Ω
150pf
10K
150Ω
.005uf
.001uf
68K
220Ω
150pf
10uf
IN273
IN751
2N1307
1
(SEE FIG. 5·8·2)
-12V.
FROM LOCAL OSCILLATOR
2N1307
(167·6 Kcps)
(SEE FIG. 5·2)
8·2K
.05uf
18K
6·8K
1·5K
2N711
150Ω
10uf
68K
470pf
8·2K
-6V
IN653
47K
3
(SEE FIG. 5·8·2)

FIG. 5·8·1

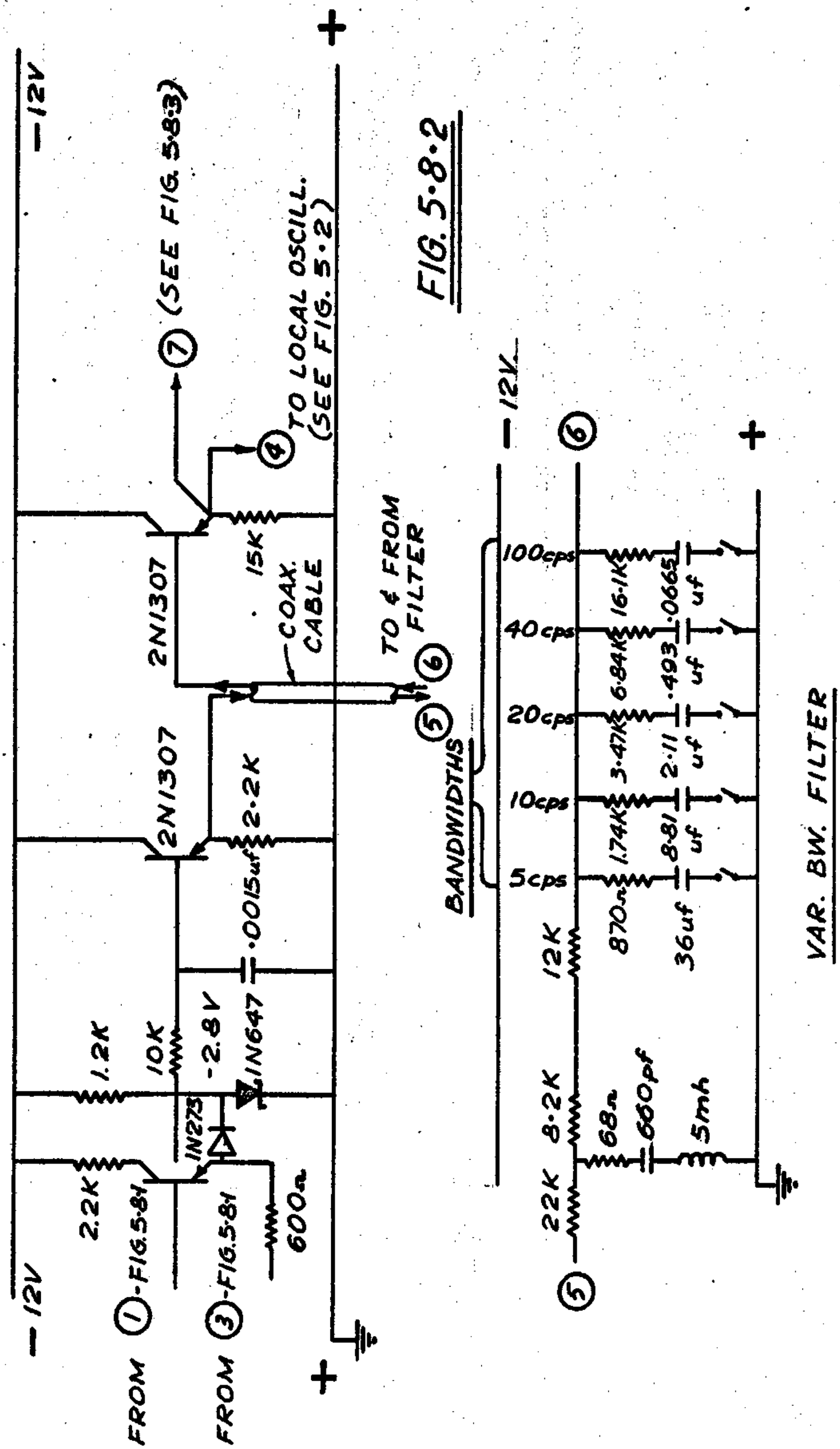

-12V
+
(SEE FIG. 5·8·3)
TO LOCAL OSCILL. (SEE FIG. 5·2)
2N1307
15K
COAX. CABLE
TO & FROM FILTER
2N1307
2·2K
·0015uf
1N647
-2.8V
10K
1.2K
1N273
2.2K
600Ω
FROM 1-FIG.5·8·1
FROM 3-FIG.5·8·1
-12V
+
BANDWIDTHS
100cps
40cps
20cps
10cps
5cps
16·1K
6·84K
3·47K
1.74K
870Ω
·0665 uf
·493 uf
2·11 uf
8·81 uf
36uf
12K
8·2K
22K
68Ω
660pf
5mh
VAR. BW. FILTER

FIG. 5·8·2

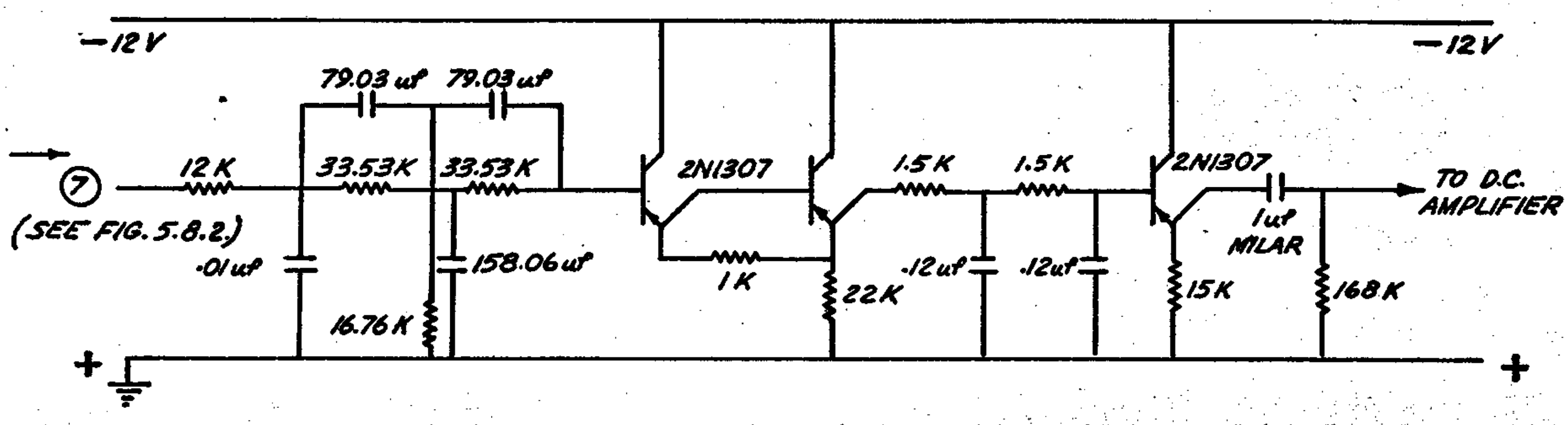
−12V
−12V
79.03 uf
79.03 uf
7
(SEE FIG. 5.8.2.)
12K
33.53K
33.53K
2N1307
1.5K
1.5K
2N1307
TO D.C. AMPLIFIER
.01 uf
158.06 uf
1K
22K
.12 uf
.12 uf
1 uf MILAR
15K
168K
16.76K
+
+

FIG. 5.8.3.

VI. PHASELOCK DETECTOR TESTS

6.0 General Discussion

Although Koehler [2] had an operational system, no experimental curves were provided regarding frequency response for the various bandwidths. In order to know exactly the various bandwidths of the phase detector, the existing system was tested experimentally. Many unexpected system peculiarities showed up, which altered field testing plans quite extensively. Where first it was planned to put the system directly into field operation and to design a prototype communication system, it soon became quite apparent that much theoretical work needed to be done.

For example, it was observed that the phase difference as noted by the rectangular wave output (wave form C in Figure 5.4) was not only a function of the frequency deviation, but also a function of the modulation frequency.

This meant that for one particular carrier frequency deviation, the lock range (π K rad./sec.), could be exceeded sooner at one modulation frequency than at another.

Changing the bandwidth affected the severity of this irregularity. In order to explain these properties, a theoretical analysis is presented next.

6.1 Phase Response Analysis

As shown in Appendix D, an equation was developed to show the relationship between the modulation frequenc; and the phase difference:

$$\Delta\phi_m(t) = \frac{\frac{AD}{t_1}(1 + t_1{}^2\omega_m{}^2)^{\frac{1}{2}}\ \mathrm{Sin}\,\omega_m t}{\left\{(\frac{K}{t_1} - \omega_m{}^2)^2 + (\frac{Kt_2 + 1}{t_1{}^2})^2\omega_m{}^2\right\}^{\frac{1}{2}}} \tag{6.1}$$

where: (1) $\Delta\phi_m(t)$ = phase difference in radians (See Figures 5.1 and 5.4)

(2) AD = frequency deviation in cps

(3) ω_m = modulation frequency in rad./sec.

(4) $K = K_1 \times K_2$

Equation 6.1 suggests a rather complex relationship and some simplification is of value. Taking into account the various values given in Table 6.I, equation 6.1 can be simplified respectively for each bandwidth, for an assumed constant frequency deviation of 1 cps. More detailed calculations are shown in Appendix E.

5 cps Bandwidth

$$\Delta\phi_m(t) = \frac{.63(1 + 2.5\,\omega_m{}^2)^{\frac{1}{2}}\ \mathrm{Sin}\,\omega_m t}{\left\{(980 - \omega_m{}^2)^2 + 980\,\omega_m{}^2\right\}^{\frac{1}{2}}} \tag{6.2}$$

10 cps Bandwidth

$$\Delta\phi_m(t) = \frac{2.52(1 + .155\,\omega_m{}^2)^{\frac{1}{2}}\ \mathrm{Sin}\,\omega_m t}{\left\{(3940 - \omega_m{}^2)^2 + 3945\,\omega_m{}^2\right\}^{\frac{1}{2}}} \tag{6.3}$$

20 cps Bandwidth

$$\Delta\phi_m(t) = \frac{10.9(1 + .00962\,\omega_m{}^2)^{\frac{1}{2}}\ \mathrm{Sin}\,\omega_m t}{\left\{(15800 - \omega_m{}^2)^2 + 15800\,\omega_m{}^2\right\}^{\frac{1}{2}}} \tag{6.4}$$

40 cps Bandwidth

$$\Delta\phi_m(t) = \frac{40.6(1 + .000625\,\omega_m{}^2)^{\frac{1}{2}}\ \mathrm{Sin}\,\omega_m t}{\left\{(62500 - \omega_m{}^2)^2 + 63200\,\omega_m{}^2\right\}^{\frac{1}{2}}} \tag{6.5}$$

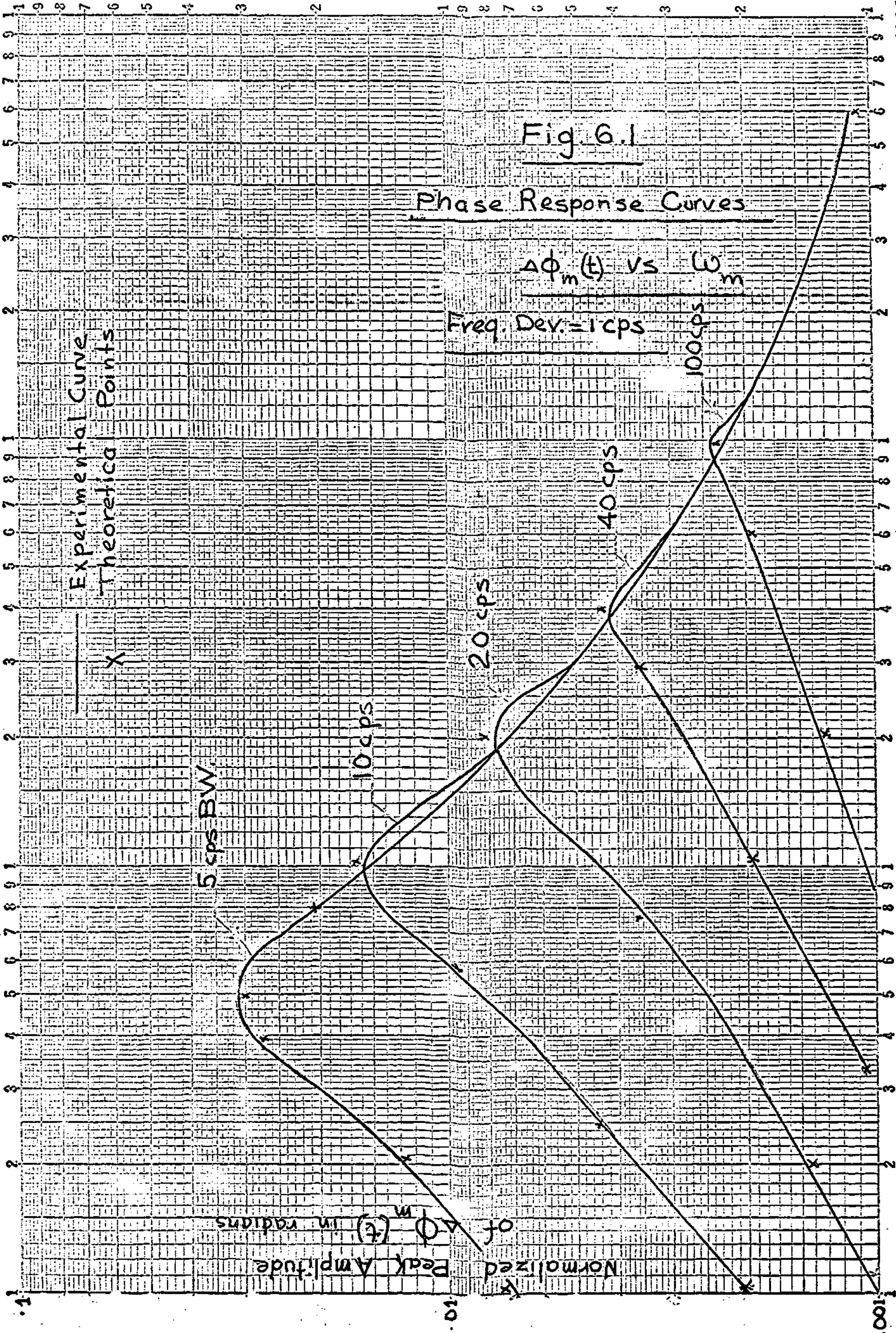
Fig. 6.1
Phase Response Curves
$\Delta\phi_m(t)$ vs ω_m
Freq. Dev. = 1 cps
—— Experimental Curve
x Theoretical Points
5 cps BW
10 cps
20 cps
40 cps
100 cps
Modulation Frequency (cps)
Normalized Peak Amplitude of $\Delta\phi_m(t)$ in radians
1
10
100
1000
.001
.01
.1

100 cps Bandwidth

$$\Delta\Phi_m(t) = \frac{252(1 + .0000152\,\omega_m^2)^{\frac{1}{2}}\ \mathrm{Sin}\,\omega_m t}{(398000 - \omega_m^2)^2 + 65000\,\omega_m^2\ ^{\frac{1}{2}}} \tag{6.6}$$

The peak amplitudes calculated from equations 6.2 to 6.6, inclusive, are plotted in Figure 6.1.

These curves were also plotted from experimental observations by measuring the width of wave form C in Figure 5.4 as a function of the modulation frequency (ω_m). The experimental curves were normalized and plotted in Figure 6.1 as well. Close correlation was observed between the theoretical and experimental curves of Figure 6.1.

It can be clearly observed that the peaks of the curves occur at the frequency representing the bandwidth. This means that for a particular frequency deviation, the phase difference is larger at the bandwidth frequency than at any other frequency. If the peaking ratio is defined as the ratio of the magnitude of $\Delta\Phi_m(t)$ when ω_m = bandwidth, to the magnitude of $\Delta\Phi_m(t)$ when $\omega_m \longrightarrow 0$, then the peaking ratio is determined as (Appendix F):

$$\text{P.R.}\ (\Delta\Phi_m(t)) = \left\{Kt_1(1 + Kt_1)\right\}^{\frac{1}{2}}/(1 + Kt_2). \tag{6.7}$$

For the system described in this thesis in which the signal bandwidth was much less than the lock range, Kt_1 and Kt_2 were much larger than unity. The peaking ratio for this condition was then simplified to yield:

$$\text{Peaking ratio of}\quad \Delta\Phi_m(t) = t_1/t_2 = \alpha \tag{6.8}$$

where; α is the network ratio.

As shown in Table (6.I), the value for α ranged from 50.4 to 3.66 for the 5 cps and 100 cps bandwidths, respectively.

A large frequency deviation was preferred, in order to obtain as large as possible a signal/noise ratio at the output. This necessitated the use of a low modulation frequency, so as not to exceed a value of π radians for $\Delta \dot{\theta}_m$.

It is interesting to note that α is related to the ratio of the lock range and the signal bandwidth (Appendix B) so that:

$$\alpha \approx \text{[illegible]} \times \text{(lock range/signal bandwidth)} \qquad \text{(B.4)}$$

where the signal bandwidth $\lll$ lock range.

Thus, for a constant signal bandwidth, a reduction in the lock range is accompanied by a corresponding decrease in the peaking ratio. Similarly, for a constant lock range, a decrease in the signal bandwidth will result in an increase of the peaking ratio.

6.2 Output Voltage-Frequency Response

Since the filter characteristics and the phase response characteristics combine to produce an output (as shown in Figure 6.2), it is significant to examine why the system voltage output response curve is a function of the bandwidth and the modulation frequency. This particular curve will also indicate the exact value of the system signal bandwidth. As shown in Figure 4.3, the output voltage is represented by $e_m(t)$. The relationship between $e_m(t)$ and $\omega_m(t)$ was calculated to be: (See Appendix G).

$$e_m(t) = \frac{K_1 DA(1 + t_2^2 \ \omega_m^2)^{\frac{1}{2}} \operatorname{Sin} \omega_m t}{t_1 \left[(K/t_1 - \omega_m^2)^2 + \left\{ (1 + Kt_2)/t_1 \right\}^2 \omega_m^2 \right]^{\frac{1}{2}}} \tag{6.9}$$

Where (1) $e_m(t)$ = output voltage

(2) AD = frequency deviation in cps

(3) ω_m = modulation frequency in rad./sec.

(4) K_1 = gain of the phase detector

(5) K = K_1K_2 in rad./sec.

For values of AD = 1 cps, K_1 = .84 volts/radian and K = 1550 rad./sec., the following equations represent the output as a function of time for the various bandwidths:

Bandwidth = 5 cps

$$e_m(t) = \frac{.53(1 + .00098 \ \omega_m^2)^{\frac{1}{2}} \operatorname{Sin} \omega_m t}{\left\{ (980 - \omega_m^2)^2 + 980 \times \omega_m^2 \right\}^{\frac{1}{2}}} \tag{6.10}$$

Bandwidth = 10 cps

$$e_m(t) = \frac{2.14(1 + .000235 \ \omega_m^2)^{\frac{1}{2}} \operatorname{Sin} \omega_m t}{\left\{ (3920 - \omega_m^2)^2 + (3940 \ \omega_m^2) \right\}^{\frac{1}{2}}} \tag{6.11}$$

Bandwidth = 20 cps

$$e_m(t) = \frac{8.55(1 + .000053 \ \omega_m^2) \operatorname{Sin} \omega_m t}{\left\{ (15800 - \omega_m^2)^2 + (15900 \ \omega_m^2) \right\}^{\frac{1}{2}}} \tag{6.12}$$

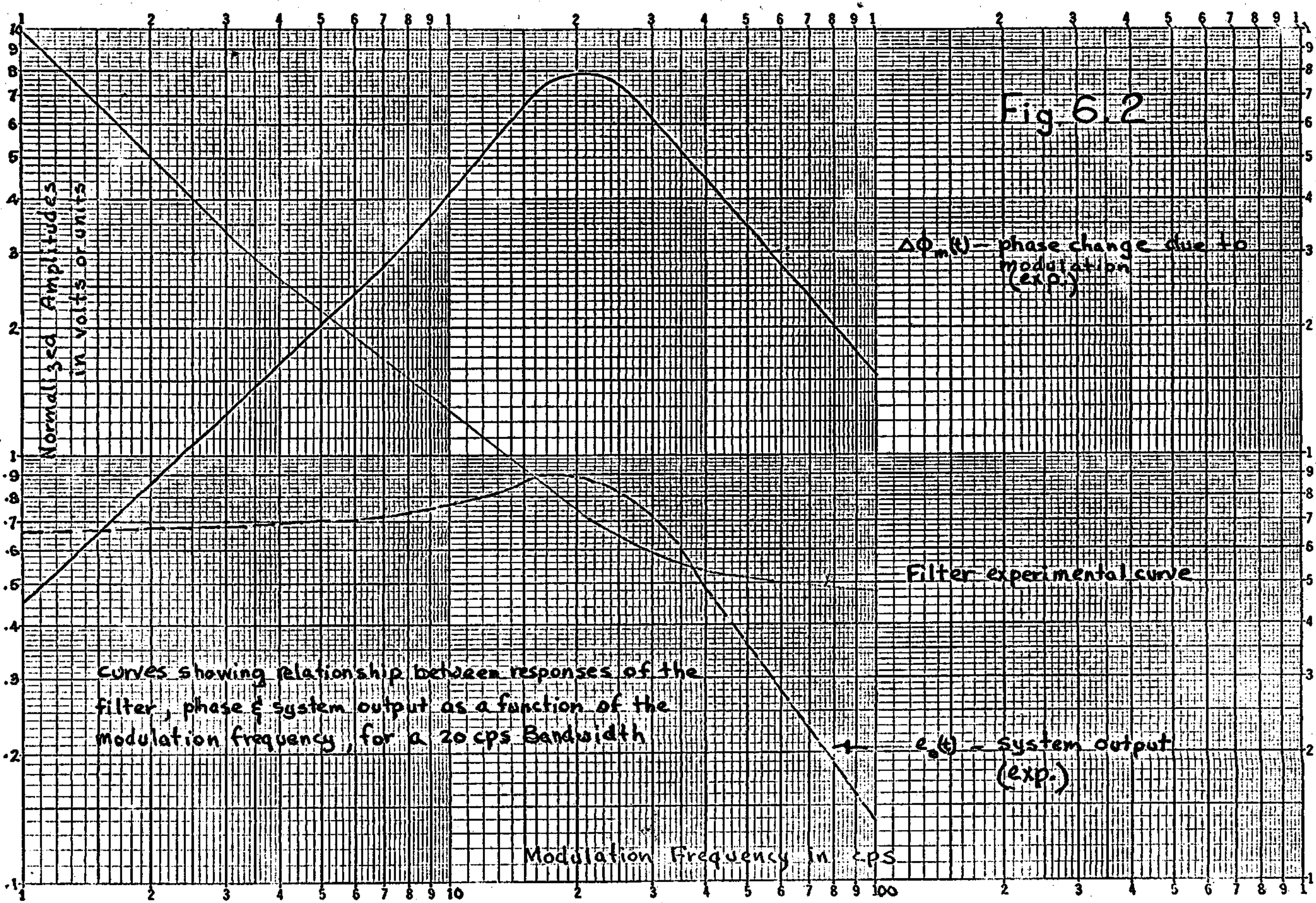
Fig. 6.2
Normalized Amplitudes in volts or units
$\Delta\phi_m(t)$ – phase change due to modulation (exp.)
Filter experimental curve
$e_o(t)$ – system output (exp.)
Curves showing relationship between responses of the filter, phase & system output as a function of the modulation frequency, for a 20 cps Bandwidth
Modulation Frequency in cps

Bandwidth = 40 cps

$$e_m(t) = \frac{34.1(1 + .000011\,\omega_m^2)\ \mathrm{Sin}\ \omega_m t}{(63000 - \omega_m^2)^2 + (64500\,\omega_m^2)} \qquad (6.13)$$

Bandwidth = 100 cps

$$e_m(t) = \frac{214(1 + .0000011\,\omega_m^2)\ \mathrm{Sin}\ \omega_m t}{(396000 - \omega_m^2)^2 + (457000\,\omega_m^2)} \qquad (6.14)$$

The peak amplitudes associated with Equations 6.10 to 6.14, inclusive, were plotted as shown in Figure 6.3. The output voltages were also measured experimentally. There was again fairly close correlation between the theoretical and the experimental curves, if compared on a normalized basis. However, both the 100 cps and 245 cps bandwidth curves show discrepancies. This is believed to be due to the affect of the 3 kc low pass filter.

Again there is some peaking evident. Theoretically, for the 5 cps bandwidth, the peaking ratio is 1.4, diminishing to 1.1 for the 100 cps bandwidth. The peaking ratio can be defined as the ratio of the output voltage when $\omega_m \rightarrow \omega_c$ to the output voltage when $\omega_m \rightarrow 0$, and is given by: (Appendix G)

$$\mathrm{P.R.}\ (e_m(t)) = (Kt_1 + K^2 t_2^2)^{\frac{1}{2}}/(Kt_2 + 1) \qquad (6.15)$$

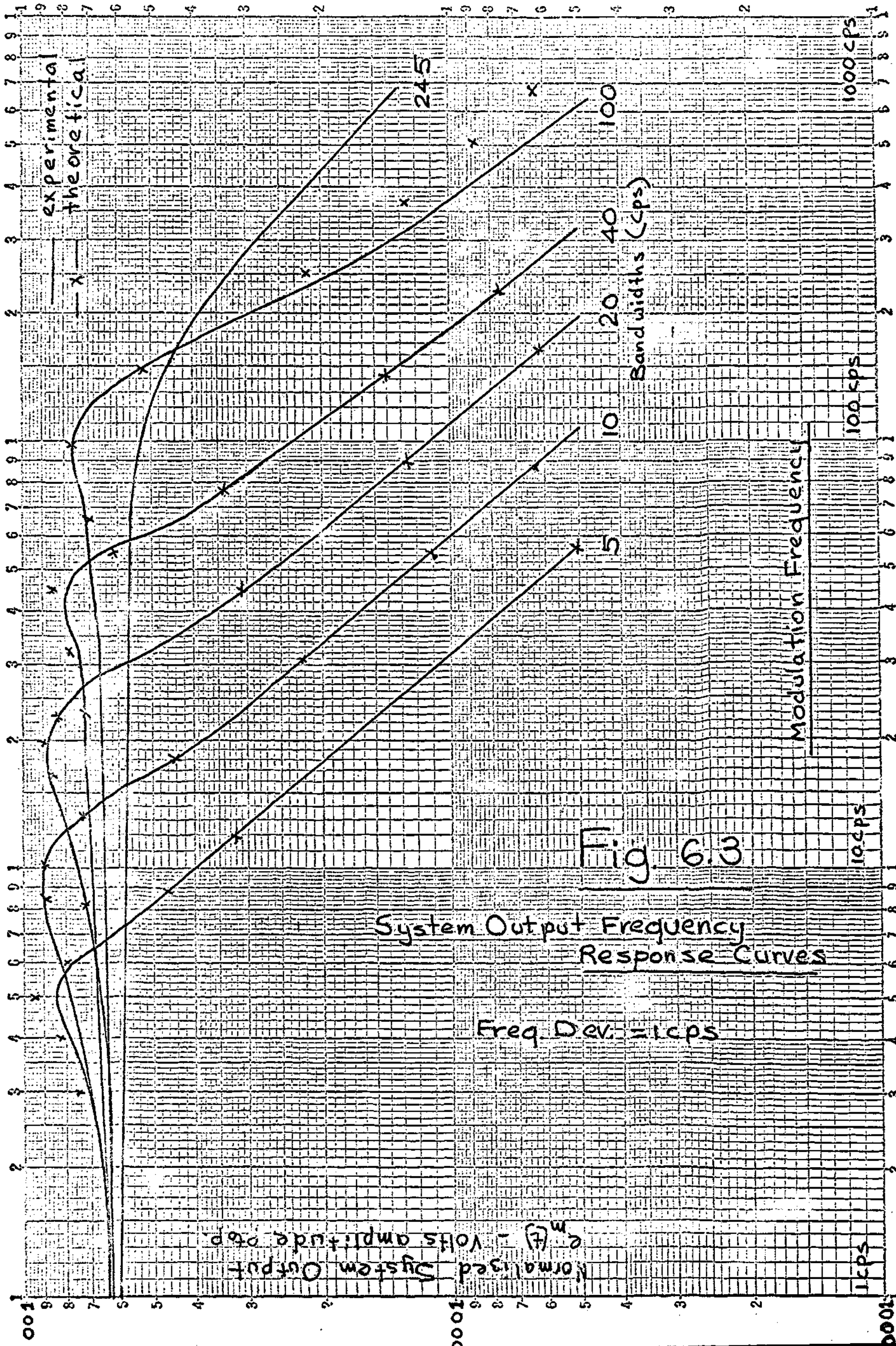

Fig. 6.3

System Output Frequency Response Curves

TABLE - 6.I

Filter Bandwidths Cps	5	10	20	40	100	245
Lock Range Cps	775	775	775	775	775	775
Capt. Range Cps	110	157	224	310	493	775
Noise Bandwidth Cps	15	30	58	104	212	387
t_2 Seconds	.0314	.0153	.00731	.00337	.00107	--
t_1 Seconds	1.58	.394	.0981	.0246	.00393	--
Network Ratio $= t_1/t_2$	50.4	25.7	13.4	7.3	3.66	--
R_1 ohms	43	43	43	43	43	43
R_2 ohms	870	1740	3470	6840	16,100	--
C - uf	36	8.81	2.11	.493	.0665	--

VII. SYSTEM OPERATION TESTS

7.0 General Discussion

So far, only the pertinent properties of the phase detector stage have been discussed. There are, however, properties associated with the receiving system as a complete unit. One of these properties is referred to as "threshold," since the system under consideration is a frequency modulated system. By testing the system first in the laboratory under simulated field conditions, and then under real field conditions, this property was examined.

By controlling the amplitude of signal and noise at the input, and measuring both signal and noise at the system output, a curve such as shown in Figure 7.1 can be obtained. For truly white Gaussian noise, the linear portions of both curves should be at a slope of 45^{o}, the horizontal and vertical scales being equal. For an amplitude modulated system, the curve will pass through the point (0,0).

The location of the curve representing the frequency modulated system depends on the magnitude of the term called modulation index, or deviation ratio. These terms are defined as:

$$\text{(1) Modulation Index} = M = \frac{\text{frequency deviation in cps}}{\text{modulation frequency in cps}}$$

$$\text{(2) Deviation Ratio} = D.R. = \frac{\text{frequency deviation in cps}}{\text{signal bandwidth in cps}}$$

In "conventional" FM systems, by which is meant an FM system using a detector other than the phase detector, the term modulation index is usually preferred over deviation ratio. The reason for this is that in conventional FM, the modulation frequency is near or exactly equal to the total bandwidth in magnitude. However, in other systems, such as the one described in this thesis, a modulation frequency lower in magnitude than the bandwidth may have to be used, in order to reduce the effect of the non-linearity in the response of the phase error versus modulation frequency.

In Figure 7.1 for the F, curve, a D.R. of 4 is used. The advantage of FM over AM can easily be seen over the linear portion of the curves. For example, if an output S/N ratio of 20 db is required, the required input S/N ratio for the AM system is 20 db, while for the FM system, an input S/N of 10 db will still produce the specified output S/N ratio.

The portion of the FM curve below the output S/N of 20 db, is referred to as the "threshold" region and in this region the advantage of FM over AM decreases rapidly. [14]

By plotting FM curves representing more than one deviation ratio, a threshold curve can be obtained as shown in Figure 7.2.

Fig. 7.1

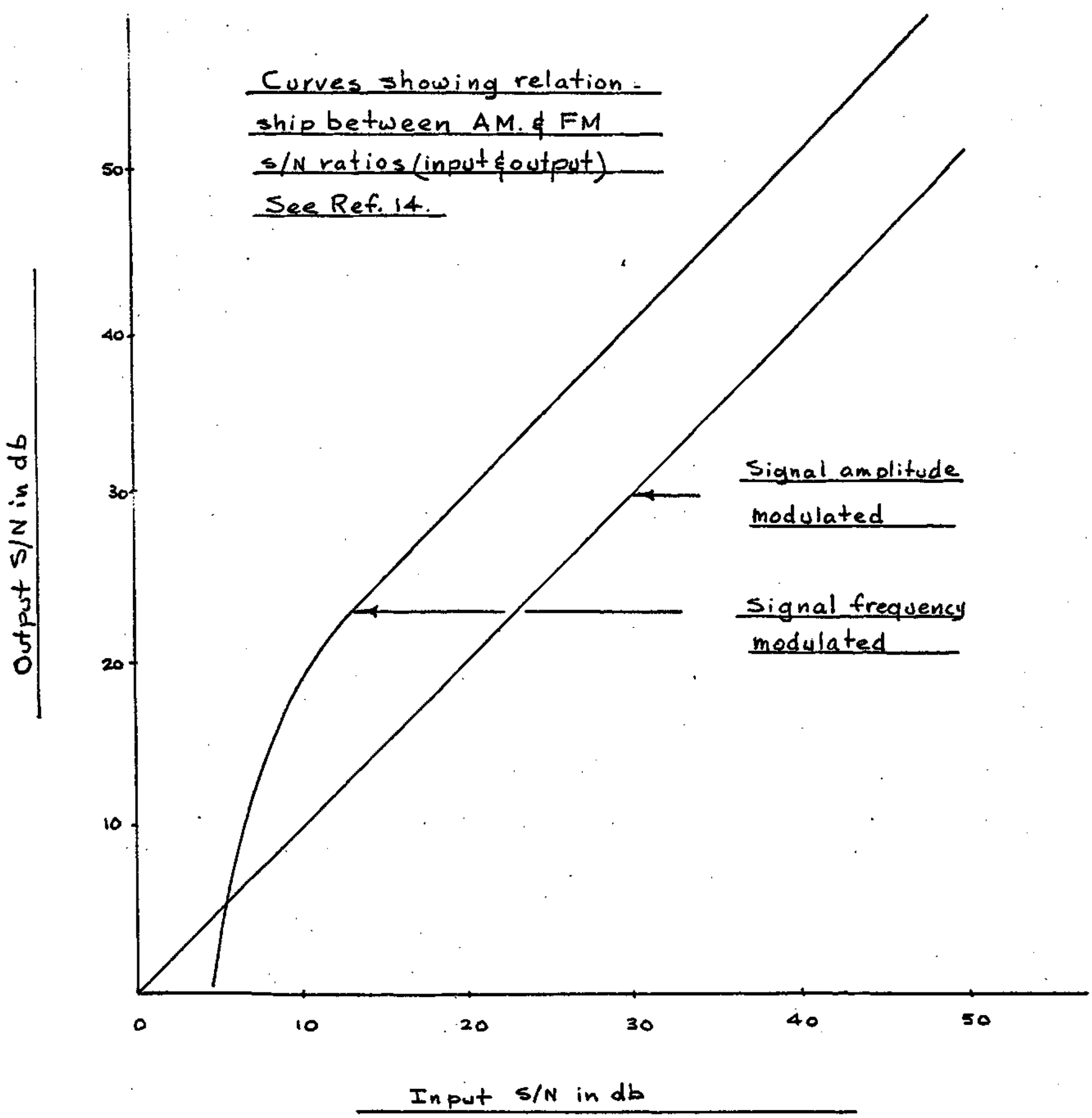
Curves showing relation-
ship between AM. & FM
s/N ratios (input & output)
See Ref. 14.
Output S/N in db
50
40
30
20
10
0
10
20
30
40
50
Signal amplitude
modulated
Signal frequency
modulated
Input S/N in db

Fig. 7.2

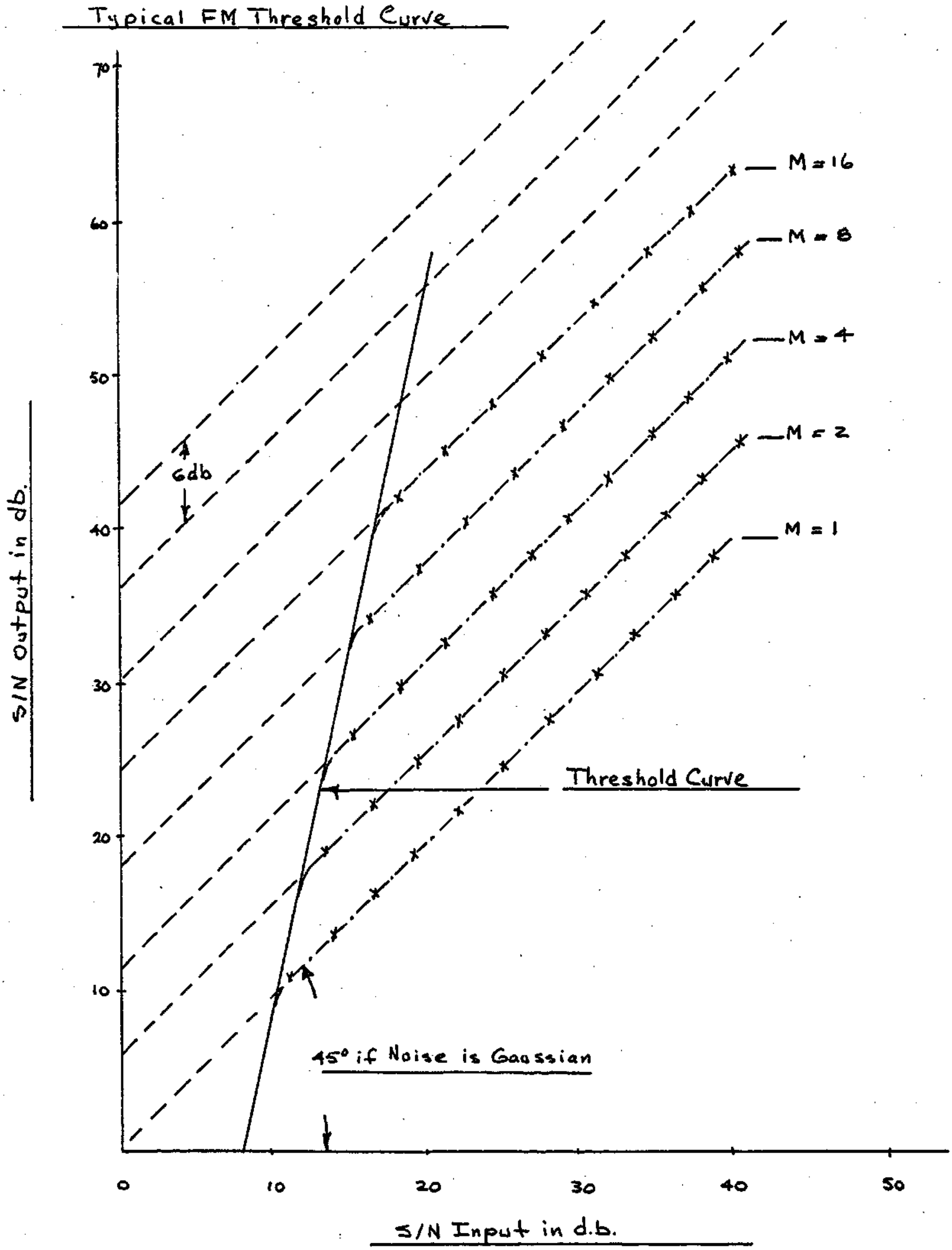
Typical FM Threshold Curve
S/N Output in db.
S/N Input in d.b.
M = 16
M = 8
M = 4
M = 2
M = 1
6db
Threshold Curve
45° if Noise is Gaussian
0
10
20
30
40
50
60
70

7.1 Threshold Considerations

7.1.1 Theoretical Predictions: Several attempts have been made in the last two or three years to predict theoretically where thresholds will occur for phase detector FM systems. However, most of these attempts have covered the operation of phase detectors which are linear over only a portion of the π radians phase change discussed in Chapter IV, section 4.1.3. A search of the literature did not discover any articles on the theoretical determination of thresholds of completely linear systems.

Develet, [15] has made an excellent attempt at determining theoretically the threshold for the phase detector system for a particular type of non-linearity.

The total phase error, $\Delta \bar{\Phi}$, is made up of modulation induced phase error and noise induced phase error. Assuming a sinusoidal modulation, the mean-square value of the modulation induced error is shown to be (in Appendix H):

$$\Delta \bar{\Phi}_m^{\,2} = \frac{M^2}{2}(1 - H(j\omega))^2 \tag{7.1}$$

where; (1) M = modulation index

(2) $H(j\omega)$ = system transfer function.

On the other hand, Heitzman [5] stated that the mean square noise induced phase error is given by (See Appendix C):

$$\Delta \bar{\Phi}_n^{\,2} = n\, B_n/C \tag{7.2}$$

$$\Delta \bar{\Phi}_n^{\,2} = \frac{n}{C} \int_0^{\infty} (H(j\omega))^2 \, d\omega \tag{7.3}$$

where; (1) n = noise power spectral density in watts/cps

(2) C = carrier power in watts.

Therefore, the total mean square phase error can be described as:

$$\Delta\phi^2 = \frac{M^2}{2}\left\{1 - H(j\omega)\right\}^2 + \frac{n}{C}\int_0^{\infty}\left|H(j\omega)^2\right| d\omega \qquad (7.4)$$

Heitzman [5] states that usually the phaselocked demodulator is said to be at threshold when the total mean phase error is equal to 1/2 radian, i.e., when $\Delta\phi^2 = .25 \text{ rad.}^2$

(However, it is assumed that the allowable phase error for a linear system would be somewhat in excess of .5 radians--say 1 radian.)

As shown in Appendix H, a threshold for carrier power is calculated in terms of the modulation index (M), by Heitzman, to produce the following equation:

$$C_t = 35.5\, M^{\frac{1}{2}}\, n\, f_m \qquad (7.5)$$

If the phase error threshold is taken to be 1 radian, then:

$$C_t = 6.28\, M^{\frac{1}{2}}\, n\, f_m \qquad (7.6)$$

To eliminate the variable quantity f_m, the modulation frequency, the carrier threshold as expressed by equation 7.5 was plotted in Figure 7.3 as C/nB_b where f_m was set equal to B_b (base bandwidth) and where n = noise power spectral density. Note that M actually is the deviation ratio in this case.

Equation 7.5 was plotted for various values of M to produce the indicated threshold curve No. 6. If equation 7.6 was plotted also, one would observe it to be several db to the left of Heitzman's curve No. 6, representing a threshold improvement. However, as indicated previously equation 7.6 is based on an assumption.

Fig. 7.3

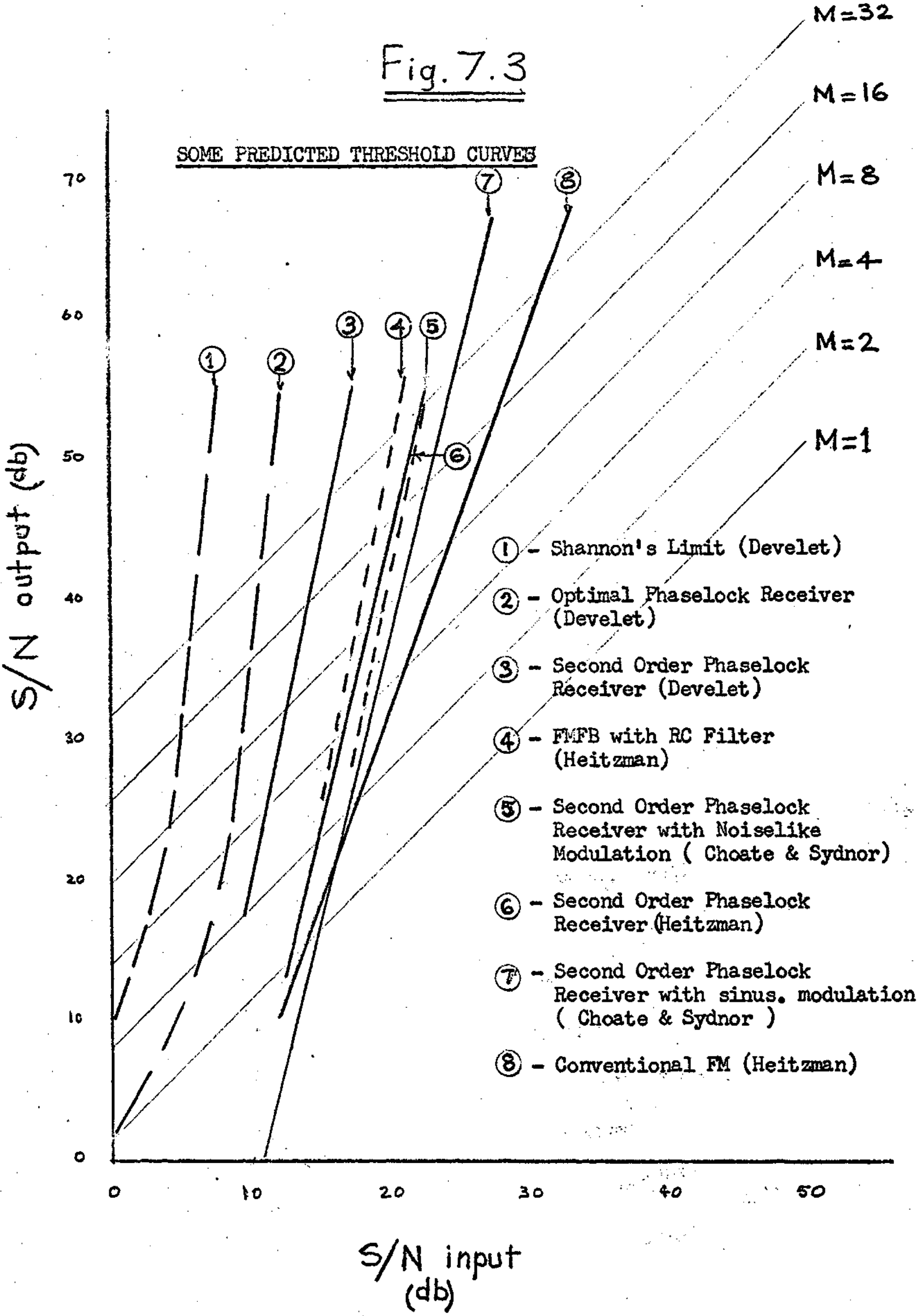
SOME PREDICTED THRESHOLD CURVES
M=32
M=16
M=8
M=4
M=2
M=1
S/N output (db)
70
60
50
40
30
20
10
0
0
10
20
30
40
50
S/N input
(db)
1 - Shannon's Limit (Develet)
2 - Optimal Phaselock Receiver (Develet)
3 - Second Order Phaselock Receiver (Develet)
4 - FMFB with RC Filter (Heitzman)
5 - Second Order Phaselock Receiver with Noiselike Modulation (Choate & Sydnor)
6 - Second Order Phaselock Receiver (Heitzman)
7 - Second Order Phaselock Receiver with sinus. modulation (Choate & Sydnor)
8 - Conventional FM (Heitzman)

Figure 7.3 also shows other curves by Heitzman for comparison. For example, No. 8 represents the threshold for a "conventional" FM receiver. Comparing No. 8 and No. 6, note the threshold improvement of the phaselocked loop over the conventional discriminator, at least above the 25 db output S/N ratio. Heitzman also predicted a threshold curve for a frequency feedback system (FMFB), (No. 4) representing even more threshold improvement over the conventional discriminator.

As mentioned previously, Develet [15] has completed much theoretical research on this subject. To calculate a threshold expression, Develet first developed a theoretical expression to determine when the phase error was actually at threshold. To do this, he used a quasi-linearization technique due to Booton. Develet's equations only hold true for the non-linear phase detector, but it is assumed that the expressions can be used to represent the linear detector without too much error. Develet developed the expression for S/N output as:

$$(S/N)_{out} = 2\,\Delta\,\Phi_m^{\,2}(S/N)_{in}/\exp.(\Delta\,\Phi^2) \tag{7.7}$$

where; (1) S/N = signal to noise ratio in db

(2) $\Delta\Phi_m$ = phase error due to modulation

(3) $\Delta\,\Phi$ = phase error due to modulation and noise

Develet then calculated from this expression, the value of $\Delta\,\Phi^2$ that would yield minimum (S/N) input ratio. He found the value of $\Delta\,\Phi^2$ to be 1.01 rad.^{2} Substituting this value back in equation 7.7 yields the following threshold expression:

$$(S/N)_{out} = 4.08(S/N)_{in}^{1/5} \tag{7.8}$$

Develet also developed the threshold equation for Shannon's limit on information flow, as:

$$(S/N)_{in} = \frac{1}{2}\,\log_e\,(1 + (S/N)_{out}) \tag{7.9}$$

Develet's equations as expressed in 7.8 and 7.9 were also plotted in Figure 7.3, along with his curve for an optimal receiver. Note that curves No. 3 and No. 6 represent the same second order phaselocked loop. However, Develet's curve should be less in error, since he calculated the magnitude of $\Delta\ \overline{\phi}^2$ to cause unlocking. Heitzman on the other hand assumed a value for $\Delta\ \phi^2$. (Note that the difference between the two curves is 10 log 1/.25 = 6 db.)

It can be expected that the experimental curve for the linear phase detector should lie somewhere between Shannon's limit curve No. 1 and the conventional discriminator curve No. 8, possibly close to Develet's curve No. 3.

7.1.2 Experimental Threshold Observations:

7.1.2.1 Measurements: In order to obtain any threshold curve experimentally it is necessary to measure both the input and the output S/N ratios. This has to be done by measuring a series of these values for several magnitudes of modulation index, as explained in section 7.0. With the proper equipment, these measurements should not be difficult to obtain in the laboratory. However, a radio frequency shielded room was not available, and a true RMS voltmeter with a frequency response to dc could not be obtained. This caused many problems.

A block diagram of the equipment used in the threshold experiment is shown in Figure 7.4. A transmitter and a noise generator were connected through a 50 ohm three-way matching pad to the input of the receiver. (Note that the output of the transmitter could be attenuated.)

The method used to obtain the necessary data for plotting the threshold curves is explained in detail below:

(1) The noise generator output was adjusted for a noise figure of 18.5 db. This value of noise figure simulated closely the magnitude of Galactic noise at the operating frequency. Mueller [16] discusses the relationships between Galactic temperature and frequency. Using a value of 20,000^{o} K from Mueller's curves, the conversion procedure to a noise figure is explained in Appendix I.

(2) The signal frequency deviation was set at one particular value, such that readings could be obtained for each of the five bandwidths under consideration. The system was then locked.

(3) The output from the transmitter, which was modified identically to the one in Uranium City, was established at .182 V rms across a 50 ohm output impedance. By means of the controllable fixed and variable attenuators, the signal was reduced and calculated at the input to the receiver.

Fig. 7.4

Block diagram of equipment used in determining FM thresholds

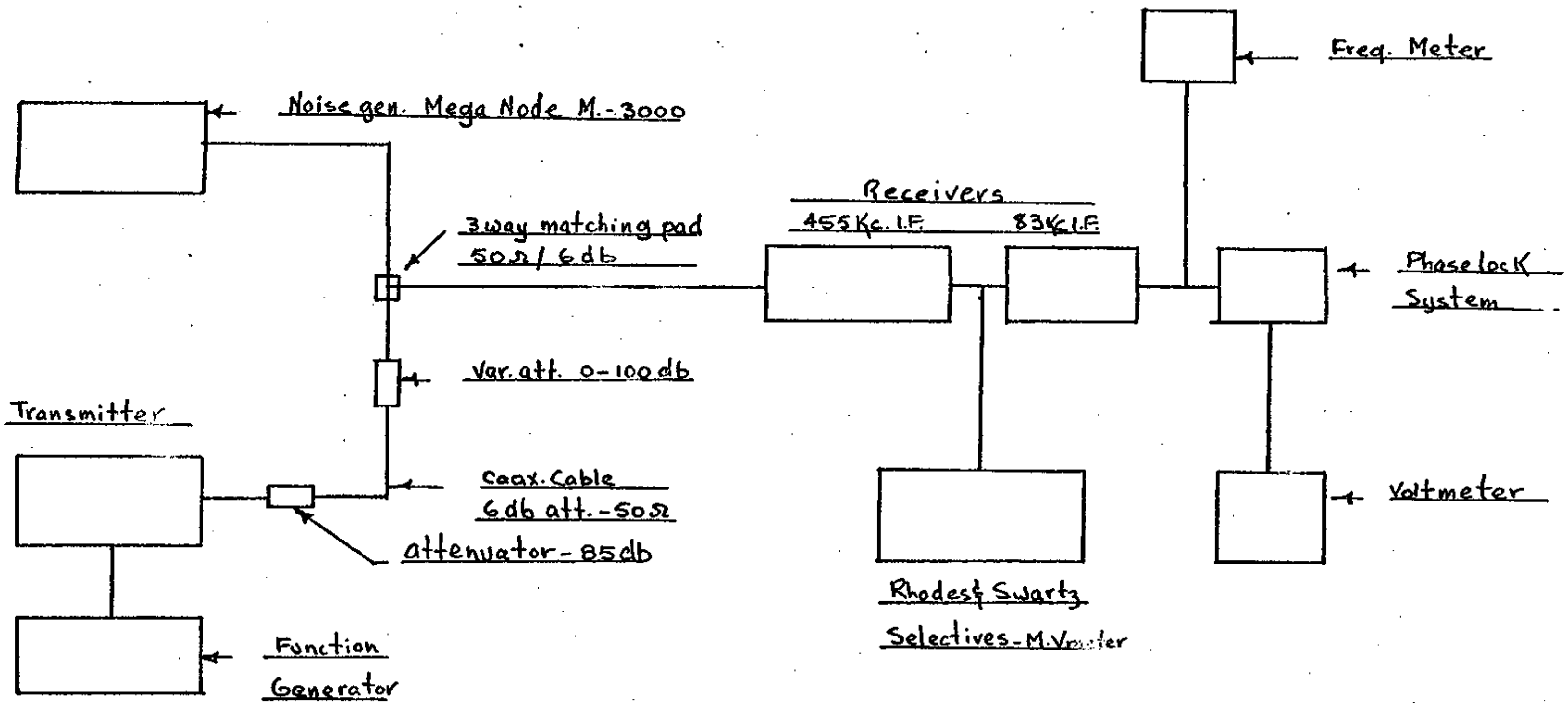

(4) The noise voltage across 50 ohm was next calculated as shown in Appendix J. Since both the noise and signal voltage were then known, the input S/N ratio could be easily obtained.

(5) The frequency deviation was measured at the 83.8 Kc IF carrier frequency. Using square wave modulation at a frequency of .1 cps, the deviation was obtained by a standard frequency meter. The modulating signal was derived from an Exact function generator.

(6) The carrier was then modulated sinusoidally such that a deviation equal to that in (5) was produced at a frequency of .5 cps, a frequency considered low enough so as not to change the magnitude of the phase error, $\Delta \Phi_m$, when switching from one bandwidth to another.

(7) The modulation index M (or in this case, the deviation ratio) was established.

(8) The output signal and noise voltage (rms) was measured. To read the rms value of the signal and noise, a thermocouple voltmeter preceded by a dc amplifier was used. Although the readings fluctuated at the lower noise frequencies, an attempt was made to obtain some average indication. (For one particular value of M, the output signal voltage level remained constant as expected, but some signal depression was noted in the 100 cps bandwidth.)

(9) The carrier input signal was attenuated stepwise until "unlocking" occurred. This unlocking point was taken to be the threshold.

(10) With the modulation removed, the rms noise output voltage was measured next. The output S/N ratios were then calculated.

(11) The experiment was repeated for a different value of M and also for different bandwidths.

The resulting curves are shown in Figures 7.5 to 7.9, inclusive. The threshold curve was obtained by drawing a line through the "unlocking" points on each M curve.

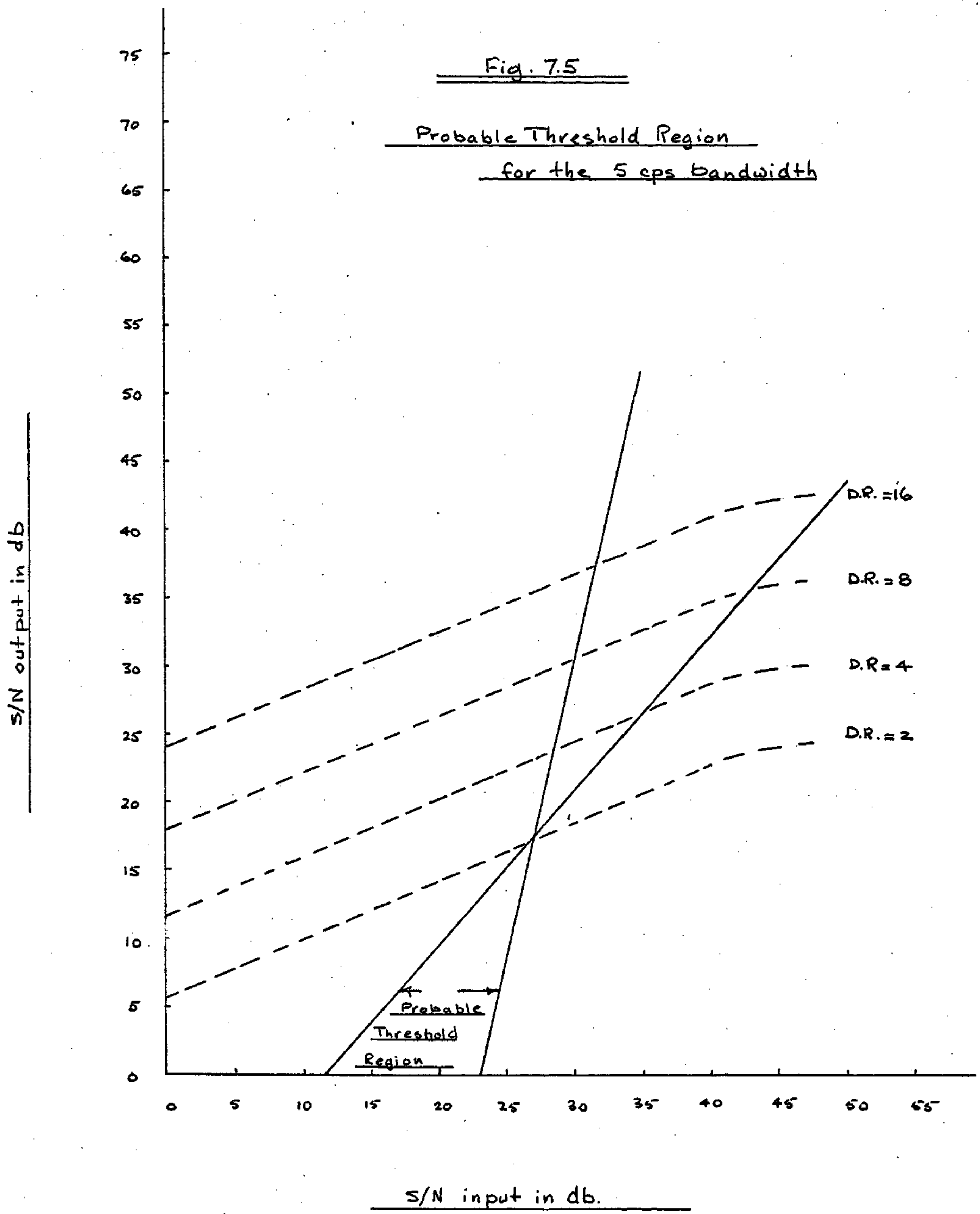

Fig. 7.5
Probable Threshold Region
for the 5 cps bandwidth
D.R. = 16
D.R. = 8
D.R = 4
D.R. = 2
Probable
Threshold
Region
S/N output in db
S/N input in db.
0
5
10
15
20
25
30
35
40
45
50
55
60
65
70
75

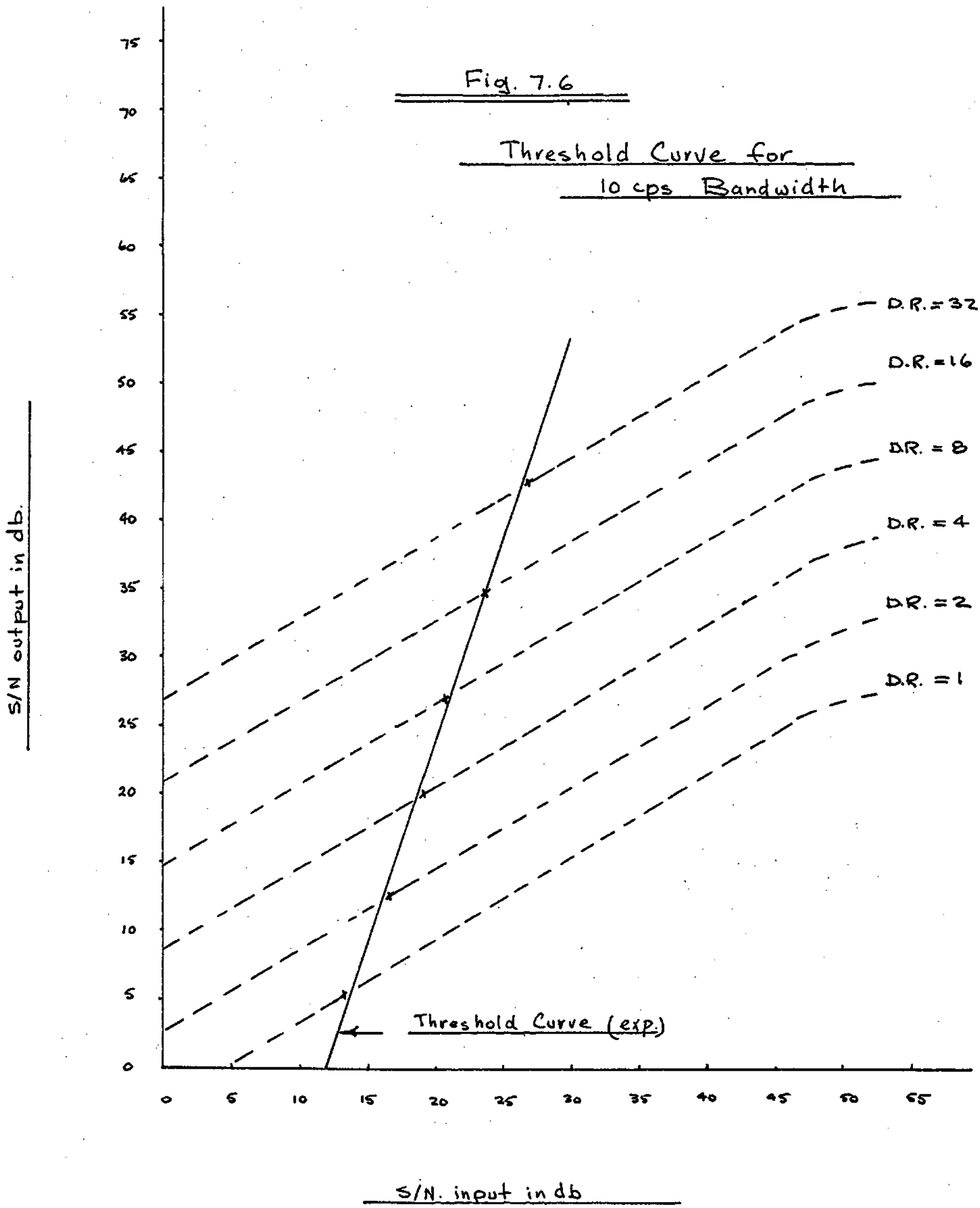
Fig. 7.6
Threshold Curve for
10 cps Bandwidth
D.R. = 32
D.R. = 16
D.R. = 8
D.R. = 4
D.R. = 2
D.R. = 1
Threshold Curve (exp.)
S/N output in db.
S/N. input in db
75
70
65
60
55
50
45
40
35
30
25
20
15
10
5
0
0
5
10
15
20
25
30
35
40
45
50
55

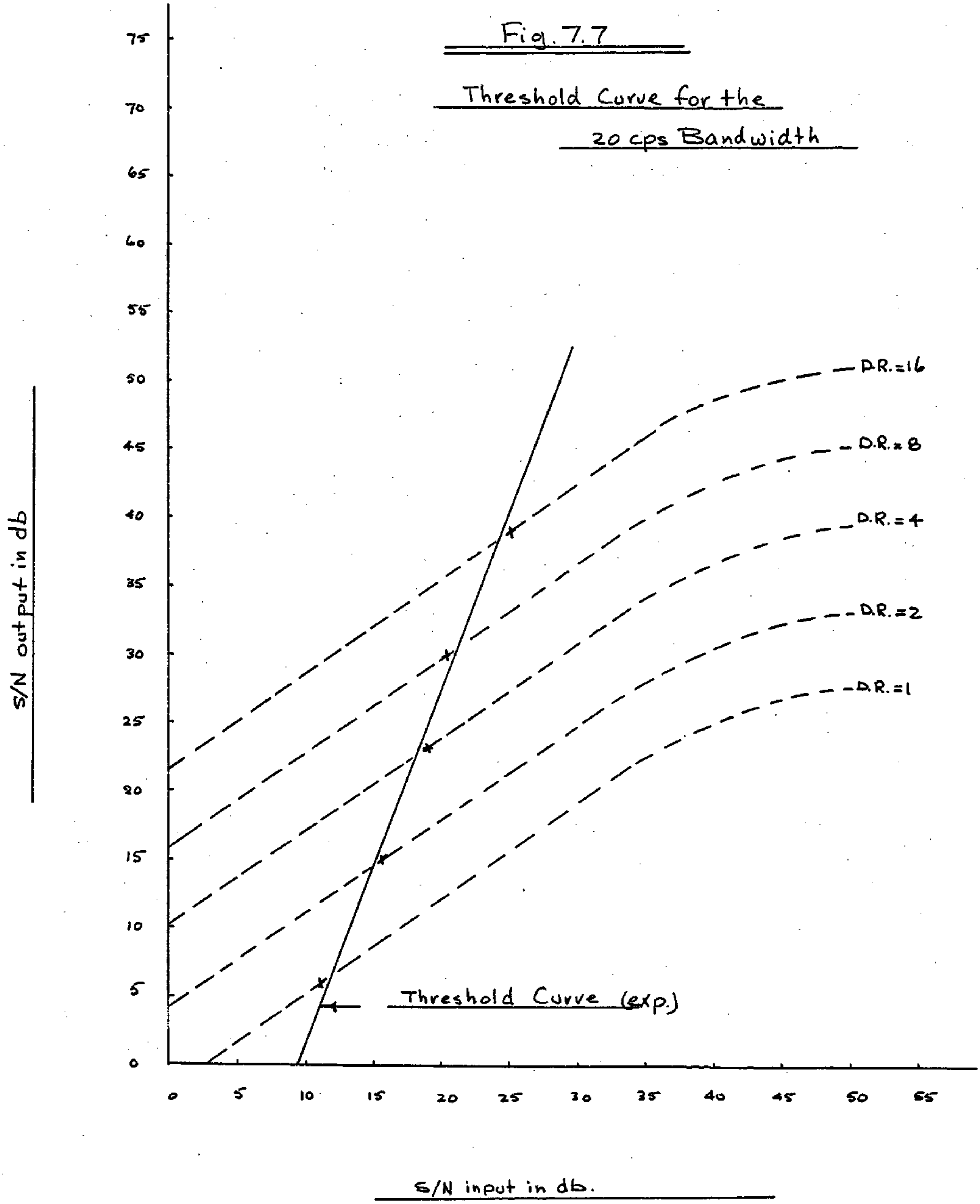
Fig. 7.7
Threshold Curve for the
20 cps Bandwidth
S/N output in db
S/N input in db.
D.R.=16
D.R.=8
D.R.=4
D.R.=2
D.R.=1
Threshold Curve (exp.)
75
70
65
60
55
50
45
40
35
30
25
20
15
10
5
0
0
5
10
15
20
25
30
35
40
45
50
55

Fig. 7.8

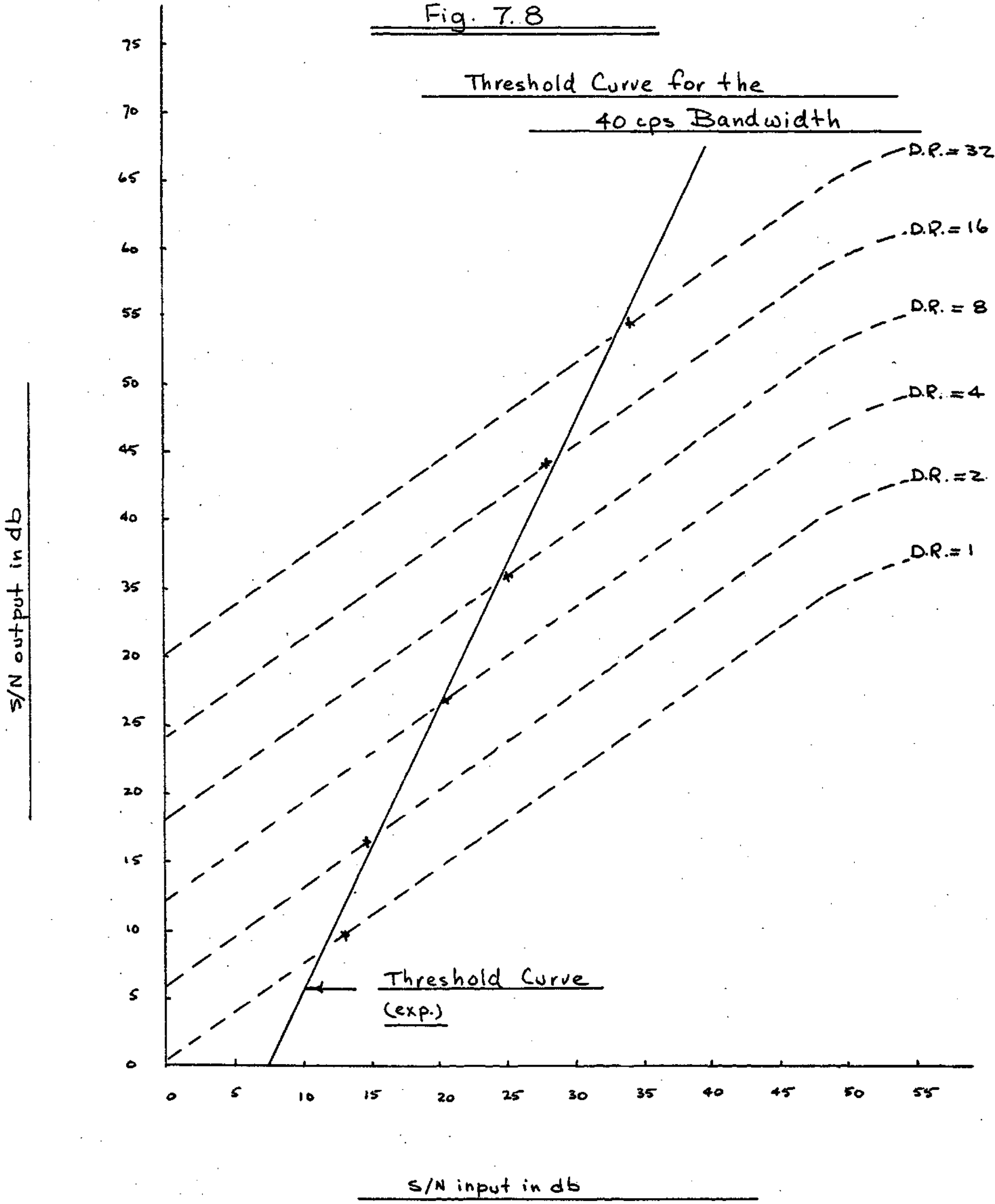
Threshold Curve for the
40 cps Bandwidth
D.R. = 32
D.R. = 16
D.R. = 8
D.R. = 4
D.R. = 2
D.R. = 1
Threshold Curve
(exp.)
S/N output in db
S/N input in db
0
5
10
15
20
25
30
35
40
45
50
55
60
65
70
75

Fig. 7.9

Threshold Curve for the 100 cps Bandwidth

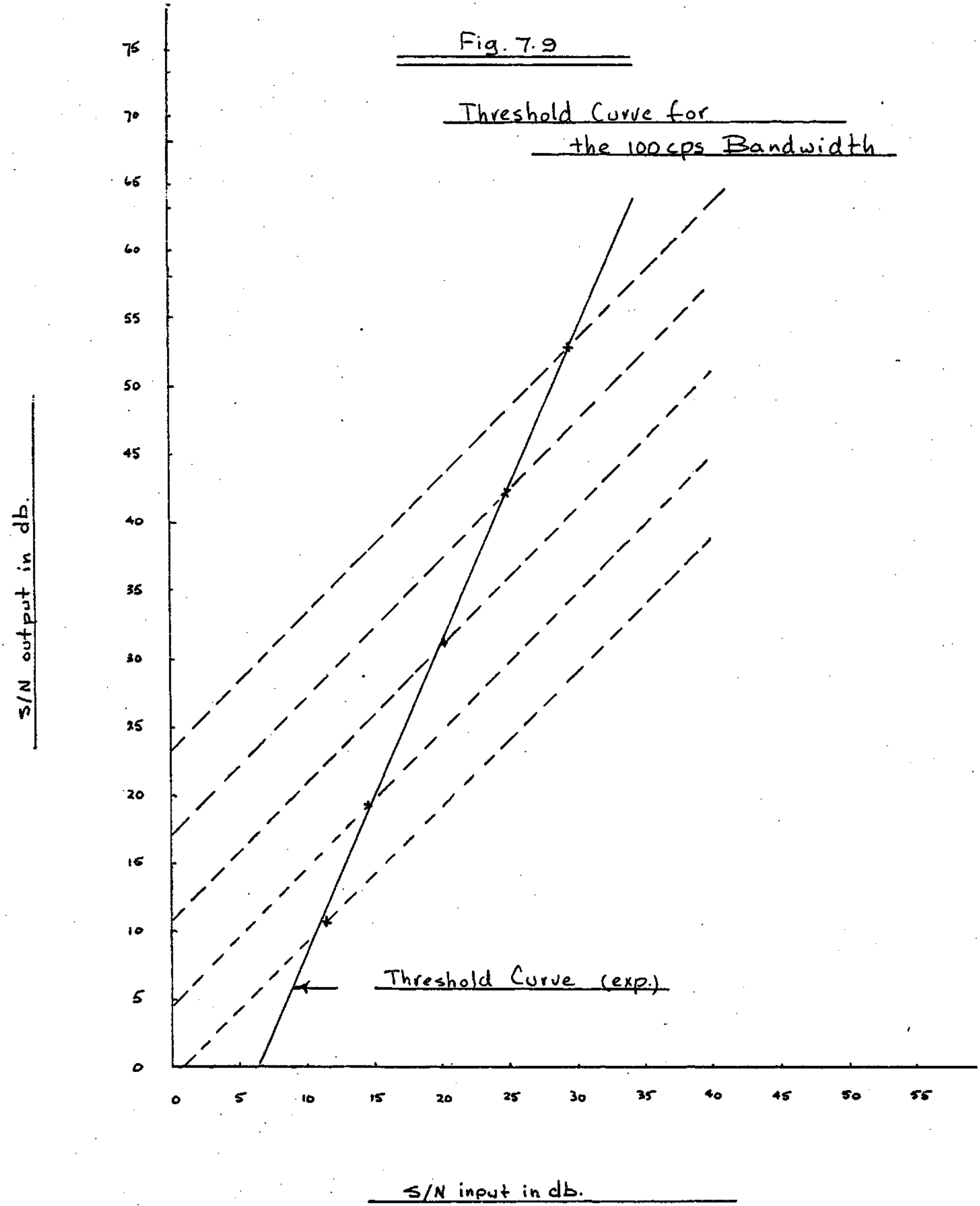

Before discussing the curves in detail, some of the problems involved in obtaining the measurements are discussed.

First of all, it was difficult to decide when "unlocking" occurred. However, after many attempts a procedure was developed:

(a) If the carrier was modulated sinusoidally, then with the system "locked," the modulating wave form could be seen at the phase detector output. As soon as this sinusoidal wave disappeared momentarily, unlocking (or threshold) was said to take place.

(b) If the receiver was not modulated, the only output was a noise-like wave form riding on a dc voltage level. By manually changing the frequency of the voltage controlled oscillator, the dc level could be raised or lowered until unlocking occurred.

Secondly, a radio-frequency shielded room was not available. This constituted quite a problem, since much stray radiation existed between the transmitter and the receiver when they were located near each other. Independent of the amount of attenuation used, the phase detector could not be unlocked.

As a result, the transmitter was removed into another laboratory, and connected to the receiver by 400 feet of 8-AU-50 ohm coax. cable. This accounts for the 6 db loss of the coax. cable shown in Figure 7.4.

However, some stray radiation must have remained because when the threshold curves were plotted, they indicated a slight improvement over Shannon's limit curve.

To correct this, the signal and noise were measured by means of a wave-analyzer (narrow band voltmeter), at the IF output from the first receiver.

Since the bandwidth of this voltmeter was 500 cps and the frequency response within the bandwidth was quite flat, the noise voltage was converted to a noise density in volts/cps. Knowing the signal bandwidth, it was then reconverted to a noise voltage. It should be noted that the receiver noise was assumed to be negligible compared to the input noise, since the noise figure of the receiver was quite low.

The signal could be read directly by this voltmeter, which indicated the true value, independent of stray radiation.

The input S/N ratios were then recalculated and the necessary corrections made to the threshold curves. This brought them more in line with expectations. Had an rf shielded room been available, this correction procedure would not have been necessary.

7.1.2.2 Discussion of the Experimental Threshold Curves: Considering first of all the curve for the 100 cps bandwidth, note that the individual M curves are at a slope of 45^{o}, as expected for white Gaussian distributed noise. Note also that the individual M curves are parallel. This is because only the signal changed (directly) with M, but the noise remained constant.

However, note with the lower bandwidths, the M curves reduce in slope and also tend to flatten out at the higher input S/N ratios. (See Figures 7.5 and 7.6.) The reduction in slope of the M curves, especially for the 5 cps bandwidth, is believed to be due to the noise spectrum at the lower frequencies, which is expected to be somewhat as shown in Figure 7.11.

If the 45^{o} slope is based on the spectrum being flat, then with a spectrum such as in Figure 7.11, an error will be introduced into the slope. Since the output S/N ratio depends on the noise power, and since the area under the curve in Figure 7.11 represents this noise power,

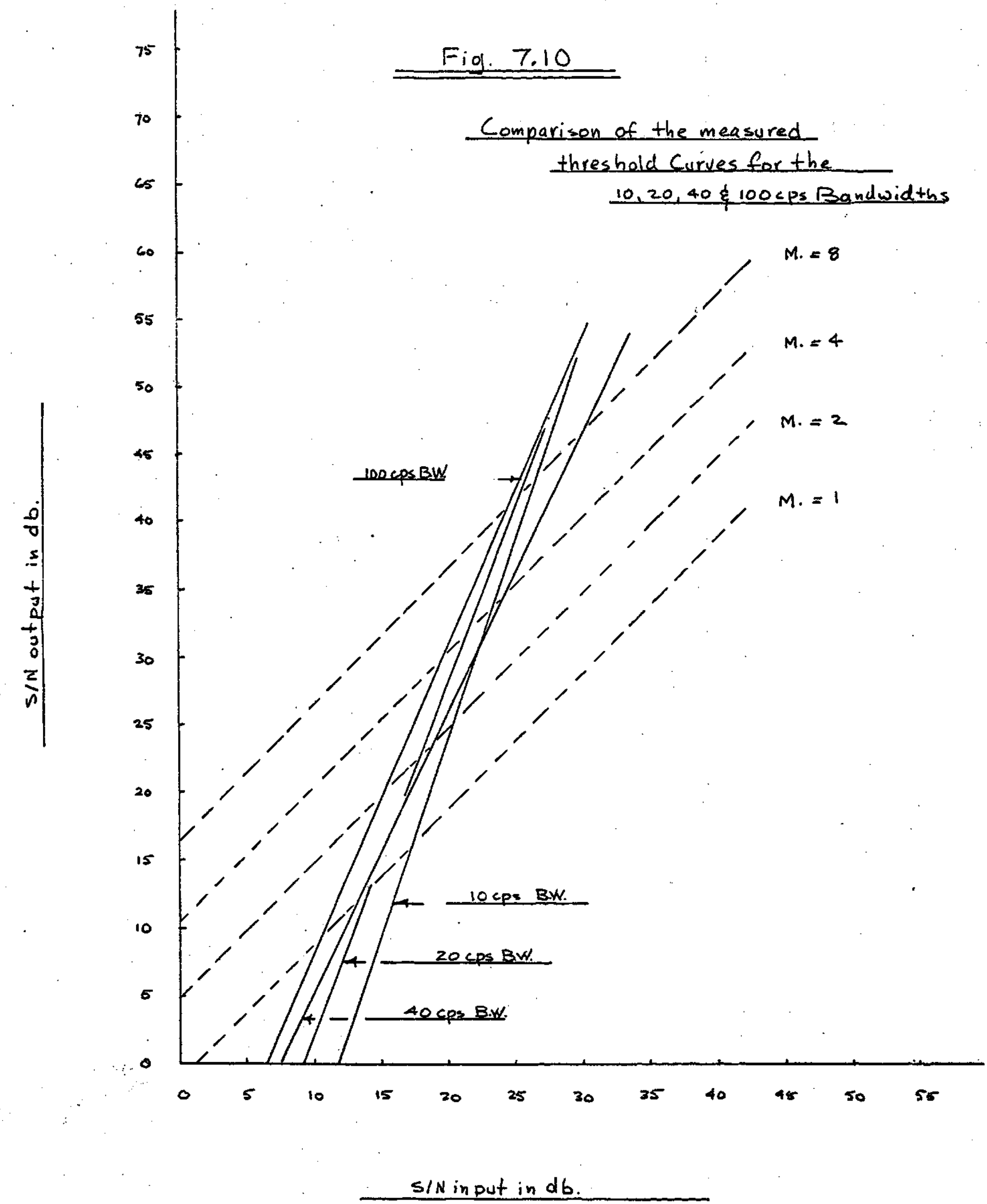
Fig. 7.10
Comparison of the measured threshold Curves for the 10, 20, 40 & 100 cps Bandwidths
M. = 8
M. = 4
M. = 2
M. = 1
100 cps BW
10 cps B.W.
20 cps B.W.
40 cps B.W.
S/N output in db.
S/N input in db.
0
5
10
15
20
25
30
35
40
45
50
55
60
65
70
75

Fig. 7.11

Possible Noise Frequency Spectrum at the Input to the Receiver.

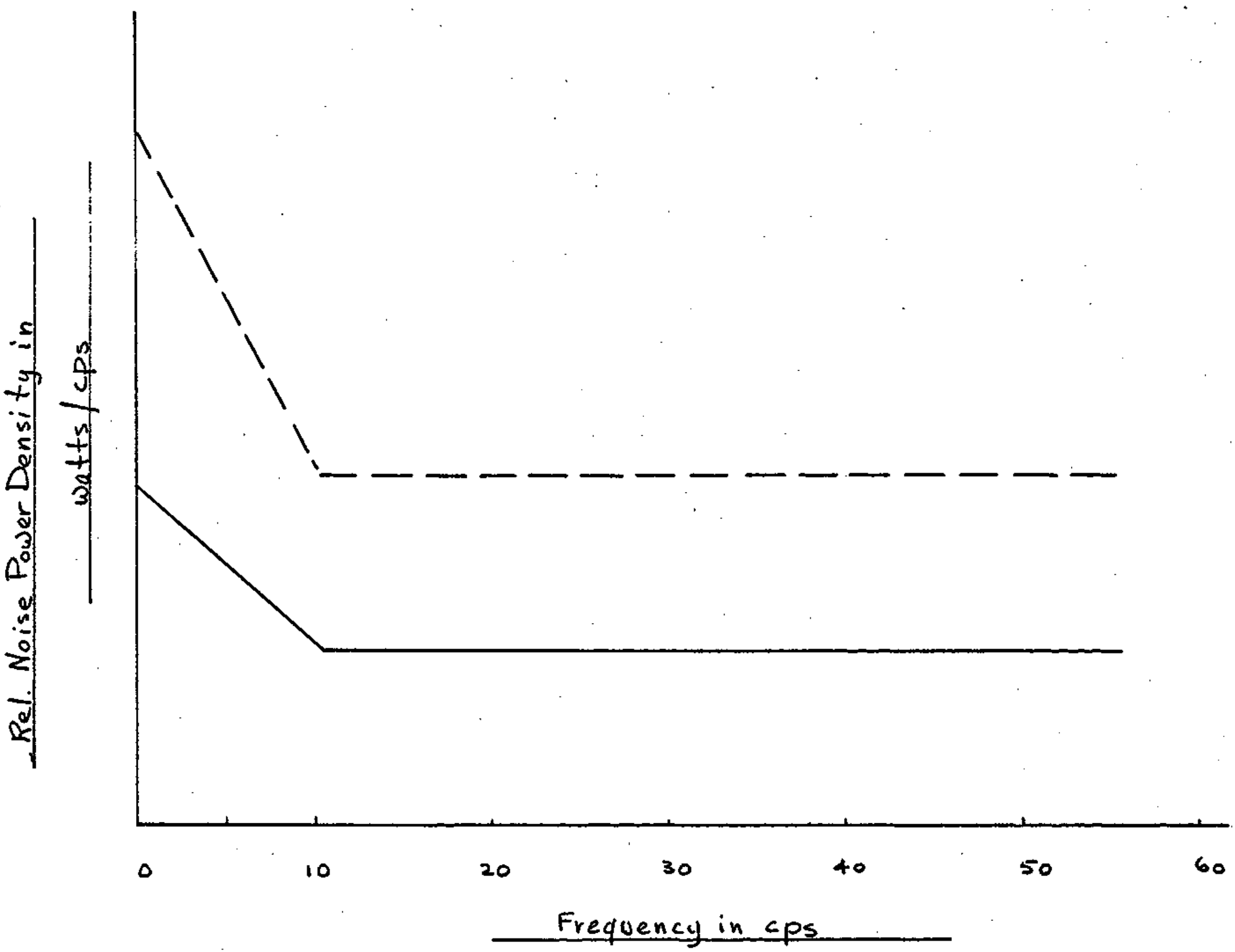

then the error in the slope of the line is a function of the error in the area under the curve. The error in the area represents an increase in noise power, and is also a constant error for a particular bandwidth. Consequently, the slope of the M curves will be less than 45^{o}, with a constant error. Since for the smaller bandwidths, this error in area is of a greater magnitude, one can expect the error in the slopes to be larger also.

The reason for the tendency of the M curves to flatten out at the higher input S/N ratios is due to the fact that the output noise could not be reduced in magnitude below a certain value, independent of how much input signal attenuation was used. (See step No. 10 in section 7.1.2.1.) Since for each M curve, the signal remains constant, the noise was the only factor affecting output S/N ratios. This remaining noise was probably produced within the system itself, and since it occurred within the bandwidth, it could not be filtered out.

Due to voltmeter reading fluctuations, it was very difficult to obtain a curve for the 5 cps bandwidth. It is believed that .5 cps modulation frequency is still too high for the 5 cps as well as the 10 cps bandwidth, so that unlocking occurred sooner than in the other bandwidths. This fact is explained by the relationship between the phase error, and the network ratio α , which is greatest for the 5 cps bandwidth. (See section 6.1.) However, a lower modulation frequency could not be used since the high pass filter has a cut-off frequency of .1 cps. Although a high pass filter was inserted at the output stage, (.1 cps), the low-frequency noise still occurred within the closed servo loop. This definitely had an effect on the unlocking of the system. Therefore, the threshold curve for the 5 cps bandwidth has been replaced by a threshold region.

The threshold curves for the 10 cps to the 100 cps bandwidths were replotted in Figure 7.10, for comparison purposes. Note that the 10 cps bandwidth curve shows the least correlation with the rest of the curves. This again is believed to be due to the high modulation frequency.

Comparing the curves in Figure 7.10 with the theoretically predicted curves in Figure 7.3, observe that close correlation only occurs for output S/N ratios below 20 db. All the experimental curves tend to have lesser slope. Had the slope of the experimental curves been steeper, then they would have closely resembled Develet's curve No. 3. Considering the difficulties experienced in obtaining the data, the curves correspond well within experimental error.

At this stage, a few conclusions can be drawn about the behaviour of the system.

(1) The system described in this thesis is nearly as good as theoretically predicted.

(2) One can now predict what values of modulation frequency and frequency deviation should be used to obtain a certain value of S/N output.

(3) One can predict what the threshold S/N input ratio should be for the larger IF bandwidth, without taking Doppler shifts into account. (See Table 7-II and Appendix J.)

(4) If the system does not operate as expected in the field, the phase detector should not be the cause. (Not considering Doppler frequency shifts.)

7.2 Field Test Discussion

7.2.1 Field Test Preparation: Although some limited field testing was completed before the threshold tests were made, the results were not very encouraging. This was one of the reasons why the threshold property was so extensively examined.

To field test the system, the following procedure was used:

(1) With the transmitter at Uranium City, an Exact function generator was adjusted to produce a frequency deviation of 20 cps. (For example, the deviation selection switch shown in Figure 2.2 was set to the No. 4 position.)

(2) The modulation frequency from the function generator was adjusted to .5 cps.

(3) With the receiver placed at a location just outside of Saskatoon, the 455 kc IF signal output was recorded so that an indication could be obtained about the input S/N ratio in the 2300 cps IF bandwidth.

(4) The system signal output was recorded separately to indicate the modulation wave form when the receiver was "locked." Since the modulation was switched off periodically, an indication of the output noise could also be obtained. Consequently, the S/N output ratio could be calculated.

(5) In order to observe locking and unlocking, an oscilloscope was used to view the phase error, $\Delta \Phi_m$, and to examine the output wave.

The operator at Uranium City was supplied with an operating and maintenance instruction brief. He forwarded a transmitter measurement log sheet once a month.

7.2.2 Field Test Observations: Figures 7.12 to 7.15 are reproductions of actual recordings made. Figure 7.12 shows the IF output from the receiver. On this recording, the transmitter breaks are clearly visible. This recording, which shows some signal enhancement, is a typical one.

A correlation between the time of unlocking in the 20 cps output signal bandwidth and the level of S/N ratio of the IF recording indicated that unlocking generally took place as soon as the IF S/N ratio decreased below +1 db. Theoretically, unlocking was to take place at -10 db in the IF bandwidth. (See Table 7-II.) This left a difference of 11 db to be explained.

Locking occurred only sporadically and many days and nights were spent at the receiving site, only to have to wait hours to obtain a clear indication of locking and unlocking. The fact was that locking never did take place, unless the signal could be observed in the IF bandwidth, and only then occasionally. It is estimated that the total locking time was probably less than 5 per cent of the total operation time.

Figure 7.14 shows the modulation recorded at the system output during a period of locking. When the modulation was switched off at the transmitter site, it was difficult to tell whether the system was locked or unlocked, making it very difficult to calculate correctly the output S/N ratio. A modulation recording taken over several hours is shown in Figure 7.15. The larger spikes indicate when locking occurred.

Although Koehler [2] indicated that the system could be locked on some bandwidths during periods of low enhancement, or even absorption, this was not reobserved at any time on any of the five signal bandwidths. The probable reasons for the above peculiarities are discussed in the following chapter.

Fig. 7.12

Recorder Calibration

Unlocking occurs at +1db-S/N in the 20cps BW.

+1db

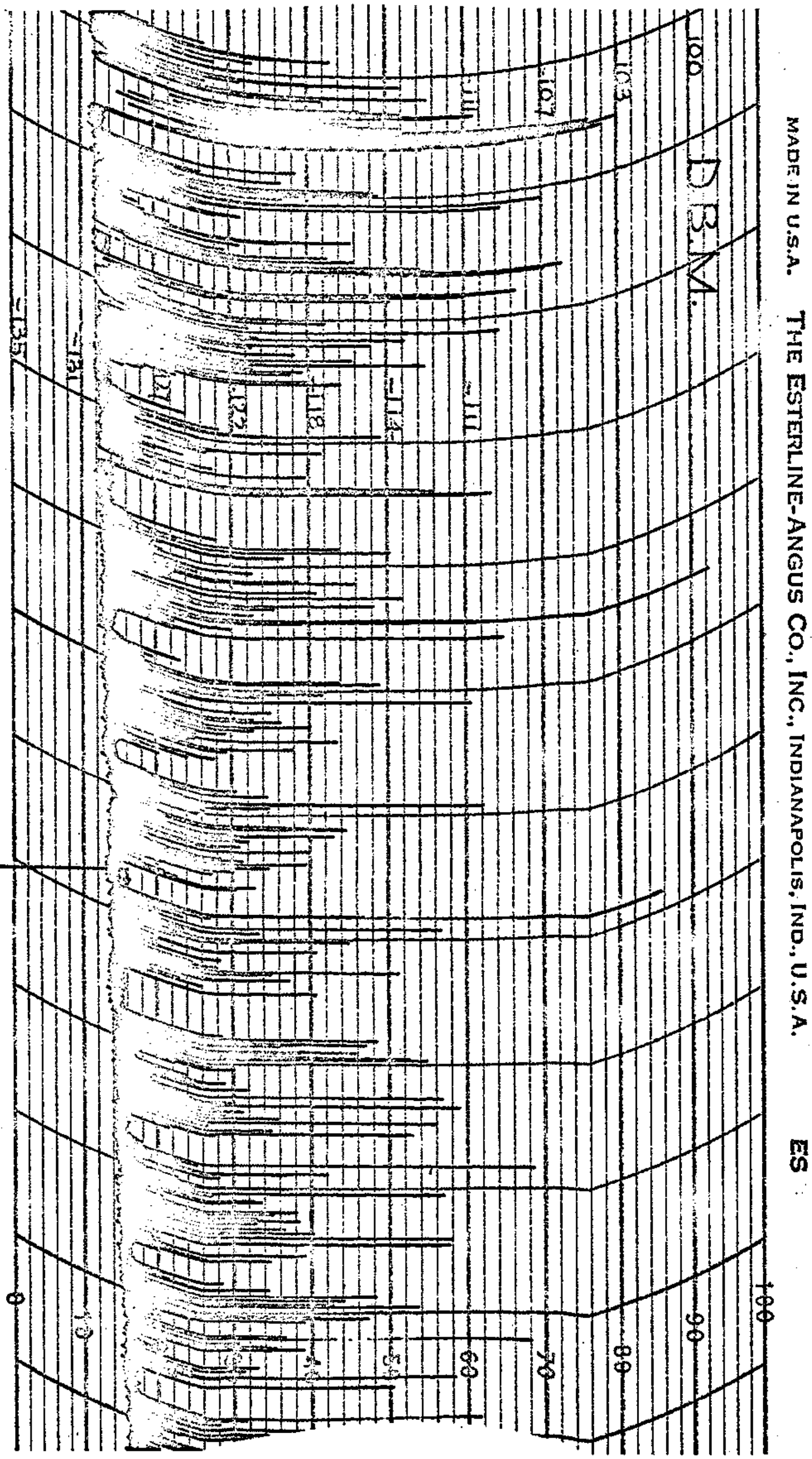

Fig. 7.13

Receiver noise & Galactic Noise Recording

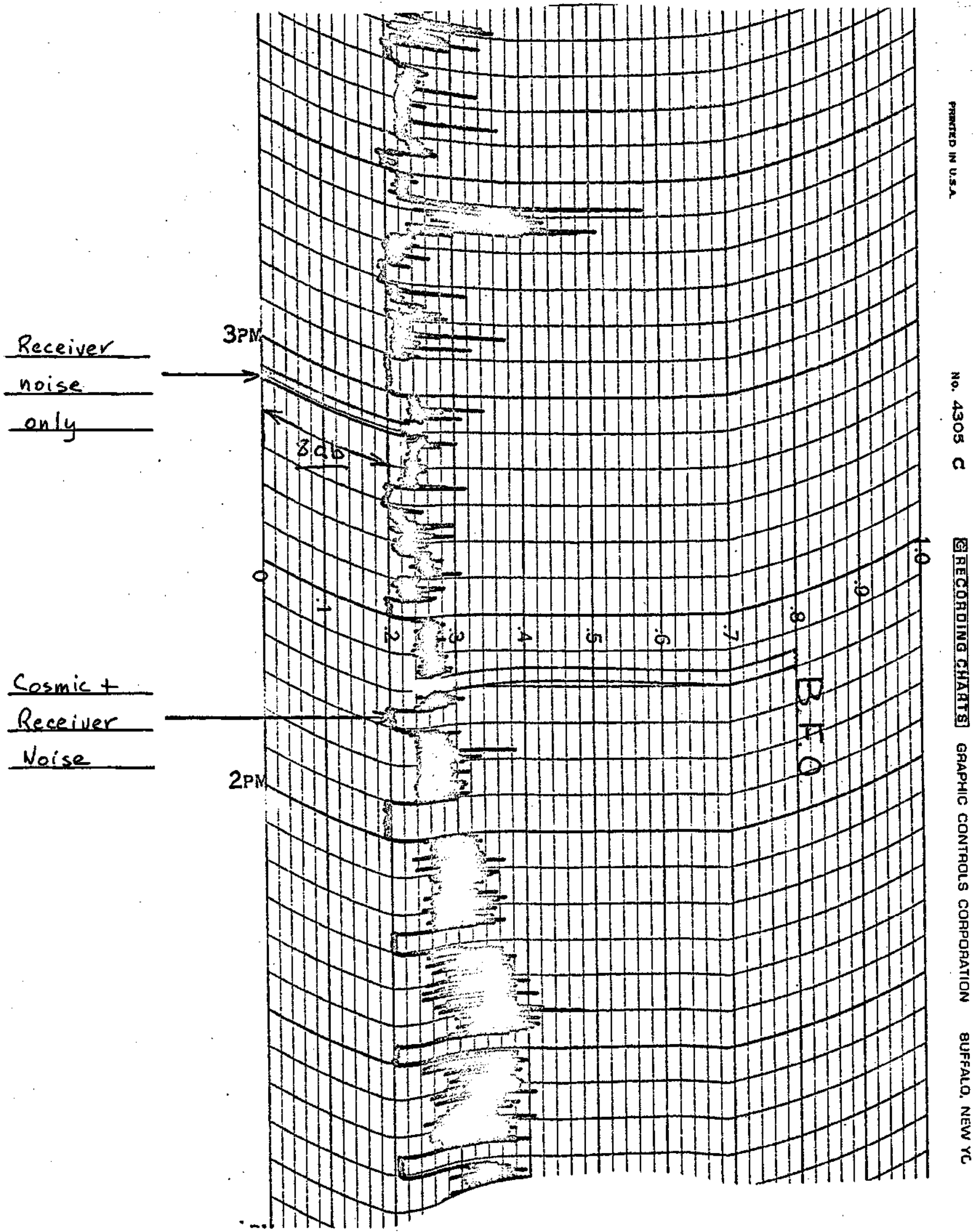

Fig. 7.14

Modulation Recording

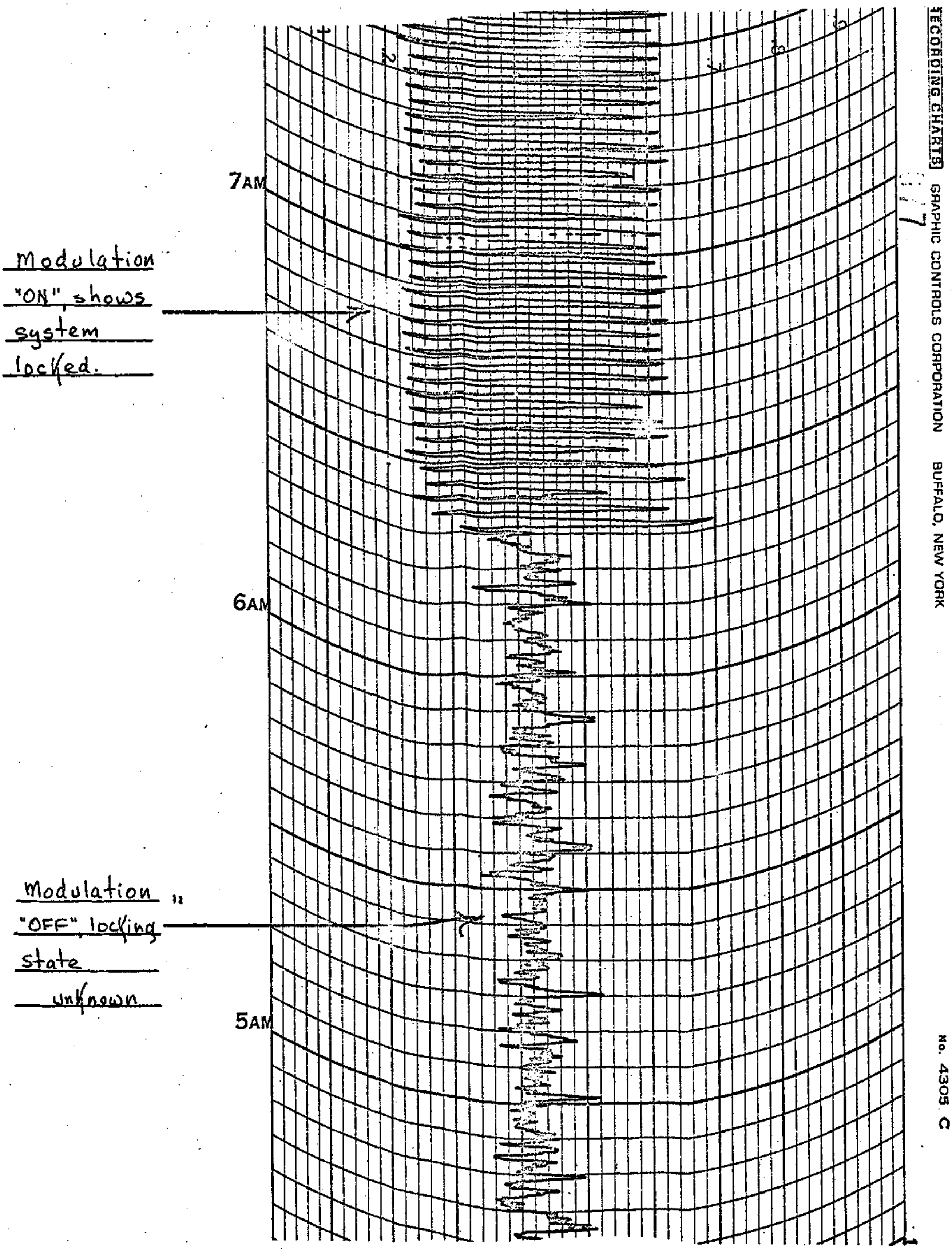

Fig. 7.15
Recording Showing the System Modulation (5 hours - typical)
This recording was made during a period of low enhancement

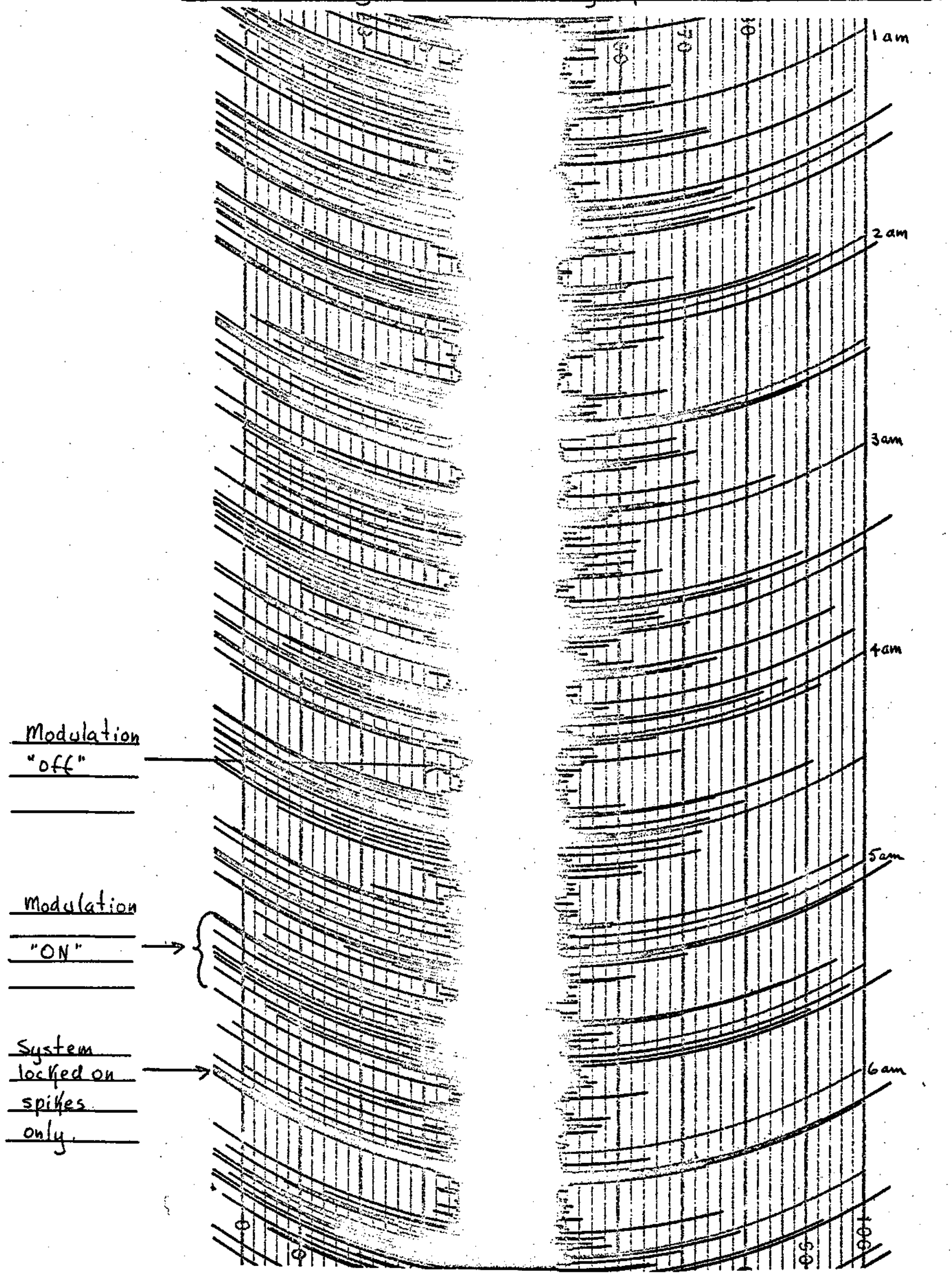

TABLE 7 - II

Frequency Deviation in Cycles/Second	Detector Bandwidth in Cycles/Second	Modulation Index	Threshold S/N Input in Detector Bandwidths	Expected Threshold S/N Input in IF Bandwidths
20	5	4	22 db	- 5 db
20	10	2	16 db	- 8 db
20	20	1	11 db	-10 db
20	40	1/2	8 db	-11 db
20	100	1/5	5 db	-11 db
40	40	1	12 db	- 7 db
50	100	1/2	8 db	- 8 db

VIII. CONCLUSIONS AND RECOMMENDATIONS

8.0 Conclusions

Although the operating results were negative, this by no means indicates that the system cannot be made to work. During the course of the experiment, many new ways of tackling the original problem, as defined in section 1.0, were discovered. However, the point remains that Koehler stated that his system did operate and the work in this thesis was to be a continuation of his experiments. Therefore, the reasons why Koehler's observations could not be verified are discussed at this time.

There is only one reason why the system should not lock and this is that the input S/N ratio is not large enough to cause the system to lock and remain locked. Two possible reasons for this are discussed below:

(1) The S/N ratio was similar to what Koehler experienced, but the detector system was not as good.

(2) The system was similar, but the S/N ratios were smaller.

The second possibility may be caused by several conditions:

(1) Different geometry of propagation.

(2) Different frequency of operation.

(3) Different ionospheric conditions.

(4) Non-clearance of the first Fresnel zone.

Koehler operated between Fort Smith and Saskatoon, which is a distance of 650 miles, compared to 528 miles between Uranium City and Saskatoon. At the same time, Koehler's operating frequency was 40.5 Mc compared to the 36.78 Mc used in this experiment.

In a paper written in 1955 by Bullington [17] the dependence of signal attenuation on frequency and distance are discussed for tropospheric and ionospheric scattering. According to Bullington, ionospheric scattering is not much dependent on distance, but extremely frequency sensitive. He claims that for distances from 400 to 600 miles, a gradual transposition takes place from tropospheric scattering to ionospheric scattering, but that no drop outs have been observed.

From Bullington's observations, it can be concluded that the lower operating frequency should have decreased the signal attenuation. On the other hand, the reduction in distance may have increased the signal attenuation. In addition, scattering may have been of a tropospheric nature; although this is unlikely since there were tropospheric propagation path obstructions.

Bailey [1] stated that distances under 2,000 km are not very useful for VHF ionospheric scattering. He also indicated that distances below 620 miles definitely should be avoided. Although it could not be determined exactly what did happen with the shorter distance, it is quite likely that the incoming S/N ratio was smaller for a larger part of the time than was the case in Koehler's experiment. This would explain why Koehler could lock his system more often.

It was observed from Koehler's records that S/N ratios of 60 db were recorded at times, suggesting forward scattering due to auroral ionization. Koehler's tests took place during a period of maximum solar activity.

Possible interference of ground obstacles with the first Fresnel zone was also examined. With the aid of a map obtained from the Department of Mines and Technical Surveys (Preliminary map 54-15 -- sheet 2 -- Uranium City), all possible propagation path obstructions were checked. The most serious obstruction was found to exist at a height of 950 feet above sea level at a distance of 1,200 feet from the transmitter. The radius of the first Fresnel zone, which contains one quarter of the total transmitted power, was calculated to be 180 feet. This left a clearance of 187 feet.

However, the presence of other antennae and housing facilities in the area may well have had an adverse effect on the transmission pattern, thereby further reducing the received S/N ratios.

The first possibility, that of the system not being as good as Koehler's, needs further consideration. It was established in section 7.1.2 that the system was nearly as good as the theoretical expressions had predicted. However, there was one large difference between the laboratory operation and the actual field operation, and that was the presence of Doppler frequency shifts in the latter case. Doppler shifts can be regarded as noise. Koehler indicated that the signal spread was approximately 10 cps. However, the rates at which these Doppler shifts take place have not been determined. It is this rate that causes FM noise, and, therefore, it is the rate along with the amount of deviation, that may cause unlocking to occur sooner than expected. This is mainly due to the magnitude of the network ratio α , which is dependent on lock range as well as bandwidth. Koehler stated that he could not lock his system often in the 5 cps bandwidth. It is also a fact that α was the greatest for the 5 cps bandwidth. Since this system used a larger lock range, with a larger magnitude of α , the Doppler effect probably was more of a contributing factor.

Since Koehler did not state that the IF S/N input ratio was -10 db at unlocking, it may very well have been larger, but still negative (say, -3 db), so that during periods of absorption, locking still was possible.

Therefore, the smaller lock range seems to have the advantage as far as threshold is concerned. But due to frequency instability, it could not be used. Presently Koehler's network is being reconstructed, and the above conclusion will be verified one way or the other. The transmitter at Uranium City is in need of repairs, thereby eliminating chances for a speedy verification.

If the conclusion regarding Doppler shifts is correct, then this will bring up another point. Since the spectral spread of the signal, as concluded by Koehler, was probably determined from measurements of the phase error, then the spectral spread will also be a function of the lock range. Therefore, the conclusion drawn by Koehler regarding spectral spread may have been in error.

In summary, the two reasons for the difference in the previous and present locking observations are:

(1) The S/N input ratio was probably not as large as before over the same period of time, thereby reducing the total locking time.

(2) If no Doppler shift had been present, the threshold curves would likely have shown the improvement expected from the theoretical examination. Presently Doppler shifts tend to increase the threshold S/N ratios by several db.

Although the present system is not practical for the intended use, an extensive analysis was made of the system itself which should prove very useful, and the knowledge gained can be applied directly in the future.

8.1 Recommendations

In order to continue the present line of research, several new approaches can be taken to arrive at meaningful results.

As a result of the work done by the author, new ideas have developed, and the following recommendations are presented to establish either a new line of research or a different method of handling the existing problem.

(1) Ultrastable Oscillators Should Be Obtained. (Frequency stability 1 in 10^8.) With these oscillators placed in the transmitter or used as a VCO, similar systems with a much smaller lock range can be built. On the other hand, the present filter can be replaced by a special filter, to eliminate the effect of non-linear phase changes. This will make the use of higher modulating frequencies possible and will reduce the effect of Doppler shifts.

(2) A Radio Frequency Shielded Room Should Be Purchased. The use of this room will facilitate the measurement of threshold data. Once this room is obtained possibly the curves in Figure 7.5 and 7.10 should be replotted.

(3) Further Tests On The Present System. Due to the fact that some propagation path obstructions may exist, the transmitting antennae should be moved to a better location, possibly to the top of a hill. It would also be advantageous to have someone with a proper technical background looking after the transmitter. The experience has been that much time is lost due to trivial technical difficulties.

To increase the path length, possibly the receiver could be moved to Regina, which is located 700 miles from Uranium City. Comparisons can then be made between Regina and Saskatoon reception.

(4) New Research. According to Heitzman, [5], a frequency feedback FM system should provide threshold improvements over a phase control system. This system should be constructed and analyzed.

Once a system has been found which will remain locked for a significant period of time, not only can the communication system be completed, but also a study can be made of the low-frequency noise spectrum. This will provide valuable information, presently not available, on Doppler frequency shifts.

LIST OF REFERENCES

(1) Bailey, Bateman, and Kirby, "Radio Transmission of VHF by Scattering and Other Processes in the Lower Ionosphere" - Proceedings of the IRE, Vol. 43, No. 10; pp. 1181 - 1209; October, 1955.

(2) J. A. Koehler, "Communication by VHF Forward Scatter in and Close to the Auroral Zone" - M.Sc. Thesis, University of Saskatchewan; 1961.

(3) J. D. Kraus, "Antennas" - McGraw Hill publication; 1950.

(4) H. T. McAleer, "A New Look at the Phase-Locked Oscillator" - IRE Proceedings; June, 1959.

(5) R. E. Heitzman, "A Study of Threshold Power Requirements of FMFB Receivers" - IRE Transactions on Space Electronics and Telemetry, Vol. Set 8, No. 4; December, 1962.

(6) D. J. Schilling, "Automatic Phase Control System Response" - IEEE Proceedings, Vol. 51, No. 10; pp. 1306 - 1316; October, 1963.

(7) T. J. Rey, "Automatic Phase Control Theory & Design" - IRE Proceedings, Vol. 48, No. 10; pp. 1760; October, 1960.

(8) G. W. Preston, "Basic Theory of Locked Oscillators in Tracking FM Signals" - IRE Transactions on Space Electronics and Telemetry, Vol. Set 5, No. 1; pp. 30 - 33; March, 1959.

(9) J. P. Frazier, "Phase Lock Loop Frequency Acquisition Study" - IRE Transactions on Space Electronics and Telemetry, Vol. Set 8, No. 3; pp. 210 - 228; September, 1962.

(10) C. R. Cahn, "Piecewise Linear Analysis of Phase-Lock Loops" - IRE Transactions on Space Electronics and Telemetry, Vol. Set 8, No. 1; pp. 8 - 13; March, 1962.

(11) Viterbi, "Phase-Locked Loop Dynamics in the Presence of Noise by Fokker - Planck Techniques" - Proceedings of the IEEE, Vol. 51, No. 12; pp. 1737 - 1753; December, 1963.

(12) K. W. Chong and R. C. S. Cobbold, "A Note on Active R.C. Low-Pass Filters" - Electronic Engineering, Vol. 35, No. 425; pp. 458 - 460; July, 1963.

(13) F. E. Nixon, "Handbook of Laplace Transformation" - Prentice Hall; 1960.

(14) M. G. Crosby, "Frequency Modulation Noise Characteristics" - Proceedings IRE, Vol. 25, No. 4; pp. 472 - 515; April, 1937.

(15) Develet, "A Threshold Criterion for Phase-Lock Demodulation" - IEEE Proceedings; pp. 349 - 356; February, 1963.

(16) G. E. Mueller, "A Pragmatic Approach to Space Communication" - IRE Proceedings, Vol. 48, No. 4; pp. 557 - 567; April, 1960.

(17) D. Bullington, "Characteristics of Beyond the Horizon Radio Transmission" - IRE Proceedings, Vol. 43, No. 10; pp. 1175 - 1180; October, 1955.

(18) R. W. Sanders, "Communication Efficiency Comparison of Several Communication Systems" - IRE Proceedings, Vol. 48, No. 4; pp. 575 - 589; April, 1960.

(19) R. L. Choate & R. L. Sydnor, "Design of PM Communication Systems" - IRE Transactions on Space Electronics and Telemetry, Vol. Set 8, No. 2; pp. 117 - 124; June, 1962.

(20) G. A. Hellwarth, "On the Performance of FM Communications in the Presence of RF Noise" - IRE Transactions Military Electronics, Vol. Mil. 6, No. 4; pp. 346 - 349; October, 1962.

(21) C. R. Laughlin, "The Diversity-Locked Loop - A Coherent Combiner" - IEEE Transactions on Space Electronics and Telemetry, Vol. Set 9, No. 3; pp. 88 - 92; September, 1963.

(22) C. S. Weaver, "Thresholds & Tracking Ranges in Phase-Locked Loops" - IRE Transactions on Space Electronics and Telemetry, Vol. Set 7, No. 3; pp. 60 - 71; September, 1961.

(23) Hiroshi Okima, "Theoretical Studies on Signal-to-Noise Characteristics on a FM System" - IEEE Transactions on Space Electronics and Telemetry, Vol. Set 9, No. 4; pp. 101 - 109; December, 1963.

(24) M. G. Morgan, "A Review of Ionospheric Propagation" - IRE Proceedings, Vol. 41; pp. 582 - 587; May, 1953.

(25) H. G. Booker, J. Atmospheric Terr. Physics, Special Supplement; pp. 52; 1957.

(26) P. A. Forsyth and E. L. Vogan, J. Atmospheric Physics, Vol. 10; 1957.

(27) C. E. Gilchriest, "Application of the Phase-Locked Loop to Telemetry as a Discriminator or Tracking Filter" - IRE Transactions on Telemetry and Remote Control; pp. 20 - 35; June, 1958.

Other Reading Material

(28) Gabriel Frenkel, "Oscillator Stability and the Second-Order Phase-Locked Loop" - IRE Proceedings, Vol. 52; pp. 65 - 69; June, 1964.

(29) P. A. Forsyth, Vogan, Hansen, and Hines, "The Principles of Janet - a Meteor Burst Communication System" - IRE Proceedings, Vol. 45; pp. 1642 - 1657; December, 1957.

(30) H. G. Booker and W. E. Gordon - "The Role of Stratospheric Scattering in Radio Communications" - IRE Proceedings; pp. 1223 - 1227; September, 1957.

(31) G. W. Pickard and H. T. Stetson, - "Tropospheric Effects in Ionosphere - Supported Radio Transmission" - IRE Proceedings; pp. 596 - 599; June, 1949.

(32) W. J. Gruen, - "Theory of AFC Synchronization" - IRE Proceedings; pp. 1043 - 1048; August, 1953.

APPENDIX A

Calculations re: Antennae and Associated Equipment

(Refer to Figures 3.3, 1.2, and 3.2)

A.0 Elevation Angle

(1) Location of the sites -

		Uranium City	Saskatoon
latitude	-	59° - 34'	52° - 9'
longitude	-	108° - 37'	106° - 37'

(2) In reference to Figure 3.3, the following distances and angles are calculated by geometric means:

$c = 90^\circ - 59^\circ\ 34' = 30^\circ\ 26'$

$a = 90^\circ - 52^\circ\ 9' = 37^\circ\ 51'$

$B = 108^\circ\ 37' - 106^\circ\ 37' = 2^\circ\ 0'$

$b = \cos^{-1}(\cos c \cos a + \sin c \sin a \cos B) = 7^\circ\ 40'$

$A = \sin^{-1}(\sin a \sin B/\sin b) = 170^\circ\ 46'$

$C = \sin^{-1}(\sin c \sin B/\sin b) = 7^\circ\ 36'$

(3) In reference to Figure 1.2:

Radius of the earth = 3960 miles

Ionospheric scattering height = 49.8 miles

(4) Since the angle $b = 7^\circ\ 40'$, then the distance between Uranium City and Saskatoon is:

$7^\circ\ 40'/\ 360^\circ \times 2\pi(3960) = 528$ miles

(5) By trigonometric means, the angle of elevation was then found to be $10^\circ\ 32'$.

A.1 Mounting Height

(1) See Figure 3.2. The vertical radiation pattern of the antennae in the presence of ground is related to the vertical radiation pattern in free space as follows:

Actual vertical radiation = $2\left\{\sin(2\pi h/\lambda)\sin\alpha\right\} H_v$

where;

λ = wave length of the carrier in space = 26.8'

h = mounting height of the antenna above ground

α = angle of elevation

H_v = vertical radiation pattern in free space

(2) For the vertical radiation pattern to have a maximum at 10° 32' (as shown in Figure 3.2), the following relationship must be valid:

$\pi/2 = (2\pi h/\lambda) \sin 10^\circ 32'$

From this:

<u>mounting height h</u> = $\pi/2 \times (\lambda /2\pi) \sin 10^\circ 32'$ = <u>36.5 ft.</u>

<u>A.2 Coaxial Cable Balun Transformer</u>

(1) Transmitter quiescent frequency = 36.777.000 cps.

(2) Wave velocity through the coaxial cable = .67 x speed of light

(3) Wave length in cable = .67 x 984 x 10^6 / 36.78 = 17.91 ft.

(4) The length of the balun loop = $\lambda /2$ = 8.96 ft.

APPENDIX B

Calculations re: Signal Bandwidth

Example

Assume that the required bandwidth is to be 5 cps and that the following information is given:

(1) $K = K_1K_2 = 1550$ radians/second,

where K_1 = gain of the phase detector in volts/radian

K_2 = gain of the local oscillator in radians/second/volt

(2) f_c = cut-off frequency = 5 cps

(3) $\omega_c = (K/t_1)^{\frac{1}{2}}$ or $2\pi f_c = (K/t_1)^{\frac{1}{2}}$

(note $t_1 = (R_1 + R_2)C$)

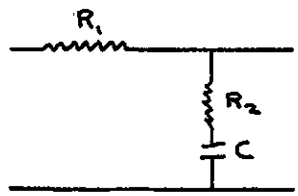

system filter

from the above data, t_1 can be calculated:

$$t_1 = K/\omega_c^2 = 1.58 \text{ sec.} \tag{B.1}$$

For minimum noise bandwidth, the network ratio $\alpha = t_1/t_2$ is obtained as in McAleer's [4] as follows: (See Equation 4.9)

$$\alpha = 1 + (1 + (K/\omega_c)^2)^{\frac{1}{2}} \tag{B.2}$$

Note that since πK is the lock range, equation B.2 can also be written as:

$$\alpha = 1 + \left\{1 + \frac{1}{\pi^2} \frac{(\text{lock range})^2}{(\text{signal bandwidth})^2}\right\}^{\frac{1}{2}} \tag{B.3}$$

If the lock range is much larger than the signal bandwidth, then:

$$\alpha \approx \frac{1}{\pi} \times \frac{\text{lock range}}{\text{signal bandwidth}} \tag{B.4}$$

Using the exact equation for α (B.2), the following value for α is obtained:

$$\alpha = 1 + (1 + \frac{1550}{31.4})^{\frac{1}{2}} = 50.4$$

The value of t_2 can now be found from equations B.1 and B.2

$$t_2 = t_1/\alpha \quad = .0314 \text{ sec.}$$

For a particular value of C, say 36×10^{-6} farads, R_2 can now be calculated, since $t_2 = R_2C$

$$R_2 = .0314/36 \times 10^{-6} = 870\ \Omega$$

Also, since $R_1C + R_2C = t_1$, then

$$R_1 = (t_1 - t_2)/C = 43\ K\ \Omega$$

To calculate values for R_1, R_2, and C for the other bandwidths, keep $R_1 = 43K$ and recalculate R_2 and C. (See Table 6.I)

APPENDIX C

Noise Bandwidth Considerations

Heitzman [5] shows that if noise is present to modulate an otherwise unmodulated carrier, the phase perturbation of the VCO can be determined as:

$$\phi^2_{rms} = \frac{n}{2C} \int_{-\infty}^{\infty} \left| H(j\omega) \right|^2 \, d\omega$$

where ϕ^2_{rms} = mean square phase perturbation caused by noise components both above and below the carrier frequency.

n = noise power spectral density in watts/cps

C = carrier power in watts

$d\omega$ = incremental portion of the frequency band

Since the quantity ϕ^2_{rms} can also be expressed as: [5]

$$\phi^2_{rms} = \frac{nB_n}{C}$$

Then it follows that

$$B_n = \frac{1}{2} \int_{-\infty}^{\infty} \left| H(j\omega) \right|^2 \, d\omega = \int_{0}^{\infty} \left| H(j\omega) \right|^2 \, d\omega$$

APPENDIX D

Development of the Phase Response Equation (6.1)

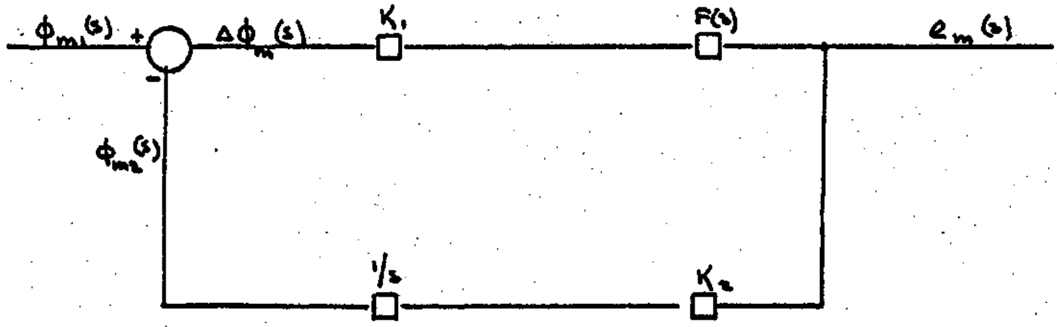

Let the incoming modulation signal be represented by:

$$I_m(t) = A \sin \omega_m t \qquad \text{cps} \tag{D.1}$$

where (1) A = constant

(2) ω_m = modulation frequency in rad./sec.

Then the incoming modulation phase signal can be derived by integration as follows:

$$\phi_m(t) = D \int I_m(t)\,dt \qquad \text{rad./sec.} \tag{D.2}$$

where (1) D = deviation constant

Note: DA = frequency deviation

Laplace transforms can be used to express equations D.1 and D.2 as:

$$I_m(s) = A\omega_m/(s^2 + \omega_m^2) \tag{D.3}$$

$$\phi_m(s) = DI_m(s)/s \tag{D.4}$$

Let the following constants be defined:

(1) $F(s)$ = filter transfer function $= \dfrac{1 + t_2 s}{1 + t_1 s}$

(2) $K = K_1 K_2$

From the diagram it can be seen that:

$$\Delta\phi_m(s) = \phi_{m1}(s) - \phi_{m2}(s) \tag{D.5}$$

$$\Delta\phi_m(s) = \frac{DI_m(s)}{s} - \Delta\phi_m(s)\left\{(K)(F(s))(1/s)\right\}$$

$$\Delta\phi_m(s) = DI_m(s)/\left\{s + K(F(s))\right\}$$

$$\Delta\phi_m(s) = \frac{DA\omega_m}{s^2 + \omega_m^{\ 2}} / \left\{s + K\frac{(1 + t_2 s)}{1 + t_1 s}\right\} \tag{D.6}$$

Equation D.6 can be rewritten as follows:

$$\Delta\phi_m(s) = \frac{(1 + t_1 s)AD\omega_m}{(s^2 + \omega_m^{\ 2})\left\{(s)(1 + t_1 s) + (K)(1 + t_2 s)\right\}}$$

$$\Delta\phi_m(s) = \frac{(1 + t_1 s)AD\omega_m}{(s^2 + \omega_m^{\ 2})(s + t_1 s^2 + K + Kt_2 s)}$$

$$\Delta\phi_m(s) = \frac{(1 + t_1 s)AD\omega_m}{(s^2 + \omega_m^{\ 2})(t_1 s^2 + s(Kt_2 + 1) + K)}$$

$$\Delta\phi_m(s) = \frac{(1 + t_1 s)AD\omega_m}{(s^2 + \omega_m^{\ 2})(K)\left\{s^2\frac{(t_1)}{K} + s\frac{(Kt_2 + 1)}{K} + 1\right\}}$$

$$\Delta\phi_m(s) = \frac{\frac{1}{t_1}(1 + t_1 s)AD}{\frac{K\omega_m}{t_1}\left\{s^2\frac{t_1}{K} + s\frac{(Kt_2 + 1)}{K} + 1\right\}\left\{\frac{s^2}{\omega_m^2} + 1\right\}} \tag{D.7}$$

Equation D.7 is now in a form in which the inverse of the Laplace transform can be obtained, [13] .

$$\Delta\phi_m(t) = \frac{\frac{(K)^{\frac{1}{2}}}{(t_1)^{1/2}}\left\{\frac{AD\,\omega_m}{t_1} / \frac{K\omega_m}{t_1}\right\}\left\{\frac{K}{t_1}\right\}^{\frac{1}{2}}\left\{1 + t_1^{\ 2}\omega_m^{\ 2}\right\}^{\frac{1}{2}}\operatorname{Sin}(\omega_m t + \psi)}{\left[\left\{\frac{(K)}{t_1} - \omega_m^{\ 2}\right\}^2 + \left\{\frac{(Kt_2 + 1)^2}{t_1^2} / \frac{(K)}{t_1}\right\}\left\{\frac{K}{t_1}\omega_m^{\ 2}\right\}\right]^{1/2}}$$

$$\Delta\phi_m(t) = \frac{\frac{AD}{t_1}(1 + t_1^{\ 2}\omega_m^{\ 2})^{\frac{1}{2}}\operatorname{Sin}(\omega_m t + \psi)}{\left[\left\{\frac{(K)}{t_1} - \omega_m^{\ 2}\right\}^2 + \left\{\frac{(Kt_2 + 1)^2}{t_1^2}\omega_m^{\ 2}\right\}\right]^{\frac{1}{2}}} \tag{D.8}$$

<u>NOTE:</u> ψ is the instantaneous phase difference between the two incoming signals. When $\omega_m = 0$, this phase difference will still exist.

APPENDIX E

Example of the calculations involved in plotting Figure 6.1 for the 20 cps bandwidth: (See Table 6.I)

Given:

(1) Bandwidth = 20 cps = 126 rad./sec.

(2) t_2 = .00731 sec.

(3) t_1 = .0981 sec.

(4) K = K_1K_2 = 1550 rad./sec.

(5) K_1 = gain of the phase detector = .84 volts/rad.

(6) K_2 = gain of the VCO = 1840 rad./sec./volt

(7) AD = 1 cps (assumed)

Then from equation 6.1:

$$\Delta\phi_m(t) = \frac{10.9(1 + .00962\,\omega_m^2)^{\frac{1}{2}}\ \mathrm{Sin}\,\omega_m t}{\left\{(137 \times 115 - \omega_m^2)^2 + (125.9)^2\,\omega_m^2\right\}^{\frac{1}{2}}}$$

$$\Delta\phi_m(t) = \frac{10.9(1 + .00962\,\omega_m^2)^{\frac{1}{2}}\ \mathrm{Sin}\,\omega_m t}{\left\{(15800 - \omega_m^2)^2 + 15800\,\omega_m^2\right\}^{\frac{1}{2}}} \qquad \text{radians}$$

Similarly equations 6.2 to 6.6 can be calculated.

APPENDIX F

Phase Peaking Ratio

The peaking ratio of $\Delta \phi_m(t)$ can be defined as:

$$P.R.(\Delta \phi_m(t)) = \frac{\text{Response when } \omega_m = (K/t_1)^{\frac{1}{2}}}{\text{Response when } \omega_m \longrightarrow 0} \qquad (F.1)$$

where; (1) ω_m = mod. frequency

(2) $K = K_1K_2$

Equation 6.1 can also be written as:

$$\Delta \phi_m(t) = AD(1 + t_1^2\omega_m^2)^{\frac{1}{2}} \sin\omega_m t \Big/ t_1\left\{(K/t_1 - \omega_m^2)^2 + \frac{(Kt_2 + 1)^2}{t_1^2}\omega_m^2\right\}^{\frac{1}{2}} \qquad (F.2)$$

Consequently, equation F.1 can be rewritten:

$$P.R.(\Delta \phi_m(t)) = \frac{AD(1 + t_1^2K/t_1)^{\frac{1}{2}}}{t_1\left\{\frac{(Kt_2 + 1)^2}{t_1^2}\frac{(K)}{(t_1)}\right\}^{\frac{1}{2}}} \Bigg/ \frac{AD}{t_1\left\{\frac{(K)}{t_1^2}^2\right\}^{\frac{1}{2}}} \qquad (F.3)$$

$$= \frac{AD(1 + Kt_1)^{\frac{1}{2}}}{(Kt_2 + 1)\left\{\frac{K}{t_1}\right\}^{\frac{1}{2}}} \Bigg/ \frac{AD}{K}$$

$$= K(1 + Kt_1)^{\frac{1}{2}} \Big/ (K/t_1)^{\frac{1}{2}}(1 + Kt_2)$$

$$= \left\{Kt_1(1 + Kt_1)\right\}^{\frac{1}{2}} \Big/ (1 + Kt_2) \qquad (F.4)$$

For Kt_1 and $Kt_2 \gg 1$

$$P.R.(\Delta \phi_m(t)) = \alpha$$

$$= t_1/t_2$$

APPENDIX G

Development of the Output Voltage-Frequency Response Equation 6.9

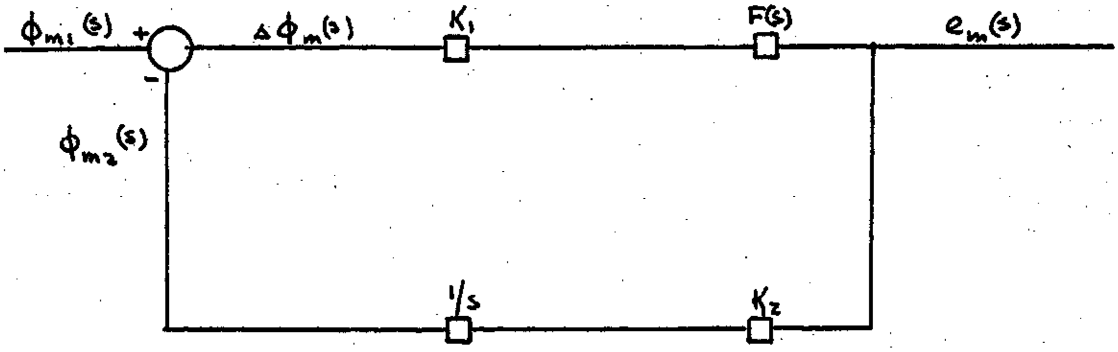

The above diagram represents the servo model of the phase lock system. The constants used in the diagram were defined in Appendix D, where it was also shown that (D.7):

$$\Delta\phi_m(s) = \frac{\frac{1}{t_1}AD(1 + t_1 s)}{\frac{K\omega_m}{t_1}\left\{\frac{s^2 t_1}{K} + \frac{s(Kt_2 + 1)}{K} + 1\right\}\left\{\frac{s^2}{\omega_m^2} + 1\right\}}$$

It can be seen from the diagram that the output voltage $e_m(s)$ can be expressed as:

$$e_m(s) = \Delta\phi_m(s)K_1F(s) \tag{G.1}$$

Substituting the expression for $\Delta\phi_m(s)$:

$$e_m(s) = \frac{\frac{1}{t_1}ADK_1\frac{(1 + t_2 s)(1 + t_1 s)}{(1 + t_1 s)}}{\frac{K\omega_m}{t_1}\left\{\frac{s^2 t_1}{K} + \frac{s(Kt_2 + 1)}{K} + 1\right\}\left\{\frac{s^2}{\omega_m^2} + 1\right\}} \tag{G.2}$$

$$e_m(s) = \frac{K_1\frac{DA}{t_1}(1 + t_2 s)}{\frac{K\omega_m}{t_1}\left\{\frac{s^2 t_1}{K} + \frac{s(Kt_2 + 1)}{K} + 1\right\}\left\{\frac{s^2}{\omega_m^2} + 1\right\}}$$

The inverse of the Laplace expression can now be found using [13] .

$$e_m(t) = \frac{K_1 D A \omega_m (\frac{K}{t_1})(1 + t_2^2 \omega_m^2)^{\frac{1}{2}} \sin(\omega_m t + \psi)}{K\omega_m \left[\left\{ \frac{K}{t_1} - \omega_m^2 \right\}^2 + \left\{ \frac{4(1 + Kt_2)^2}{4Kt_1} \right\} \left\{ \frac{K}{t_1} \omega_m^2 \right\} \right]^{\frac{1}{2}}}$$

$$e_m(t) = \frac{K_1 D A \omega_m K (1 + t_2^2 \omega_m^2)^{\frac{1}{2}} \sin(\omega_m t + \psi)}{K \omega_m t_1 \left[\left\{ (\frac{K}{t_1}) - \omega_m^2 \right\}^2 + \left\{ \frac{1 + Kt_2}{t_1} \right\}^2 \omega_m^2 \right]^{\frac{1}{2}}}$$

$$e_m(t) = \frac{K_1 D A (1 + t_2^2 \omega_m^2)^{\frac{1}{2}} \sin(\omega_m t + \psi)}{t_1 \left[\left\{ (\frac{K}{t}) - \omega_m^2 \right\}^2 + \left\{ \frac{Kt_2 + 1}{t_1} \right\}^2 \omega_m^2 \right]^{\frac{1}{2}}} \tag{G.3}$$

NOTE: ψ is the instantaneous phase difference between the two incoming signals as explained in Appendix D. Usually ψ is neglected, since only the amplitude and frequency are of interest.

<u>Example of the calculations involved in plotting Figure 6.3 for the 20 cps bandwidth:</u> (See Table 6.I)

(1) Bandwidth	= 20 cps =	126 rad./sec.
(2) t_2	=	.00731 sec.
(3) t_1	=	.0981 sec.
(4) K_1	=	.84 volts/rad.
(5) K_2	=	1840 rad./sec./volt
(6) K	=	1550 rad./sec.
(7) AD	=	1 cps (assumed)

Then from equation 6.9, for the 20 cps bandwidth:

$$e_m(t) = \frac{.84(1 + (.00731)^2 \omega_m^2)^{\frac{1}{2}} \operatorname{Sin}(\omega_m t + \psi)}{.0981 \left[\left\{ \frac{1550}{.0981} - \omega_m^2 \right\}^2 + \left\{ \frac{((1550)(.00731) + 1}{.0981} \right\}^2 \omega_m^2 \right]^{\frac{1}{2}}}$$

$$e_m(t) = \frac{8.55(1 + .000053\,\omega_m^2)^{\frac{1}{2}} \operatorname{Sin}(\omega_m t + \psi)}{\left\{ (15800 - \omega_m^2)^2 + 15900\,\omega_m^2 \right\}^{\frac{1}{2}}} \qquad \text{(G.4)}$$

Similarly equations 6.10 to 6.14 can be calculated.

<u>Peaking ratio for $e_m(t)$</u>

$$\text{Ratio} = \frac{\text{Response when } \omega_m = (K/t_1)^{\frac{1}{2}}}{\text{Response when } \omega_m \longrightarrow 0}$$

$$= \frac{ADK_1 \left\{ (1 + t_2^2(K/t_1) \right\}^{\frac{1}{2}}}{t_1 \left[\left\{ \frac{Kt_2 + 1}{t_1} \right\} \left\{ \frac{K}{t_1} \right\} \right]^{\frac{1}{2}}} \Big/ \frac{ADK_1}{K}$$

$$= K(1 + t_2^2 \frac{K}{t_1})^{\frac{1}{2}} \Big/ (Kt_2 + 1) \left\{ \frac{K}{t_1} \right\}^{\frac{1}{2}}$$

$$= K(\frac{t_1}{K} + t_2^2)^{\frac{1}{2}} \Big/ (Kt_2 + 1)$$

$$= (Kt_1 + K^2 t_2^2)^{\frac{1}{2}} \Big/ (Kt_2 + 1)$$

<u>Peaking ratios</u> (See Table 6.I for values of t_2 and t_1)

Bandwidth	Ratio
5 cps	1.40
10 cps	1.37
20 cps	1.35
40 cps	1.30
100 cps	1.1

APPENDIX H

Development of Expressions Used in Theoretical Threshold Predictions in Chapter 7

H.0 Phase Error Due to Modulation

According to Figure 4.3, and as shown by Heitzman [5], the mean square modulation induced phase error can be obtained as follows:

$$\Delta\phi_m = \phi_{m1}(t) - \phi_{m2}(t) \tag{H.1}$$

where; (1) $\phi_{m1}(t) \rightarrow$ due to sinusoidal modulation from the transmitter

(2) $\phi_{m2}(t) \rightarrow$ due to sinusoidal modulation from the V.C.O.

Factoring out ϕ_{m1} produces:

$$\Delta\phi_m = \phi_{m1}(t)\left\{1 - \phi_{m2}(t)/\phi_{m1}(t)\right\}$$

$$= \phi_{m1}(t)(1 - H(j\omega))$$

Since ϕ_{m1} can be expressed as $\int AD \sin\omega_m(t)$, then the mean square modulation induced phase error is:

$$\phi_m^2 = \frac{1}{2}\left\{\frac{AD}{2\omega_m}\right\}^2 / \left\{1 - H(j\omega)\right\}^2 = \frac{M^2}{2}\left\{1 - H(j\omega)\right\}^2 \tag{H.2}$$

H.1 Carrier Power Threshold Equation (see Heitzman [5])

According to equation 7.4, the total mean square phase error is:

$$\Delta\phi^2 = \frac{M^2}{2}\left\{1 - H(j\omega)\right\}^2 + \frac{n}{C}\int_0^{\infty} H(j\omega)^2\, d\omega \tag{H.3}$$

where; (1) M = modulation index

(2) n = noise power density

(3) C = carrier power

NOTE: H(s) = Laplace transform expression of $H(j\omega)$ = system transfer function

$$H(s) = \left\{K/t_1 + K(t_2/t_1)s\right\} / \left\{K/t_1 + (1/t_1 + Kt_2/t_1)s + s^2\right\} \tag{H.4}$$

(Equation H.4 was partly derived in section 4.1.1)

If B_b is defined as the signal bandwidth or basebandwidth, then for a damping factor Υ = .707 and with $Kt_2 \gg 1$ for the larger of the 5 bandwidths under consideration, the function H(s) can be simplified to read:

$$H(s) = B_b^2 + 1.4\left\{\frac{B_b s}{B_b^2}\right\} + 1.4\ B_b s + s^2 \tag{H.5}$$

Equation H.5 can be combined with equation H.3 so that:

$$\Delta\phi_2 = M^2/2\ (\ \omega_m^4/B_b^4 + \omega_m^4) + 3nB_b/4\sqrt{2}\ C$$

For $\omega_m \ll B_b$, the above equation reduces to:

$$\Delta\phi^2 = \frac{M^2\ \omega_m^4}{2B_b^4} + \frac{3nB_b}{4\sqrt{2}\ C} \tag{H.6}$$

The minimizing value of B_b is then found by setting the derivative of $\Delta\phi^2$, taken with respect to B_b, equal to zero.

$$B_b(\min) = \left\{\frac{8\sqrt{2}\ M^2\ C\ \omega_m^4}{3n}\right\}^{1/5} \tag{H.7}$$

If this value in equation H.6 is now set equal to .25, as described in section 7.1.1, then the carrier threshold power C_t is:

$$C_t = 35.5\ M^{\frac{1}{2}}\ nf_m \tag{H.8}$$

APPENDIX I

Simulation of Galactic Noise by the Mega-Node Noise Generator

The expression relating thermal noise to Galactic temperature is:

$$E_n^2 = 4RKT\Delta f \qquad (I.1)$$

where; (1) E_n = noise rms voltage

(2) K = Boltzman's constant = 1.38×10^{-23} joules/^oK

(3) T = absolute temperature in ^oK = $20{,}000^oK$

(4) R = input impedance to the receiver = 50 ohm

(5) f = bandwidth of receiver of interest

From the above information, the following equation can be derived:

$$\frac{E_n^2}{R\Delta f} = 4 \times 1.38 \times 10^{-23} \times 20 \times 10^3 \text{ watts/cps}$$

$$= 11 \times 10^{-19} \text{ watt/cps} \qquad (I.2)$$

The noise generator is calibrated in terms of noise figure and the expression relating noise power to noise figure is obtained as follows:

(1) $$\frac{E_n^2}{R\Delta f} = 2eI_bR \qquad (I.3)$$

where; (1) I_b = dc noise gen. diode plate current

= 4.5×10^{-3} amps

(2) e = charge on an electron = 1.59×10^{-19} cls

(2) $$F = 20I_bR \qquad (I.4)$$

where; (1) F = noise figure

(2) R = output impedance of the n.g. = 50 ohm (for a matched gen.-load combination)

Equations I.3 and I.4 can be combined to produce:

$$E_n^2/R\Delta f = eF/10 \qquad (I.5)$$

Equation I.5 can now be solved for F

$$F = 10(11 \times 10^{-19}) / 1.59 \times 10^{-19} = 70$$

Or, expressed in decibels:

$$\underline{F} = 10 \log_{10}\left\{\frac{F}{1}\right\} = \underline{18.5 \text{ db}}$$

APPENDIX J

Calculations for Noise Voltage

Noise generator setting is 18.5 db = 70

As shown in Appendix I, by equation I.5, the noise density is:

$$\frac{E_n^{\,2}}{R\Delta f} = \frac{eF}{10} = 11 \times 10^{-19} \text{ watts/cps}$$

where; (1) E_n = rms noise voltage

(2) R = impedance of the noise gen. load = 50 Ω

(3) f = signal bandwidth

(4) e = charge on an electron

(5) F = noise figure

From the above information, E_n can now be found:

$$E_n = (50 \times 1.1 \times 10^{-18} \times \Delta f)^{\frac{1}{2}} \text{ volts} \qquad \text{(J.1)}$$

$$= 7.32 \times 10^{-9} \times (\Delta f)^{\frac{1}{2}} \text{ volts}$$

For each bandwidth, the noise voltages are calculated below:

Bandwidth (cps)	Rms Noise Voltage
5	16.5×10^{-9}
10	24.5×10^{-9}
20	32.7×10^{-9}
40	46.2×10^{-9}
100	73.2×10^{-9}

APPENDIX K

Conversion of threshold S/N ratios from the signal bandwidth to the IF bandwidth.

Example:

Given: Bandwidth = 20 cps

Deviation = 20 cps

Mod. Index = 1

Threshold = 11 db S/N input

This corresponds to a S/N input ratio in the 2300 cps IF bandwidth of:

$$S/N \text{ in } (2300 \text{ cps}) = 11 \text{ db} - 10 \log \frac{\text{IF} \rightarrow \text{BW}}{\text{detector} \rightarrow \text{BW}}$$

$$= 11 \text{ db} - 10 \log 2300/20$$

$$= \underline{-10 \text{ db}}$$

Other values are shown in Table 7 - II.